

ABSTRACT

Title of Document: STRUCTURE, REACTIVITY AND
 SOLUTION DYNAMICS OF THE Sn_9^{4-} ION

Fatma Sanem Kocak
Doctor of Philosophy, 2011

Directed By: Professor Bryan W. Eichhorn
 Department of Chemistry and Biochemistry

In this thesis, the nature of the Sn_9^{4-} in solution and its reactivity with transition metal atoms and electrophiles have been studied. The Sn_9^{4-} ion is a very strong Brønsted base that deprotonates en to form the Sn_9H^{3-} ion and is a potent ion sequestering agent that competes with 2,2,2-crypt for binding K^+ . The Sn_9H^{3-} ion has a pK_a in a range of 32.2- 44 in dmsO and can be reversibly interconverted to K_3Sn_9^- through addition of K^+ and base. Addition of K^+ to Sn_9H^{3-} in the absence of base gives the proposed coupled $\text{Sn}_9\text{-Sn}_9^{6-}$ dimer. The diamagnetic Sn_9H^{3-} ion was mischaracterized as the Sn_9^{3-} paramagnetic radical in numerous publications since 1983. The Sn_9H^{3-} ion reacts with $\text{Ni}(\text{cod})_2$ and $\text{Pd}(\text{PPh}_3)_4$ complexes and give the $\text{M@Sn}_9\text{H}^{3-}$ clusters (M= Ni, Pd). The $\text{Ni@Sn}_9\text{H}^{3-}$ ion reacts with (arene) $\text{M}(\text{CO})_3$ complexes to form is the $\text{Ni@Sn}_9\text{M}(\text{CO})_3^{4-}$ ion. Endohedral d-10 atoms do not affect

the pK_a 's of the hydrido clusters, whereas coordination of $M(CO)_3$ group ($M= Cr, Mo$) significantly increases the acidity.

The $M@Sn_9SnCy_3^{3-}$ ions, where $M= Ni$ and Pd , have been prepared with two different synthetic routes from $Ni@Sn_9H^{3-}$ and $Sn_9SnCy_3^{3-}$ ions, respectively. The $Ni@Sn_9H^{3-}$ ion reacts with Cy_3SnCl and gives the $Ni@Sn_9SnCy_3^{3-}$ ion. The $Sn_9SnCy_3^{3-}$ ion reacts with $Pd(PPh_3)_4$ and gives the $Pd@Sn_9SnCy_3^{3-}$ cluster. The $Pd@Sn_9PdSnCy_3^{3-}$ ion has been prepared from a new type of reaction, where the Pd metal is oxidatively inserted into the *exo*-bond of $Pd@Sn_9-SnCy_3$.

Two new fused deltahedral clusters have been prepared from Sn_9^{4+} , Ge_9^{4+} , $Pd(PPh_3)_4$, and $Ni(cod)_2$ precursors to give the $Pd_2@Sn_{18}^{4+}$, the largest-known deltahedral cluster to-date, and $Ni@Sn_8(\mu-Ge)Ni@Sn_8^{4+}$, the first example of an endohedral heteroatom cluster.

^{119}Sn , 1H , ^{13}C NMR studies show these clusters to be highly dynamic. The $Sn_9SnR_3^{3-}$ ions ($R= Cy$ and nBu) and $M@Sn_9R^{3-}$ ions ($M= Ni, Pd$ and $R= H, SnCy_3$) exhibit fast intramolecular exchange of the all 9-Sn atoms, while the *exo*-substituent groups scramble around the clusters. The $Sn_9^iPr^{3-}$ ion has non-mobile alkyl substituent, which removes the *exo*-bonded Sn atom from exchanging with the remaining 8-Sn atoms of the cluster.

STRUCTURE, REACTIVITY AND SOLUTION DYNAMICS OF THE Sn_9^{4+} ION

by

Fatma Sanem Kocak

Dissertation submitted to the Faculty of the Graduate School of the
University of Maryland, College Park, in partial fulfillment
of the requirements for the degree of
Doctor of Philosophy
2011

Advisory Committee:
Professor Bryan W. Eichhorn, Chair
Professor Gregory S. Jackson
Professor Christopher Jarzynski
Professor Lawrence R. Sita
Professor Andrei Vedernikov

© Copyright by
Fatma Sanem Kocak
2011

Dedication

To my family, and in memory of my grandmother.

Acknowledgements

I would like to express my sincere gratitude to Prof. Bryan Eichorn for his guidance, support and suggestions he has given throughout this thesis. I have been inspired by his scientific approach and strength for finding out the true knowledge. If I were to start over my PhD again, I would definitely work with him. Thank you for everything!

I would like to thank to Prof. Andrei Vedernikov for his contributions with with his great knowledge about the acid-base chemistry and his DFT calculations for visualizing the hydrides for us. I am also very grateful to Dr. Peter Zavalij for solving numerous of the crystal structures and for his valuable discussions. I am deeply indebted to Dr. Yiu-Fai Lam for teaching me NMR and his great help and support with my NMR experiments. I also had a great pleasure working with him for about two years, and I would like to thank to him for giving me that opportunity.

I want to thank to my past and present lab mates Dr. Selim Alayoglu, Dr. Oktay Demircan, Dr. Zhufang Liu, Dr. Chunjuan Zhang, Dr. Yang Peng, Dr. Aldo Ponce, Dr. Tony Dylla, Pavan Bellamkonda, Domonique Downing, Dennis Mayo, Chris Sims, Yi Yu, for making my life more memorable for the time I spent at University of Maryland. I also would like to thank to Dina Jaber, Dr. Suleyman Can, Dr. Serpil Gonen Williams, Dr. Emren Esenturk and Dr. Okan Esenturk for their friendships and supports.

My cousin Hatice Ozel Abaan and her family, Ogan Abaan and Ata Abaan, have filled the gap of having a family during the time here in Maryland, and I am very grateful to them.

I owe to my beloved family for their support and their love that they kept sending from Turkey.

Last, but not least, I would like to thank Dr. Aydin Balkan for providing me with motivation, his love, and never ending support during the writing of this thesis.

Table of Contents

Dedication	ii
Acknowledgements.....	iii
Table of Contents	v
List of Tables	ix
List of Figures.....	xi
List of Abbreviations	xiv
Chapter 1: Introduction.....	1
1.1. Introduction.....	1
1.2. Zintl Ions	3
1.3. Transition Metal Derivatives of Zintl Ions	8
1.4. Solution Dynamics of Group 14 Zintl Ions.....	13
1.5. Overview of the Thesis	17
Chapter 2: The Sn_9H^{3-} ion and $\text{Sn}_9\text{-Sn}_9^{6-}$ dimer	18
2.1. Introduction.....	18
2.2. Results and Discussion.....	21
2.2.1. Synthesis	21
2.2.2. Solid State Structure.....	22
2.2.3. NMR Spectroscopic Studies.....	27
2.2.4. Acid-base Chemistry and Alkali Metal Sequestering	30
2.2.5. Coupling of Sn_9H^{3-} ions	37
2.3. Conclusion	39

2.4. Experimental Section	40
2.4.1. General Data	40
2.4.2. Chemicals	41
2.4.3. Synthesis	41
Chapter 3: Sn_9R^{3-} (R= ^iPr , SnCy_3 , $\text{Sn}(\text{nBu})_3$) clusters and their solution dynamics ..	43
3.1. Introduction	43
3.2. Results and Discussion	45
3.2.1. Synthesis	45
3.2.2. Solid State Structure	46
3.2.3. NMR Spectroscopic Studies	50
3.3. Conclusion	61
3.4. Experimental Section	62
3.4.1. General Data	62
3.4.2. Chemicals	63
3.4.3. Synthesis	63
Chapter 4: Endohedral Derivatives of Exo-substituted Zintl Clusters	66
4.1. Introduction	66
4.2. Results and Discussion	68
4.2.1. Synthesis	68
4.2.2. Solid State Structure	73
4.2.3. NMR Spectroscopic Studies	84
4.3. Conclusion	93
4.4. Experimental Section	97

4.4.1. General Data	97
4.4.2. Chemicals	97
4.4.3. Synthesis	98
Chapter 5: Ni@Sn ₉ M(CO) ₃ ⁴⁺ (M= Cr, Mo)	102
5.1. Introduction.....	102
5.2. Results and Discussion.....	104
5.2.1. Synthesis	104
5.2.2. Solid State Structure.....	106
5.2.3. IR Spectroscopy	111
5.2.4. NMR Spectroscopic Studies.....	113
5.3. Conclusion	113
5.4. Experimental Section	114
5.4.1. General Data	114
5.4.2. Chemicals	115
Chapter 6: Fused Deltahedral Clusters	117
6.1. Introduction.....	117
6.2. Results and Discussion.....	119
6.2.1. Synthesis	119
6.2.2. Solid State Structure.....	121
6.2.3. NMR Spectroscopic Studies.....	125
6.3. Conclusion	131
6.4. Experimental Section	132
6.4.1. General Data	132

6.4.2. Chemicals	133
6.4.3. Synthesis	133
Chapter 7: Conclusion	135
Appendix	139
References	144

List of Tables

Table 2.1. Different polymorph structures of the reported Sn_9^{3-} ions and Sn_9H^{3-} ion.	22
Table 2.2. Selected bond lengths (\AA) for the Sn_9H^{3-} ion.....	25
Table 2.3. ^{119}Sn NMR data of $\text{K}_x\text{Sn}_9^{(4-x)-}$ recorded at room temperature.	31
Table 2.4. Acidities of related weak acids in dmsO solution at 25°C	37
Table 3.1. Crystallographic data for the Sn_9R^{3-} ($\text{R} = \text{}^i\text{Pr}, \text{SnCy}_3$) ions.....	46
Table 3.2. Selected bond lengths of the $\text{Sn}_9\text{-}^i\text{Pr}^{3-}$ anion in \AA	49
Table 3.3. Selected bond lengths of the $\text{Sn}_9\text{SnCy}_3^{3-}$ anion in \AA	50
Table 3.4. ^{119}Sn NMR data of the clusters anions Sn_9R^{3-}	50
Table 4.1. Crystallographic data for the $\text{M@Sn}_9\text{H}^{3-}$ ($\text{M} = \text{Pd}, \text{Ni}$) ions.	74
Table 4.2. Selected Bond Lengths [\AA] for the $\text{M@Sn}_9\text{H}^{3-}$ ($\text{M} = \text{Ni}, \text{Pd}$) clusters	77
Table 4.3. Crystallographic data for the $\text{M@Sn}_9\text{SnCy}_3^{3-}$ ($\text{M} = \text{Pd}, \text{Ni}$).....	79
Table 4.4. Selected Bond Lengths [\AA] for the $\text{M@Sn}_9\text{SnCy}_3^{3-}$ ($\text{M} = \text{Ni}, \text{Pd}$) clusters.	81
Table 4.5. Crystallographic data for the $\text{Pd@Sn}_9\text{PdSnCy}_3^{3-}$ ion.	82
Table 4.6. Selected Bond Lengths [\AA] for the $\text{Pd@Sn}_9\text{PdSnCy}_3^{3-}$ ion.	84
Table 4.7. Summary of the average Sn-Sn bond distances and NMR data of the Sn_9R^{3-} and $\text{M@Sn}_9\text{R}^{3-}$ ions ($\text{R} = \text{H}, \text{SnCy}_3$ and $\text{M} = \text{Ni}, \text{Pd}$)	84
Table 5.1. Crystallographic data for the $\text{Ni@Sn}_9\text{M}(\text{CO})_3^{4-}$ ($\text{M} = \text{Cr}, \text{Mo}$) ion.....	107
Table 5.2. Selected Bond Lengths [\AA] and angles ($^\circ$) for the $\eta^5\text{-Ni@Sn}_9\text{Mo}(\text{CO})_3^{4-}$ ion.....	111

Table 6.1. Crystallographic data for the Pd ₂ @Sn ₁₈ ⁴⁻ ion.	122
Table 6.2. Selected Bond Lengths [Å] for the Pd ₂ @Sn ₁₈ ⁴⁻ ion.	123
Table 6.3. Crystallographic data for the Ni@Sn ₈ (μ-Ge)Ni@Sn ₈ ⁴⁻ ion.	124
Table A1. Crystallographic data for the PtH(PPh ₃)(Cy ₃ Sn) ₂ ⁻ and Pd@Sn ₉ PtSnCy ₃ ³⁻	141
Table A2. Selected Bond Lengths [Å] and angles (°) for the PtH(PPh ₃)(Cy ₃ Sn) ₂ ⁻ ..	141
Table A3. Selected Bond Lengths [Å] for the Pd@Sn ₉ PtSnCy ₃ ³⁻ ion.	142

List of Figures

Figure 1.1. Structures of homoatomic Group 14 Zintl ions.....	5
Figure 1.2. Low dimensional binary assemblies of A_xSn_9 in layer and chain.....	6
Figure 1.3. Structures of the non-interstitial transition metal derivatives of Group 14 Zintl ions.....	10
Figure 1.4. Structures of the endohedral high symmetry group 14 ions.....	11
Figure 1.5. ^{119}Sn NMR spectrum of the $Sn_{9-x}Pb_x^{4-}$ anion series.....	15
Figure 2.1. The structures of Sn_9^{n-} ; tricapped trigonal prism (D_{3h}) and monocapped square anti prism (C_{4v}).....	23
Figure 2.2. ORTEP drawing of the structure of the Sn_9H^{3-}	24
Figure 2.3. Proposed structure of the $Sn_9-Sn_9^{6-}$ ion.	26
Figure 2.4. NMR spectra of the Sn_9H^{3-}	27
Figure 2.5. ^{119}Sn NMR spectrum of the $Sn_9-Sn_9^{6-}$ anion.	29
Figure 2.6. ^{119}Sn and 1H NMR spectra for the titration of the ethylenediamine solution of K_4Sn_9 with molar equivalents of 2,2,2-crypt.....	33
Figure 2.7. ^{119}Sn NMR spectrum of the reactions of Sn_9H^{3-} with KCl and CsCl salts in the absence of a base.....	38
Figure 3.1. Exchange mechanism of the Sn_9^{4-} ion between the two lowest energy structures.....	44
Figure 3.2. ORTEP drawing of the Sn_9R^{3-} ions, where R is iPr in (a) and $SnCy_3$ in (b).....	47
Figure 3.3. ^{119}Sn NMR spectrum of the $Sn_9SnCy_3^{3-}$ anion.....	53
Figure 3.4. 1H spectrum of $[K(2,2,2-crypt)]_3[Sn_9Sn(Cy)_3].2py$	54

Figure 3.5. ^{119}Sn NMR spectrum of the $\text{Sn}_9\text{Sn}(\text{}^n\text{Bu})_3^{3-}$ anion.	54
Figure 3.6. ^{119}Sn NMR spectrum of the $\text{Sn}_9\text{-}^i\text{Pr}^{3-}$ anion.....	56
Figure 3.7. Variable temperature ^{119}Sn NMR spectra for the Sn_9R^{3-} ion.	57
Figure 3.8. Proposed exchange mechanisms for the Sn_9R^{3-} ions; a) $\text{R} = \text{SnCy}_3$, $\text{Sn}(\text{}^n\text{Bu})_3$ and b) $\text{R} = ^i\text{Pr}$	58
Figure 4.1. ORTEP drawing of the $\text{M@Sn}_9\text{H}^{3-}$ ($\text{M} = \text{Ni}, \text{Pd}$) ions	75
Figure 4.2. ORTEP drawings of the $\text{M@Sn}_9\text{SnCy}_3^{3-}$ clusters.....	78
Figure 4.3. ORTEP drawing of the $\text{Pd@Sn}_9\text{PdSnCy}_3^{3-}$ ion.....	83
Figure 4.4. NMR spectra of the $\text{Ni@Sn}_9\text{H}^{3-}$ ion	86
Figure 4.5. NMR spectra of the $\text{Pd@Sn}_9\text{H}^{3-}$ ion	86
Figure 4.6. ^1H NMR spectrum of the $\text{Ni@Ge}_9\text{H}^{3-}$	87
Figure 4.7. ^{119}Sn NMR spectra of the $\text{M@Sn}_9\text{SnCy}_3^{3-}$ ($\text{M} = \text{Ni}, \text{Pd}$).	90
Figure 4.8. ^{119}Sn NMR spectrum of the $\text{Pd@Sn}_9\text{PdSnCy}_3^{3-}$	92
Figure 4.9. Graphical representations of stepwise conversions; a) $\text{Sn}_9^{4-} \rightarrow \text{Sn}_9\text{H}^{3-}$ $\rightarrow \text{Ni@Sn}_9\text{H}^{3-} \rightarrow \text{Ni@Sn}_9\text{SnCy}_3^{3-}$, b) $\text{Sn}_9^{4-} \rightarrow \text{Sn}_9\text{SnCy}_3^{3-} \rightarrow \text{Pd@Sn}_9\text{SnCy}_3^{3-} \rightarrow$ $\text{Pd@Sn}_9\text{PdSnCy}_3^{3-}$	94
Figure 5.1. Structures of the Pb clusters from the reaction of Pb_9^{4-} with corresponding transition metal precursors.....	102
Figure 5.2. Conversion of $\text{Sn}_9^{4-} \rightarrow \text{Sn}_9\text{H}^{3-} \rightarrow \text{Ni@Sn}_9\text{H}^{3-} \rightarrow \text{Ni@Sn}_9\text{M}(\text{CO})_3^{4-}$ ($\text{M} = \text{Cr},$ Mo).....	105
Figure 5.3. ORTEP drawings of the $\eta^5\text{-Ni@Sn}_9\text{M}(\text{CO})_3^{4-}$ ions	108
Figure 5.4. The $\nu(\text{C}=\text{O})$ region of the IR spectra of a) $\eta^5\text{-Ni@Sn}_9\text{Cr}(\text{CO})_3^{4-}$ and b) $\eta^5\text{-}$ $\text{Ni@Sn}_9\text{Mo}(\text{CO})_3^{4-}$	112

Figure 6.1. Polyhedral structures of the fused deltahedral clusters; a) $\text{Pt}_2@Sn_{17}^{4-}$, b) $\text{Pd}_2@Ge_{18}^{4-}$, c) $\text{Ni}_2@Sn_{17}^{4-}$, d) $\text{Ni}_3@Ge_{18}^{4-}$	118
Figure 6.2. ORTEP drawing of the structures; a) $\text{Pd}_2@Sn_{18}^{4-}$ and, b) preliminary structure of $\text{Ni}@Sn_8(\mu\text{-Ge})\text{Ni}@Sn_8^{4-}$ ion..	121
Figure 6.3. ^{119}Sn NMR spectrum of the $\text{Pd}_2@Sn_{18}^{4-}$ ion.	126
Figure 6.4. ^{119}Sn NMR spectrum of the $\text{Ni}@Sn_8(\mu\text{-Ge})\text{Ni}@Sn_8^{4-}$ ion.....	127
Figure 6.5. ^{119}Sn NMR spectra a) K_4Sn_9 , b) reaction mixture of K_4Sn_9 with $\text{Ni}(\text{cod})_2$ complex, c) $\text{Ni}@Sn_9\text{H}^{3-}$ ion, and d) reaction mixture of KCl salt and $\text{Ni}@Sn_9\text{H}^{3-}$ ion, prepared <i>in-situ</i> in the presence of 2,2,2-crypt.	129
Figure A1. ORTEP drawing of the $\text{PtH}(\text{PPh}_3)(\text{Cy}_3\text{Sn})_2^-$ complex (a) and $\text{Pd}@Sn_9\text{PtSnCy}_3^{3-}$ ion (b).	140

List of Abbreviations

NPs	Nanoparticles
NMR	Nuclear magnetic resonance
IR	infrared
ORTEP	Oakridge thermal ellipsoid parameters
XRD	x-ray diffraction
EPR	electron paramagnetic resonance
2,2,2-crypt	4,7,13,16,21,24-hexaoxa-1,10-diazabicyclo[8.8.8]hexacosane
18-crown-6	1,4,7,10,13,16-hexaoxacyclooctadecane
en	ethylenediamine
RNH ₂	ethylenediamine
tol	toluene
dmf	dimethylformamide
DMSO	dimethylsulfoxide
py	pyridine
thf	tetrahydrofuran
Cy	cyclohexyl
Ph	phenyl
cod	cyclooctadiene
Bu	butyl
Me	methyl
mes	mesityl
TMS	tetramethyl silane

eq	equation
equiv	equivalent
cbe	cluster bonding electrons
CO	carbon monoxide
Pr	propyl
ppm	parts per million
hrs	hours
min	minute
MHz	mega hertz
calc	calculated
Abs coeff	absorption coefficient
avg	average
mmol	millimole
ml	milliliter

Chapter 1: Introduction

1.1. Introduction

Zintl ions are typically classified as the polyanions of the heavier main group elements of group 14 and 15. They are generally obtained from dissolution of binary phases with alkali metals. Recent studies in this field have resulted in a remarkable number of new clusters with interesting structures and bonding.^[1-4] In this thesis, I describe my studies mainly on the synthesis of new Zintl clusters, unraveling the complex mechanism of their formations. By elucidating the dynamic and the spectroscopic properties of the clusters resulted in resolving long standing misconceptions of acid-base chemistry and ion pairing in Zintl complexes. Introductions to these topics are given below.

Zintl ions are an important member of molecular cluster compounds. Highly symmetrical clusters derived from Zintl ions have novel solid state structures, unusual electronic structures, and interesting gas phase chemistry and solution dynamic properties. In addition to these features, their similarities to the fullerenes and metalloid clusters sparked interest towards synthesis and characterization of such clusters.^[5] Remarkable progress in isolation of new Zintl clusters revealed many chemical properties, such as functionalization of the clusters, formation of oligomers, inclusion and coordination of transition metals. Recent developments with oxidatively coupled clusters and mesoporous materials have triggered new advances in this field

towards obtaining cluster-assembled nanomaterials from these molecular building blocks.^[6, 7]

The Zintl ions with their precise sizes and compositions can be considered as the interface between large molecules and small nanoparticles (NPs). Transition metal derivatives of these polyanions are thought to be potential precursors for bimetallic and trimetallic NPs, owing to their stability without supporting ligands, and their precise compositions.^[8, 9] In most cases, bimetallic systems have superior catalytic properties such as in hydrocarbon reforming reactions, preferential H₂ oxidation with CO tolerance compared to monometallic systems due to effects on the electronic band structure.^[10-12]

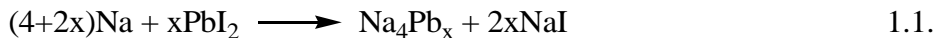
Atomic mobility significantly affects the reactivity of catalysts in heterogeneous transformations.^[13] Therefore, the mobility of metal atoms in bare metal clusters and small metallic NPs is of fundamental importance to cluster science and nanochemistry. Surface restructuring in bimetallic NPs and cluster catalysts is particularly relevant, because changes in the local environment of a metal atom can alter its chemical activity.^[11, 14] Recent studies suggest that small NPs are far more fluid than initially thought.^[15, 16] Lower melting points and the dominance of surface energies in small NPs suggest that these systems may be quite dynamic. However, little is known about the dynamic properties and processes of NPs due to lack of suitable experimental techniques. On the other hand, studies have shown that most Zintl ion clusters show highly dynamic liquid-like behavior in the solution. The similarities between Zintl ions and NPs suggest that studying solution dynamics of Zintl ions may help uncover dynamic properties of NPs.

Below I have reviewed and summarized the chemistry of Zintl ions, their transition metal derivatives, and their solution dynamics.

1.2. Zintl Ions

The first discovery of Zintl ions dates back to the 1890s, when Joannis obtained sodium plumbide precipitates from the ammonia solution of sodium and metallic lead.^[17, 18] The compositions of the precipitates were determined to be $\text{NaPb}_4 \cdot 2\text{NH}_3$ and NaPb_2 depending on the reaction conditions. Later, in 1907 Kraus showed that these plumbides were actually salts that dissociate into Na^+ and Pb^{n-} ions ($n = 2, 4$) in liquid ammonia.^[19, 20] The subsequent electrolysis studies by Smyth and Peck showed that Te/Na, Sb/Na polyanionic salts have compositions of 4:1 and 2.33:1, respectively.^[21, 22] As a result of these experimental analyses, the actual compositions of the polyanions were concluded to be $\text{Na}_4\text{Pb} \cdot \text{Pb}_8$, $\text{Na}_3\text{Sb} \cdot \text{Sb}_6$ and $\text{Na}_4\text{Te} \cdot \text{Te}_3$.^[19, 21, 22] They are now known as sodium salts of Pb_9^{4-} , Sb_7^{3-} and Te_4^{4-} anions.

In the 1930's, Zintl and his coworkers were the first to correlate the structure and bonding of solid state intermetallics of the heavier main group elements (e.g. NaTl), which are now known as Zintl phases. In addition, they studied the chemistry of soluble main-group polyanions by reducing halide salts of main group metals such as PbI_2 and BiI_3 in a charge transfer reaction with sodium and potassium as given in eq.1.1.^[23, 24] They also prepared a variety of polyatomic anions having molecular formulas of E_9^{4-} ($\text{E} = \text{Sn}, \text{Pb}$) and E_7^{3-} ($\text{E} = \text{Sb}, \text{Bi}$), E_5^{3-} ($\text{E} = \text{As}, \text{Bi}$) and E_3^{3-} ($\text{E} = \text{As}, \text{Sb}, \text{Bi}$).^[25]



The first soluble polyanion to be isolated in solid state, $\text{Na}_4(6-8\text{en})\text{Sn}_9$, has been obtained by dissolution of melt of nominal composition of $\text{NaSn}_{2.4}$ alloy in ethylenediamine.^[26, 27] Its structural analysis showed that it is a three dimensional salt with a composition of $\text{Na}_4(\text{en})_7\text{Sn}_9$ and has an Sn_9^{4-} polyhedron and Na^+ ions surrounded by ethylenediamine solvate molecules in the lattice. This new discovery was followed by isolation and structural analysis of several free-standing metal clusters including Ge_9^{4-} ,^[28] E_7^{3-} (E= P, As),^[29, 30] and P_{16}^{2-} .^[31]

The structure of the pnicogen (group 15) Zintl ions are hydrocarbon-like and polycyclic in nature, as in cyclic E_4^{2-} (E= P, As, Sb, Bi)^[32, 33] ions and nortricyclane E_7^{3-} (E= P, As, Sb)^[34] ions. In these ions, the E and E⁻ are electronically equivalent to CH and CH₂, such that they form localized bonds. In contrast, group 14 Zintl ions form electron deficient structures, and many group 14 polyhedrons follow Wade-Mingos rules.^[35, 36] The *closo* clusters of E_4^{4-} (E=Ge, Sn) (Figure 1.1a),^[37, 38] E_5^{2-} (E= Si, Ge, Sn, Pb) (Figure 1.1b)^[39, 40] and E_{10}^{2-} (E= Pb^[41] and Ge in $\text{Ge}_{10}\text{Mn}(\text{CO})_4^{3-}$ ion)^[42] (Figure 1.1d) have $2n+2$ electron configuration, and the *nido*-clusters E_9^{4-} (E= Si, Ge, Sn, Pb) (Figure 1.1c)^[43, 44] have $2n+4$ electron configurations, where n is the number of vertex atoms. On the other hand, the 9-vertex structures of E_9^{3-} (E= Si, Ge, S, Pb) ions are distorted tricapped trigonal prisms, which deviated from a Wade-Mingos description of a *nido* structure.^[45-48] These ions have been proposed to be paramagnetic ions. However, as it will be discussed in this thesis, Sn_9^{3-} ion and potentially together with the other group 14 ions are diamagnetic E_9H^{3-} clusters.

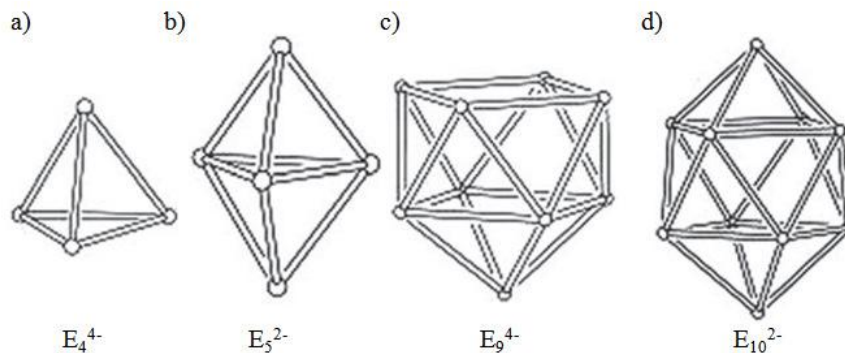


Figure 1.1. Structures of homoatomic Group 14 Zintl ions a) E_4^{4-} , E= Ge, Sn; b) E_5^{2-} , E= Ge, Sn, Pb; c) E_9^{4-} , E= Si, Ge, Sn, Pb; d) E_{10}^{2-} , E= Pb and Ge in $Ge_{10}Mn(CO)_4^{3-}$ (taken from reference [3]).

In 1976, Corbett and co-workers first used 4,7,13,16,21,24-hexaoxa-1,10-diazobicyclo[8,8,8]hexacosane (known as 2,2,2-crypt) as a alkali ion sequestering agent.^[49] Further studies showed that metallic potassium and group 14 elements in the presence of 18-crown-6 forms Sn_9^{4-} and Pb_9^{4-} ions when heated at 40°C, well below the melting points of elements.^[50] The group 14 and group 15 clusters isolated with 2,2,2-crypt and 18-crown-6 include E_5^{2-} (E=Si, Ge, Sn, Pb),^[39, 40, 51] E_9^{n-} (E= Si, Ge, Sn, Pb, n= 3, 4),^[45, 52] E_9^{2-} (Si)^[53] and, E_7^{3-} (E= P, As, Sb).^[32, 37, 43] In these studies, the E_9^{n-} ions (E= Ge, Sn, Pb, n= 3, 4) and their derivatives have been isolated through dissolution of melts of nominal composition A_4E_9 (A= Li, Na, K, Cs, Rb). However, due to limited solubility of the A_4Si_9 binary phase, the Si_9^{n-} (n= 3, 4) has been obtained from the $A_{12}E_{17}$ binary phase in liquid ammonia.^[44] The E_5^{2-} (E=Si, Ge, Sn, Pb) ions have been isolated by dissolution of alkali metal rich binary phases (e.g. $K_{1.33}Sn$).

Crystallization of group 14 polyhedra with less than four equivalents of sequestering agents often results in the isolation of 1 and 2 dimensional compounds containing infinite layers of anions separated by alkali metal-cryptate ions such as 2D layer of $\text{Rb}_2\text{Sn}_9^{2-}$ in the $[\text{K}(18\text{-crown-6})]_2[\text{Rb}_2\text{Sn}_9(\text{en})_{1.5}]$ (Figure 1.2a), and linear chains of $[\text{KSn}_9]^{3-}$ in $[\text{K}(18\text{-crown-6})]_3[\text{KE}_9]$ (Figure 1.2b).^[50, 54-59] In these low dimensional binary assemblies, the non interacting cluster ions are linked by alkali metal cations.

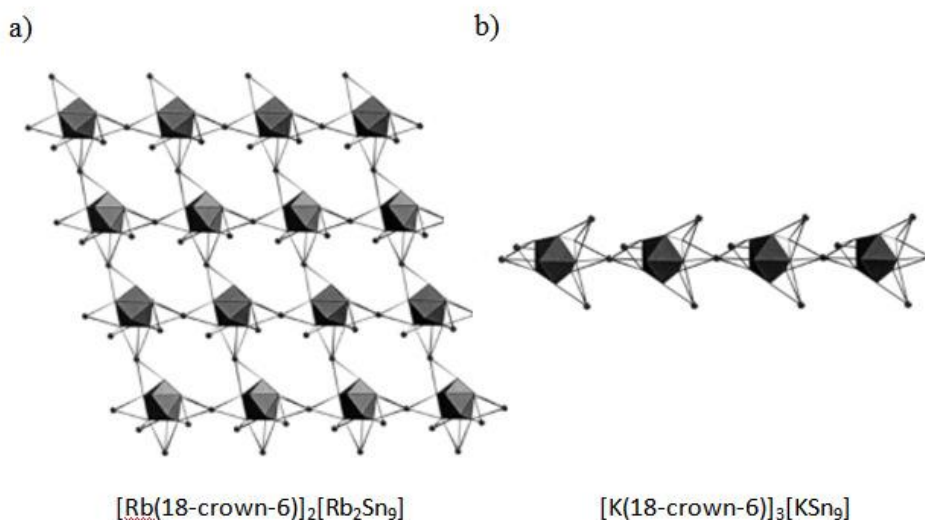


Figure 1.2. Low dimensional binary assemblies of A_xSn_9 in layer and chain. a) 2D layer of $\text{Rb}_2\text{Sn}_9^{2-}$ in the $[\text{K}(18\text{-crown-6})]_2[\text{Rb}_2\text{Sn}_9(\text{en})_{1.5}]$; b) linear chain of $[\text{KSn}_9]^{3-}$ in $[\text{K}(18\text{-crown-6})]_3[\text{KE}_9]$. Polyhedra represent main group clusters and alkali ions are shown as spheres. Organic groups are omitted for clarity. (taken from reference [55])

The first oxidatively coupled group 15 oligomer was studied by Haushalter and coworkers.^[60] In this As_{14}^{4-} ion dimer, the norticyclane-structured As_7^{3-} ions are connected through a 2-center-2-electrons *exo*-bond exterior the cluster. Subsequent studies showed that Ge_9^{4-} clusters can also give oxidatively coupled ions e.g. $(\text{Ge}_9)_m^{n-}$ ($n=6$ for $m=2,3$ and $n=8$ for $m=4$).^[61-65] The Ge_9 oligomers have mono-capped

square antiprismatic cluster units, connected by two-center-two-electron exo-bond(s). Moreover, usage of 18-crown-6 as sequestering agent in the Ge_9^{4+} solution allowed isolation of the $1\infty[\text{Ge}_9^{2-}]$ polymer.^[66] Further oxidation of Ge_9^{4+} clusters to the zero oxidation state resulted in clathratic and mesoporous materials.^[67-71] These results show that the controlled growth of Ge_9^{4+} ions can result in materials with ordered structures in uniform compositions. Coupled clusters with other members of the group 14 Zintl ions are not as common. Recently, a coupled cluster for the Sn_9^{4+} analog has been obtained by Ag^+ ion coordination in the $\mu\text{-Ag}[\text{Sn}_9]_2^{5-}$ cluster.^[72] In spite of extensive studies of group 14 and 15 Zintl ions, to-date, the coupling mechanism is not fully understood.

The group 14 and 15 Zintl ions have been shown to form *exo*-functionalized derivatives containing covalently-bonded substituents on the exterior of the clusters. Several R_xE_7 compounds ($x=1-3$) have been prepared in earlier studies, where $\text{E} = \text{P}, \text{As}$, and $\text{R} = \text{H}, \text{Me}, \text{Et}, \text{Bu}, i\text{-Pr}, \text{SnCy}_3, \text{SiMe}_3, \text{SnMe}_3, \text{and PbMe}_3$.^[73-75] More recent studies have shown that the E_9^{4+} ions ($\text{E} = \text{Ge}, \text{Sn}$) can also form substituted deltahedral clusters e.g. $\text{RGe}_9^{3-}, \text{R}_2\text{Ge}_9^{2-}, \text{RGe}_9\text{-Ge}_9\text{R}^{4+}$ and RSn_9^{3-} , where R is an *exo*-bonded alkyl or post-transition metal group.^[76-81] Although the formation of the alkyl substituted RGe_9^{3-} ions have not been fully explained, nucleophilic substitution reactions have been proposed. The effects of the substituent group on the highly dynamic nature of E_9^{4+} ions and reactivity with transition metal complexes have not been studied.

The substituted Zintl clusters bridge two fields of molecular cluster chemistry due to their structural similarities; namely Zintl ions and metalloid clusters. Metalloid

clusters are highly substituted clusters of E_xR_y , where the number of E-E bonds is greater than the E-R bonds. They have been prepared by different synthetic methods than Zintl ions. Some of the examples of the group 14 metalloids clusters are Sn_8R_4 ($R = C_6H_3-2,6-(2,4,6-Me_3C_6H_2)_2$),^[82] Sn_9R_3 ($R = 2,6-(2,4,6-iPr_3C_6H_2)_2C_6H_3$)^[83] and Pb_nR_6 ($R = Si(SiMe_3)_3$, $n = 10, 12$).^[84] Unlike the metalloids clusters, substitution of the E_9^{4-} ($E = Ge, Sn$) Zintl ions gives a maximum of two substituent groups, as in the $Ge_9R_2^{2-}$ ($R = SbPh_2$ and $BiPh_2$) ions.^[77, 78]

Although numerous examples of homoatomic series of group 14 and 15 ions have been isolated, the examples of isolated heteroatomic Zintl ions are rather limited. The isolated heteroatom naked clusters have been obtained by dissolution of the ternary phases from the corresponding nominal melts (e.g. $K_2Sn_2Bi_2$). Some examples of these clusters include $Tl_2Te_2^{2-}$, $As_2Se_6^{3-}$, $Sn_2Bi_2^{2-}$, $Pb_2Sb_2^{2-}$, $InBi_3^{2-}$, $GaBi_3^{2-}$, $In_4Bi_5^{3-}$ and co-crystallized $TlSn_8^{3-}$, $TlSn_9^{3-}$ ions.^[60, 85-88] Although, the series of the $Sn_{9-x}Ge_x^{4-}$ and $Sn_{9-x}Pb_x^{4-}$ heteroatom clusters were characterized by solution studies, their isolation in the solid state has not been reported.^[38, 89] Recently, the $Sn_8Ge(C_2H_3)^{3-}$ and $Sn_7Ge_2(C_2H_3)^{3-}$ ions have been isolated from alkyl substitution reactions, where the vinyl groups are attached to the Ge atom.^[90] However, a rational synthesis and isolation method is needed for obtaining other potential free standing heteroatom clusters.

1.3. Transition Metal Derivatives of Zintl Ions

The reactivity of the group 14 Zintl ions with transition metals and more recently lanthanides has resulted in many transition-metal Zintl-ion adducts in

different nuclearities and geometries.^[3, 91] These binary and ternary ions are of importance, since they can be building blocks for nanoparticles and cluster assembled nanomaterials.^[9] The increased numbers of examples for such clusters in the last decade has enhanced the understanding of structure, bonding and solution dynamics. However the differences in reaction mechanisms resulting in diversity of the products have not been fully understood.

In 1983, Rudolph and his coworkers showed the reactivity of K_4Sn_9 and K_4Pb_9 in the ethylenediamine with transition metal complexes of $Pt(PPh_3)_4$ and $Pd(PPh_3)_4$.^[92, 93] They identified the new cluster ions in the solution by means of NMR studies and proposed these new compounds as $(PPh_3)_2ME_9^{4-}$ (M= Pd, Pt, E= Sn, Pb). However, since these cluster compounds were not been isolated, the actual compositions of these clusters are not known.

The first isolated transition-metal group 14 Zintl ions synthesized from nine-atom cluster precursors were $\eta^4-E_9Cr(CO)_3^{4-}$ (E=Sn, Pb) clusters (Figure 1.3 a).^[94, 95] Later, a new isomer for the $\eta^5-Sn_9W(CO)_3^{4-}$ and $\eta^5-Pb_9Mo(CO)_3^{4-}$ anions was reported.^[96, 97] Eichhorn et al described the equilibrium between η^4 and η^5 isomers by NMR studies.^[96-98] In recent years, this class of anions have been expanded by isolation of other η^4 coordinated cluster anions, with examples including $Ge_9M(L)^{3-}$ (M= Ni, R= CO, and for M=Pd L= PPh_3),^[99, 100] $E_9Ir(cod)^{3-}$ (E= Sn, Pb),^[72, 101] $E_9Zn(C_6H_5)^{3-}$ (E= Si, Ge, Sn, Pb)^[102, 103] and E_9CdR^{3-} (E= Sn, Pd, R= C_6H_5 , $SnBu_3$).^[103]

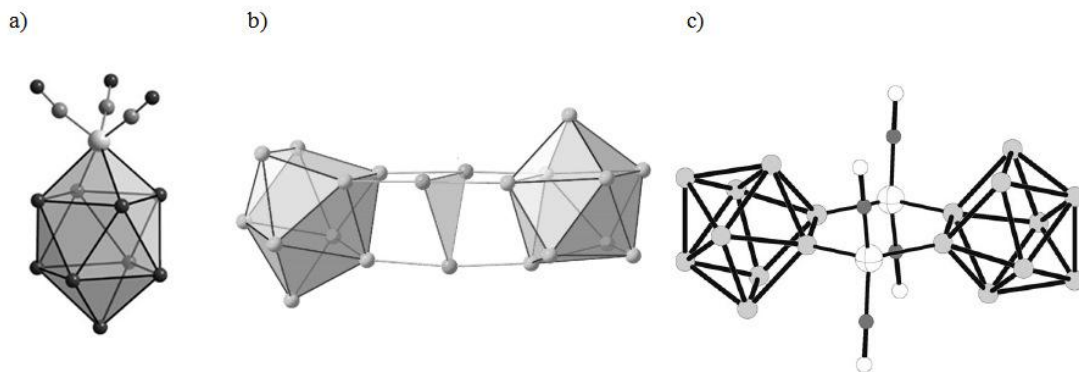


Figure 1.3. Structures of the non-interstitial transition metal derivatives of Group 14 Zintl ions. a) $E_9M(CO)_3^{4-}$, $E = Sn, Pb$, $M = Cr, Mo, W$; b) $Ge_9Au_3Ge_9^{5-}$; c) $Si_9\{Ni(CO)_2\}_2Si_9^{8-}$. (taken from references [96, 104, 105])

Another important class of transition metal-group 14 Zintl ions are the deltahedral clusters linked by the transition metal atom(s) in various different fashions as in the $Ge_9Au_3Ge_9^{5-}$ (Figure 1.3 b), $Si_9\{Ni(CO)_2\}_2Si_9^{8-}$ (Figure 1.3 c), $Pb_9Cd-CdPb_9^{6-}$ and polymeric $1\infty[HgGe_9]^{2-}$ ions.^[104-108] The isolated $Au_3Ge_{45}^{9-}$ ion combines the two reactivity profiles of the Ge_9^{4-} ions; oxidative coupling and linkage with the transition metals.^[109] Thus, controlled growth of the cluster ions is also possible by using transition metal atoms.

Many reactions with transition metal complexes and E_9^{4-} ($E = Ge, Sn, Pb$) starting clusters yield products that conserve the initial nuclearity of 9. However, some studies reported fragmentation of the cluster ions^[110-112] or occurrence of negatively charged coordination compounds instead of transition metal adduct.^[112-114] The reason of this unusual reactivity has not been investigated.

Further studies showed that transition metal atoms can be inserted into the clusters to form endohedral compounds with 9 or more atoms by using low valent transition metal complexes with labile ligands such as PPh_3 . In the endohedral

clusters, the transition metal atoms occupy the central position in the clusters coordinating to cluster atoms. The smallest endohedral ions isolated to date are the $\text{Cu}@E_9^{3-}$ ($E = \text{Sn}, \text{Pb}$) (Figure 1.4 a), $\text{Pt}@Sn_9H^{3-}$ and $\text{Ni}@Ge_9^{3-}$ ions.^[53, 115, 116] The reaction of K_4E_9 and the Cu^+ ion represents a both charge and mass balanced reaction. Most other reactions appear to involve partial oxidation of the E_9^{4-} ions with sacrificial reduction of ligands or solvent. The E_9^{4-} ($E = \text{Ge}, \text{Sn}$) clusters react with the group 10 transition metal complexes to give endohedral cluster ions *e.g.* $\text{Pt}@Sn_9Pt(\text{PPh}_3)^{2-}$.^[117] Eichhorn et al. showed that 1:2 ratio of Sn_9^{4-} and $\text{Pt}(\text{PPh}_3)_4$ react in an oxidation process to give $\text{Pt}@Sn_9Pt(\text{PPh}_3)^{2-}$ and H_2 gas resulting from reduction of the ethylenediamine (en) solvent.^[117] Various examples of isostructural Ge analogs of this cluster have been isolated with different coordinated ligands to the vertex transition metal atom, such as the $\text{Ni}@Ge_9Ni(L)^{2-}$ ($L = \text{CO}, \text{PPh}_3$), $\text{Ni}@Ge_9Pd(\text{PPh}_3)^{2-}$ and $\text{Ni}@Ge_9Ni(L)^{3-}$ ($L = \text{en}, -\text{CCPh}$) ions.^[4, 99, 100] The $\text{Ni}@Ge_9Ni(\text{CO})^{2-}$ ion was obtained from the $\text{Ni}@Ge_9^{3-}$ ion in a stepwise conversion, but this conversion does not clearly explain the one lost electron.^[99]

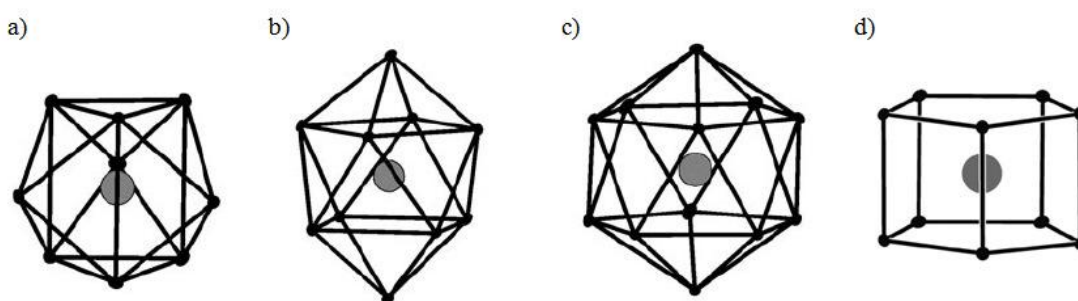


Figure 1.4. Structures of the endohedral high symmetry group 14 ions. a) $\text{Cu}@E_9^{3-}$, $E = \text{Sn}, \text{Pb}$; b) $\text{Ni}@Pb_{10}^{2-}$; c) $\text{M}@E_{12}^{n-}$, for $E = \text{Pb}$, $M = \text{Ni}, \text{Pd}, \text{Pt}$, and $n = 2$, for $E = \text{Sn}$, $M = \text{Ir}$, and $n = 3$; d) $\text{M}@Ge_{10}^{3-}$ ($M = \text{Fe}, \text{Co}$). (taken from reference [118])

Highly symmetric closed shell group 14 ions without any attending ligands have gained significant attention due to similarities of their structures with the platonic solids and their σ -aromatic properties. The icosahedral clusters Ir@Sn_{12}^{3-} and M@Pb_{12}^{2-} (M= Ni, Pd, Pt) are landmark examples of high symmetry in the group 14 Zintl ions (Figure 1.4 c).^[119-121] Eichhorn et al reported that in the reaction of Pb_9^{4-} with $\text{M}(\text{PPh}_3)_4$ (M= Pd, Pt) metal precursors, C_6H_6 and Ph_2P^- are forming as byproducts.^[122] However, the reaction of Pb_9^{4-} ion with $\text{Ni}(\text{cod})_2$ to give Ni@Pb_{12}^{2-} ion proceeds via reduction of cod to cyclooctene. Fassler et al. succeeded in converting $\text{Sn}_9\text{Ir}(\text{cod})^{3-}$ into Ir@Sn_{12}^{3-} ion.^[123] However, the detailed reaction mechanisms of formation for these clusters are not clear. Having a lower symmetry, deltahedral Ni@Pb_{10}^{2-} ion (Figure 1.4 b) has a bicapped square antiprismatic structure, whereas non-deltahedral M@Ge_{10}^{3-} (M= Fe, Co) ions adopt a pentagonal prismatic structure (Figure 1.4 d).^[124, 125]

In the fused deltahedral clusters, two endohedral transition metal atoms can be encapsulated in two-focus clusters. The reported examples are $\text{Ni}_2\text{@Sn}_{17}^{4-}$, $\text{Pt}_2\text{@Sn}_{17}^{4-}$, $\text{Pd}_2\text{@Ge}_{18}^{4-}$ and $\text{Ni}_3\text{Ge}_{18}^{4-}$ ions. The $\text{Pt}_2\text{@Sn}_{17}^{4-}$ and $\text{Pd}_2\text{@Ge}_{18}^{4-}$ ions are single cage clusters with two endohedral transition metal atoms.^[115, 126-128] In the $\text{Ni}_2\text{@Sn}_{17}^{4-}$ and $\text{Ni}_3\text{Ge}_{18}^{4-}$ ions, two endohedral cluster units are bound to each other with a common vertex atom, Sn and Ni, respectively.^[126, 128] Although they have similar geometries, the reasons for the differences in nuclearity are unexplored.

In addition to starting with the 9-atom clusters, reaction of 4-atom cluster Si_4^{4-} with $\text{Cu}(\text{mes})$ resulted in $\text{Si}_4\{\text{Cu}(\text{mes})\}_2^{4-}$ showing prospect for reactivity of group 14 Zintl ions such as E_5^{2-} (E= Si, Ge, Sn, Pb).^[129] More recently, two new clusters have

been isolated starting from $\text{Sn}_2\text{Bi}_2^{2-}$ heteroatom Zintl ion. Similar to the fused deltahedral ions, $\text{Ni}_2@\text{Sn}_7\text{Bi}_5^{3-}$ has two transition metal atoms in a single cage heteroatom cluster.^[130] The second ion, $\text{Eu}@\text{Sn}_6\text{Bi}_8^{4-}$, is a fuller type Zintl ion with a lanthanide endohedral atom.^[131]

1.4. Solution Dynamics of Group 14 Zintl Ions

The fortuitous presence of almost equal abundance of $I = \frac{1}{2}$ ^{119}Sn and ^{117}Sn isotopes provides a direct measure of the number of Sn atoms in a given cluster. A statistical evaluation of the isotope distributions in the clusters gives the relative populations the different isotopimers (*i.e.* clusters having different distributions of isotopes). In NMR analyses, the multiplicity of the resonance associated with each isotopimer (*i.e.* singlet, doublet, triplet, etc.) and its relative abundance dictates the satellite pattern and intensity.^[132] Evaluation of data collected over the last 30 years shows that satellite patterns and coupling constants can provide significant insight into the number of spin-active vertex atoms in the cluster, the positions of metal atoms in a cluster (*i.e.* interstitial or vertex) and the number of atoms in dynamic exchange.^[133] For example, when an X nucleus (*e.g.* $X = ^{195}\text{Pt}$, $^{63/65}\text{Cu}$, ^1H , $^{119/117}\text{Sn}$) couples to nine equivalent Sn atoms, a characteristic satellite pattern is observed regardless of the identity of X. Moreover, the magnitudes of the coupling constants provide insight into mechanisms of dynamic exchange.

In 1978, Rudolph and coworkers provided the first experimental evidence for dynamic exchange of A_4E_9 ($\text{A} = \text{Li}, \text{Na}, \text{K}, \text{Cs}, \text{Rb}$, and $\text{E} = \text{Sn}, \text{Pb}$).^[134] They obtained the ^{119}Sn and the ^{207}Pb spectra from the melts of nominal compositions of Na_4E_9 in

ethylenediamine (en). Instead of finding 3 signals in 4:4:1 ratio as expected from the C_{4v} solid state structure, they reported that Na_4Sn_9 has a single resonance at $\delta^{119}Sn = -1230$ ppm (upfield from $SnMe_4$). The Na_4Pb_9 resonance was reported at $\delta^{207}Pb = -4150$ ppm, upfield from the $PbMe_4$ (see Figure 1.5). Single resonance in NH_3 solvents from 30 °C to -40 °C represents a rapid intramolecular exchange of all 9 E atoms on the NMR time scale. The intramolecular nature of exchange and the nuclearity of the cluster are conveniently evidenced by the presence and intensities of the ^{117}Sn satellites on the ^{119}Sn resonance. The chemical shifts of Sn_9^{4-} and Pb_9^{4-} ions are both solvent and cation dependent, and they systematically move downfield from Li^+ to Cs^+ . These trends of downfield shifts with increasing size and “softness” of alkali counter ion are attributed to increased ion pairing with the larger alkali ions.^[135]

The exchange mechanism of such 9-atom fluxional clusters is widely accepted to involve the interconversions of the D_{3h} and C_{4v} structures in a “diamond-square-diamond” mechanism common to the boranes.^[45, 136] Corbett showed that the energy difference between the two structures was negligible^[45] and more recent studies have shown the calculated energy barrier for interconversion to be < 0.01 eV in Sn_9^{4-} cluster.^[137] The ^{119}Sn Mössbauer studies and related EXAFS studies of Sn_9^{4-} suggest that the cluster still shows dynamic behavior in the solid state.^[138, 139] Recently, SCF-CNDO-MO calculations showed that if three vertices in this cluster are replaced by Bi^+ atoms, as in the $Sn_6Bi_3^-$ ion, the optimized energy difference between C_{4v} and D_{3h} symmetries increases (0.22 eV), and the cluster should become static in solution, however this ion has not been isolated to date.^[137]

The fluxionality of the Sn_9^{4-} ion are evidenced not only by the observation of a single NMR chemical shift, but also by reduced ^{119}Sn - ^{117}Sn coupling constants, $J(^{119}\text{Sn}$ - $^{117}\text{Sn})$ which are less affected by the nature of the counter cation. A typical Sn-Sn single bond in a Zintl complex shows $J(^{119}\text{Sn}$ - $^{117}\text{Sn})$ values between 1975-1043 Hz in a static compound.^[38, 98] For example, NMR studies of tetrahedral Sn_4^{2-} , $\text{Sn}_2\text{Bi}_2^{2-}$ ions and trigonal bipyramidal cluster Pb_5^{2-} ion have relatively larger coupling constants.^[38, 135] These results indicate that the latter clusters are static or in slow exchange on the NMR time scale. However, the Sn_9^{4-} ion shows $J(^{119}\text{Sn}$ - $^{117}\text{Sn})$ values between 250 – 310 Hz, depending on solvent.^[140] The small coupling constants in a fluxional ion are due to averaging of one-bond, two-bond and three-bond couplings present in the static structures.

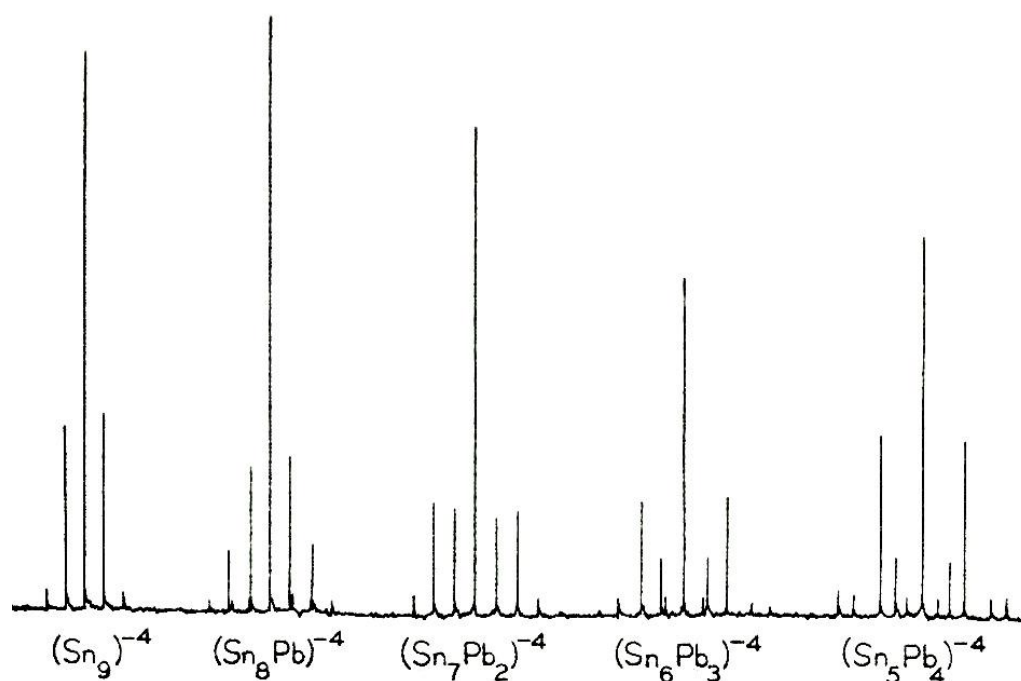


Figure 1.5. ^{119}Sn NMR spectrum of the $\text{Sn}_{9-x}\text{Pb}_x^{4-}$ anion series. (taken from the reference [132])

The $\text{Sn}_{9-x}\text{Ge}_x^{4-}$ and $\text{Sn}_{9-x}\text{Pb}_x^{4-}$ clusters (Figure 1.5) ($x = 1 \rightarrow 8$) have also been characterized by ^{119}Sn and ^{207}Pb NMR spectroscopy.^[38, 89, 134] The $\text{E}_{9-x}\text{E}'_x^{4-}$ ions are highly fluxional and also show systematic trends in chemical shifts and coupling constants. The crystallized 50:50 mixture of TlSn_9^{3-} and TlSn_8^{3-} was characterized by single-crystal X-ray diffraction.^[86] However, only one diamagnetic cluster was observed in the solution, and it was proposed as TlSn_8^{5-} , which is also highly fluxional showing a single time-averaged ^{119}Sn resonance with distinct coupling to a Tl atom and pronounced Sn satellites as well.^[140]

The solution dynamics of transition metal derivatives of the group 14 Zintl ions have also been shown in detailed studies. These studies also give insights about the rigidity of the polyhedron structure ranging from static ions to highly dynamic structures in solution. The $\eta^4\text{-Sn}_9\text{Ir}(\text{cod})^{3-}$ ion has a single ^{119}Sn resonance indicative of fast global exchange of all 9 Sn atoms at room temperature.^[121] In contrast, isostructural $\eta^4\text{-E}_9\text{M}(\text{CO})_3^{4-}$ ions (M= Cr, Mo, W) are the only E_9 clusters with diminished fluxionality at room temperature.^[98, 110]

In most of the solution studies, the interstitial Sn clusters, centered with a transition metal atom, have been shown to be highly fluxional in solution. The Cu@Sn_9^{3-} , and $\text{Pt@Sn}_9\text{H}^{3-}$ ions are highly fluxional with a single ^{119}Sn resonance in solution.^[115, 116] In the latter ion, the exchange mechanism also involves a facile mobility of the proton ligand beside a fast exchange of the cluster vertices. The $\text{Pt@Sn}_9\text{Pt}(\text{PPh}_3)^{2-}$ ion, has unusual dynamic properties displaying a “static” Pt-Pt- PPh_3 unit inserted into a highly dynamic Sn_9^{2-} cage.^[117]

The large deltahedral clusters $\text{Pt}_2@\text{Sn}_{17}^{4-}$ and $\text{Ni}_2@\text{Sn}_{17}^{4-}$ have also been shown to be fluxional.^[115, 128] The $\text{Ni}_2@\text{Sn}_{17}^{4-}$ ion is the only example, whose limiting ^{119}Sn NMR spectrum can be achieved at lower temperatures, whereas the other examples such as $\text{Pt}@\text{Sn}_9\text{Pt}(\text{PPh}_3)^{2-}$ ion shows gradual broadening of the ^{119}Sn signal at lower temperatures up to -70°C .^[117]

1.5. Overview of the Thesis

In the following chapters of this thesis, the synthesis and characterization of new clusters derived from Sn_9^{4-} ion and their reactivity with group 10 and group 6 transition metal complexes will be presented. The unique stepwise reactions, structural properties of the resulting clusters and their solution dynamics are discussed.

Chapter 2 presents the true nature of the Sn_9H^{3-} ion and a facile synthesis of $\text{Sn}_9\text{-Sn}_9^{6-}$ dimer. The synthesis and solution behavior of the three new substituted Sn_9R^{3-} ($\text{R} = \text{}^i\text{Pr}, \text{SnCy}_3, \text{SnBu}_3$) ions are discussed in Chapter 3. Following that, Chapter 4 focuses on the reactivity of these substituted clusters Sn_9R^{3-} ($\text{R} = \text{H}, \text{SnCy}_3$) with group 10 transition metals. In Chapter 5, stepwise synthesis of two new ternary Zintl ions, $\text{Ni}@\text{Sn}_9\text{M}(\text{CO})_3^{4-}$ ($\text{M} = \text{Cr}, \text{Mo}$), will be discussed. Finally, in Chapter 6, the synthesis of two new members of the fused deltahedral clusters, $\text{Pd}_2@\text{Sn}_{18}^{4-}$ and $\text{Ni}@\text{Sn}_8(\mu\text{-Ge})\text{Ni}@\text{Sn}_8^{4-}$ will be presented with their structural and solution dynamics. This chapter also discusses intermolecular exchange mechanism in solution dynamics.

Chapter 2: The Sn_9H^{3-} ion and $\text{Sn}_9\text{-Sn}_9^{6-}$ dimer

2.1. Introduction

The organotin hydrides e.g. HSnBu_3 have been known for a long time for their applications in organic synthesis, such as hydrogenation of alkyl halides.^[141] Recent discoveries showed that low valent group 14 hydrides, $[\text{Ar}^*\text{Sn}(\mu\text{-H})_2]$, can be stabilized by bulky aryl ligands ($\text{Ar}^* = \text{C}_6\text{H}_3\text{-2,6-(C}_6\text{H}_2\text{-2,4,6-}^i\text{Pr}_3)_2$).^[142] Moreover, these low valent group 14 hydrides have been used as one of the synthetic methods of obtaining metalloids clusters such as Sn_9Ar^*_3 ($\text{Ar}^* = \text{C}_6\text{H}_3\text{-2,6-(C}_6\text{H}_2\text{-2,4,6-}^i\text{Pr}_3)_2$).^[83] Although the synthetic approaches are different, these substituted metalloids clusters are now considered to be part of the class of substituted Zintl ions in their structural similarities.

Zintl phase hydrides, which are also known as interstitial hydrides, are intermetallic phases of alkali metal p-block binaries with hydrogen atoms as intercalated groups (e.g. Ca_3SnH_2) or with hydrogen ligands bound as terminating ligands to the p-block polyanions (e.g. SrAlSiH).^[143] The potential applications of these hydrogenous Zintl phases are unexplored.

As molecular cluster ions, group 15 Zintl ions of hydrido clusters have been extensively studied.^[144-149] Several studies demonstrated that proton substitution reactions on clusters, e.g. on the P_7^{3-} and As_7^{3-} ions, are similar with the other substituted RE_7^{2-} ($\text{R} = \text{Me}, ^i\text{Pr}$ etc.) derivatives.^[73, 75, 150, 151] Alkyl and post transition metal group substituted Ge and Sn clusters have also been reported.^[58, 78, 79, 152]

However, none of these studies considered hydride substitution on group 14 E_9^{4-} (E= Si, Ge, Sn, Pb) Zintl ions.

The Sn_9^{4-} ion with C_{4v} symmetry has been isolated in three dimensional salt structures of $Na_4(6-8en)Sn_9$ and $Li(NH_3)_4Sn_9 \cdot NH_3$.^[153, 154] Later, sequestering agents such as 2,2,2-crypt and 18-crown-6 have been used for better crystallization. The $[Na(2,2,2-crypt)]_4Sn_9$ salt is the only example of -4 charged cluster of group 14, where the Na^+ ions are fully sequestered by 2,2,2-crypt.^[49] The nonastannide structure is close to the idealized C_{4v} symmetry.

Strong-ion pairing of E_9^{4-} (E= Sn, Pb) and alkali metals have been observed in NMR studies.^[140] Less-encapsulating 18-crown-6 sequestering agent does not fully prevent alkali-metal coordination, and in the $[K(18-crown-6)]_4Sn_9 \cdot en$ structure Sn_9^{4-} ion has coordination to two $(K-18-crown-6)^+$ ions.^[32] According to conventional wisdom, 4 equivalents of 2,2,2-crypt in a solution of dissolved melts of nominal composition K_4Sn_9 has been thought to fully sequester the K^+ ions to form $(K(2,2,2-crypt))^+$ ions.

On the other hand, using 4 equivalents of 2,2,2-crypt in a solution of melts of nominal composition of K_4Sn_9 results in isolation of Sn_9H^{3-} ion, which has been reported to be a paramagnetic Sn_9^{3-} ion in numerous studies.^[45, 52, 155] The paramagnetism of the Sn_9^{3-} clusters has been explained in the existing hypothesis by an equilibrium process between the Sn_9^{4-} , Sn_9^{3-} and Sn_9^{2-} clusters and the solvated electrons.^[4, 136] The EPR signal lacks hyperfine splitting and was obtained from the $[K(2,2,2-crypt)]_6[Sn_9]_2$ crystalline sample at room temperature and was reported as weakly paramagnetic ion.^[52] The EPR signal of Sn_9^{3-} ion show even a weaker

paramagnetism in dmf solution, no EPR signal for the Pb_9^{3-} ion has been reported in solution. Thus, the Sn_9^{3-} ion together with the Ge_9^{3-} , Pb_9^{3-} , Si_9^{3-} ions have been widely accepted as a paramagnetic clusters in about 35 publications since the first proposal in 1983. However, as it will be discussed in this chapter, our studies clarify that it is a hydride substituted cluster analogous to the other Sn_9R^{3-} clusters (R= alkyl, post transition metal group).^[81, 152]

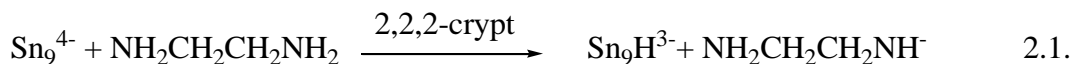
Recently, oxidatively coupled clusters of the dimer, trimer and tetramer $(\text{Ge}_9)_n^{m-}$ clusters, where $n= 2, 3, 4$ and $m= 6, 6, 8$ respectively, have been obtained by different synthetic methods.^[61-63, 65] Increasing the Ge_9^{4-} concentration in the solution in the presence of 2,2,2-crypt gave a $\text{Ge}_9\text{-Ge}_9^{6-}$ dimer.^[61] Using AsPh_3 or PPh_3 as oxidizing agents resulted in a trimer $\text{Ge}_9=\text{Ge}_9=\text{Ge}_9^{8-}$ ion.^[62] To date, the only example Sn analog of the coupled clusters is the $\mu\text{-Ag}(\text{Sn}_9)_2^{5-}$ ion, where the Ag^+ ion is coordinated to the dimer cluster.^[72] The existence of the coupled clusters has also been cited as support that the E_9^{3-} clusters (E= Si, Ge, Sn, Pb) are paramagnetic ions, which are proposed to form from the coupling the two E_9^{3-} radicals.^[3, 4] However, isolation of the stable E_9^{3-} radicals and the oxidative coupling process have not been fully explained.

In this study, we describe the nature of the isolated Sn_9^{3-} ion to be a protonated Sn_9H^{3-} cluster by extensive NMR studies. Furthermore, the existence of equilibrium between KSn_9^{3-} and Sn_9H^{3-} ions will be discussed. Finally, the proposed $\text{Sn}_9\text{-Sn}_9^{6-}$ dimer is characterized in the solution, and a generic synthetic method is proposed to obtain the coupled clusters.

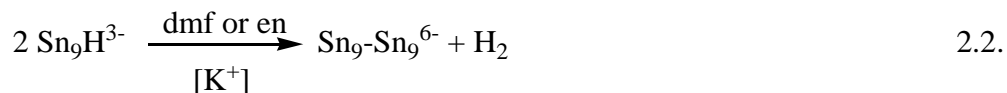
2.2. Results and Discussion

2.2.1. Synthesis

Melts of nominal composition of K_4Sn_9 and 4 equivalents of 2,2,2-crypt dissolved in ethylenediamine (en) solution give the Sn_9H^{3-} cluster anion according to eq. 2.1, and have been isolated in 60% crystalline yield as $[\text{K}(2,2,2\text{-crypt})]^+$ salts. The air and moisture sensitive black-red crystals have been characterized by single crystal XRD, ^1H and ^{119}Sn NMR spectroscopy. When the crystalline samples are dissolved in en and dimethylformamide (dmf) solvents, they give a characteristic green color to the solutions, and slowly decompose at temperatures higher than 60 °C.



The dmf solutions prepared from dissolving crystals of $[\text{K}(2,2,2\text{-crypt})]_3[\text{Sn}_9\text{H}]$ react with KCl or CsCl to give a red colored solution (eq. 2.2). The resulting cluster species is tentatively assigned as an oxidatively coupled $\text{Sn}_9\text{-Sn}_9^{6-}$ cluster on the basis of NMR analysis (see below). Alternatively, Sn_9H^{3-} ions in ethylenediamine solution, which was neutralized by adding NH_4Cl , react with KCl resulting in the $\text{Sn}_9\text{-Sn}_9^{6-}$ dimer.



The proposed equation (eq.2.2) for the conversion of Sn_9H^{3-} to the oxidatively coupled $\text{Sn}_9\text{-Sn}_9^{6-}$ dimer catalyzed by K^+ , involves a two net electron oxidation and elimination of H_2 gas. Although crystalline salts of the $\text{Sn}_9\text{-Sn}_9^{6-}$ have not been, the $\text{Sn}_9\text{-Sn}_9^{6-}$ ion has been characterized by ^{119}Sn NMR spectroscopy.

2.2.2. Solid State Structure

Reported solid state structures for the Sn_9^{3-} ion (Sn_9H^{3-} , see below) are given in the Table 2.1. The triclinic structure, P-1, contains a non-interacting Sn_9^{3-} anion and 3 $[\text{K}(2,2,2\text{-crypt})]^+$ cations in the unit cell.^[45, 47, 48] They can also crystallize in monoclinic space group, $P2_1/c$, with two non-interacting Sn_9^{3-} anions and 6 $[\text{K}(2,2,2\text{-crypt})]^+$ cations.^[155] Moreover, these structures have crystallographic modifications depending on the number of solvent molecules in the lattice. The triclinic structure with one Sn_9^{3-} ion per cell is more crystallographically ordered compared to that of the monoclinic structure.

Table 2.1. Different polymorph structures of the reported Sn_9^{3-} ions and Sn_9H^{3-} ion.

Structure	Space group	h/e	d_2/d_1	ref
$[\text{K}(2,2,2\text{-crypt})]_3[\text{Sn}_9]\text{en}_{1.5}$	Triclinic	1.08	1.45	[45]
$[\text{K}(2,2,2\text{-crypt})]_3[\text{Sn}_9]\text{en}_{0.5}$	Triclinic	1.07	1.32	[47, 48]
$[\text{K}(2,2,2\text{-crypt})]_6[\text{Sn}_9]_2\text{en}_{1.5}\text{tol}_{0.5}$	Monoclinic	1.08	1.34	[155]
$[\text{K}(2,2,2\text{-crypt})]_3[\text{Sn}_9\text{H}]\text{en}_{0.5}$	Triclinic	1.07	1.46	This work

We have also obtained two different polymorphs with similar unit cell parameters for the Sn_9H^{3-} ions. As the triclinic structure of the Sn_9H^{3-} anion is crystallographically ordered, structural analysis of the $[\text{K}(2,2,2\text{-crypt})][\text{Sn}_9\text{H}]\text{-en}_{0.5}$ crystals of triclinic unit cell, P-1, will be explained in detail.

The distortion from an idealized monocapped square antiprism of C_{4v} symmetric Sn_9^{4-} anion towards tricapped trigonal prism and D_{3h} symmetry can be represented by the deviation of the diagonal ratio from the ideal value (Table 2.1). For an ideal C_{4v} geometry of Sn_9^{4-} , the ratio of the diagonals on the open square face is 1.^[49] The tricapped trigonal prism is defined by the smallest ratio of average prism height (h) divided by average prism edge (e) among three virtual trigonal prisms in

the distorted Sn_9H^{3-} structure.^[156] The dihedral angle between the two planes defined by Sn1-4-3 and Sn1-2-3 atoms (Figure 2.1) on the open square is another indication of the deviation from an idealized C_{4v} symmetry. This torsion angle for the reported structures of the Sn_9H^{3-} ions varies between 7° - 17° . For comparison, the dihedral angles for the idealized C_{4v} symmetric $[\text{Na}(2,2,2\text{-crypt})]_4[\text{Sn}_9]$ and $\eta^4\text{-Sn}_9\text{Cr}(\text{CO})_3^{4-}$ are 3° and 0° , respectively.^[43, 94]

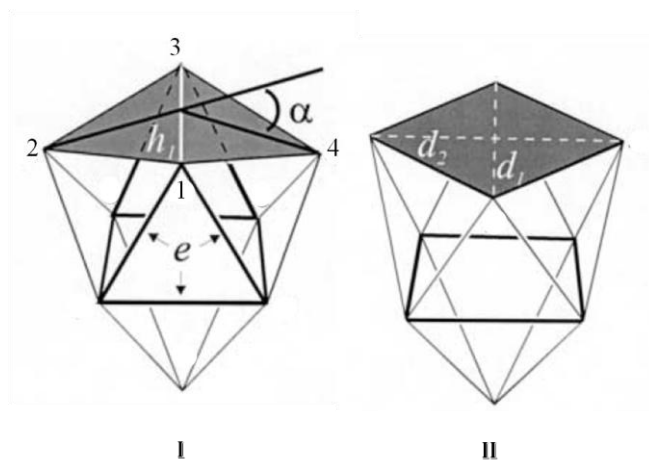


Figure 2.1. The structures of Sn_9^{n} ; tricapped trigonal prism (D_{3h}) and monocapped square anti prism (C_{4v}). Figure adapted from ref. [156]

Our structure of the Sn_9H^{3-} ion shown in Figure 2.2 is also a distorted tricapped trigonal prism. The structure of Sn_9H^{3-} is a 9-vertex *nido* structure with an *exo*-substituted hydride atom. The virtual symmetry for the Sn_9 cluster framework is C_{2v} . A two-fold rotation axis passes through Sn9 and intersects the contact of Sn1-3. Because the hydrogen atom could not be located crystallographically, minimized DFT structures were calculated by Prof. Andrei Vedernikov with several different starting points for the hydrogen atom location. In all cases, the structure converged to that shown in Figure 2.2 c in which the Sn_9 core and the position of the *exo* hydrogen atom are virtually identical to that of the Sn_9R^{3-} ($\text{R} = \text{}^t\text{Bu}, \text{}^i\text{Pr}, \text{SnCy}_3$) ions.^[81, 152]

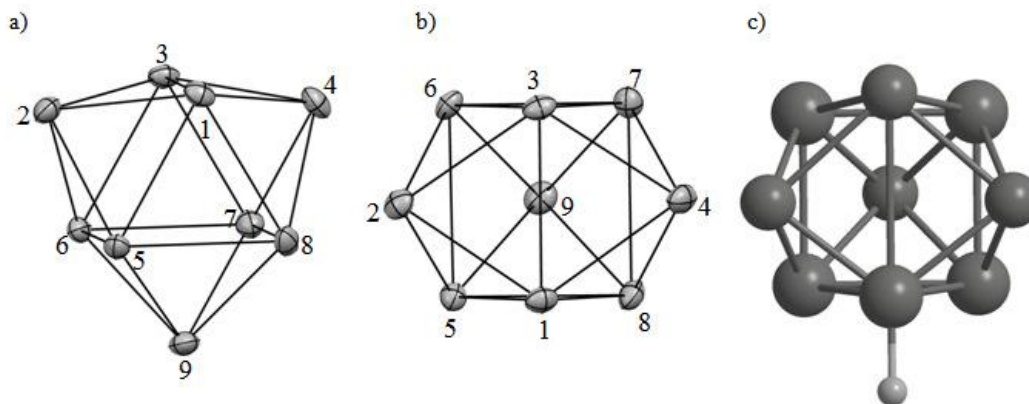


Figure 2.2. ORTEP drawing of the structure of the Sn_9H^{3-} in a), top view in b), and c) DFT energy minimized structure.

The bond lengths of the Sn_9H^{3-} are given in Table 2.2. The idealized D_{3h} tricapped trigonal prism has 21 edges and is used as a reference for evaluating the structural metric parameters. The Sn_9H^{3-} cluster ion has Sn-Sn contacts in a range between 2.951 (4) - 3.302 (4) Å (avg 3.035 ± 0.120 Å), which is consistent with the known Sn_9H^{3-} ions ($(\text{Sn-Sn})_{\text{avg}} = 3.027 \pm 0.125$ Å and 3.041 ± 0.146 Å).^[45, 157] The idealized C_{4v} symmetric Sn_9^{4-} has an average $d(\text{Sn-Sn})_{\text{avg}} = 3.075 \pm 0.274$ Å for these 21 Sn-Sn contacts.^[49] Thus, a hydride substituent does not significantly affect the Sn-Sn bond distances, and are similar within a ± 0.1 Å estimated standard deviation.

However, the *exo*-bonding reduces one of the diagonal distances on the open-square relative to the idealized C_{4v} symmetry of Sn_9^{4-} . This distance for the Sn_9H^{3-} structure is Sn1-3 = 3.302 (4) Å in consistency with the reported Sn_9H^{3-} structure (3.315 Å).^[45] As a result of this contraction in the open-square, the diagonal ratio in the Sn_9H^{3-} ion is 1.47 (Sn1-Sn3/Sn2-Sn4 refer to Figure 2.2) in consistency with the reported structures (Table 2.1). This observation is also valid for the other substituted clusters Sn_9R^{3-} which also distort towards D_{3h} symmetry. These distances in the other

substituted clusters are 3.780 Å for R= ^tBu, 3.810 Å for R= ⁱPr, and 3.652 Å for R= SnCy₃ resulting in the diagonal ratio of 1.18, 1.17, and 1.26, respectively.^[81, 152]

Table 2.2. Selected bond lengths (Å) for the Sn₉H³⁻ ion.

Atoms	Distances	Atoms	Distances
Sn1-2	2.962(5)	Sn4-7	2.939(4)
Sn1-3	3.302(4)	Sn4-8	2.951(4)
Sn1-4	2.987(5)	Sn5-6	3.288(4)
Sn1-5	3.062(5)	Sn5-8	3.054(4)
Sn1-8	3.067(4)	Sn5-9	2.945(4)
Sn2-3	2.949(5)	Sn6-7	3.071(4)
Sn2-5	2.960(4)	Sn6-9	2.952(4)
Sn2-6	2.965(4)	Sn7-8	3.301(4)
Sn3-6	3.086(5)	Sn7-9	2.952(4)
Sn3-7	3.065(4)	Sn8-9	2.968(4)

The contraction of the Sn1-3 bond relative to the C_{4v} symmetric Sn₉⁴⁻ ion is a common effect of substituent groups. On the other hand, the orientation of the substituent group relative to the open square in Sn₉R³⁻ differs for various substituents. Such clusters with R= ⁱPr and SnCy₃ will be discussed in Chapter 3. The measured Sn3-Sn1-H angle from minimized DFT structure of Sn₉H³⁻ ion is 173°, which is between the angles of Sn₉R³⁻ (161° R= ^tBu and 162° for R= ⁱPr) and Sn₉SnCy₃³⁻ (197°) ions.^[81, 152]

The Sn₉H³⁻ cluster is a 9-vertex 22e⁻ *nido* cluster as expected from a Wade-Mingos analysis. In this analysis, each vertex Sn atom contributes 2 electrons, and 1 additional electron contribution comes from the hydride ligand. The sum of all contributions and three electrons from the -3 charge gives 22 electrons, corresponding

to a $2n+4$ ($n= 9$) *nido* cluster. It is isoelectronic with the known substituted Ge_9R^{3-} and Sn_9R^{3-} clusters.^[78, 81, 158, 159]

Although the $\text{Sn}_9\text{-Sn}_9^{6-}$ ion could not be isolated in solid state, it was characterized by ^{119}Sn NMR spectroscopy. Therefore, based on the solution studies of the $\text{Sn}_9\text{-Sn}_9^{6-}$ coupled ion, the structure of the clusters is proposed to be similar to the dimer of the germanium analog (Figure 2.3). In the reported structures of the $\text{Ge}_9\text{-Ge}_9^{6-}$ ion, two cluster units are connected with an *exo*-bond on the non-capped square of the two monocapped trigonal prisms in a *trans* orientation. On the other hand, in the reported $\mu\text{-Ag}(\text{Sn}_9\text{Sn}_9)^{5-}$ ion the two cluster units align in a *cis* orientation due to a bridging Ag^+ ion.^[61, 72]

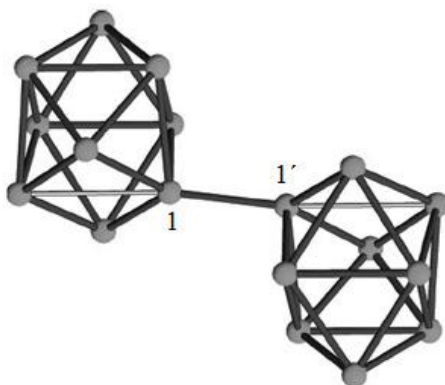


Figure 2.3. Proposed structure of the $\text{Sn}_9\text{-Sn}_9^{6-}$ ion. Figure adapted from ref. [4]

The overall cluster bonding electron count for the $\text{Sn}_9\text{-Sn}_9^{6-}$ dimer is $42 e^-$. However, each half of dimer can be viewed as a $22 e^-$ cluster considering $1 e^-$ contribution from an *exo*-substituent. Thus, they represent $22e^-$ *nido* clusters ($2n+4$) in a Wade-Mingos analysis that are bound to each other through an *exo*-bond.

2.2.3. NMR Spectroscopic Studies

The NMR spectroscopic data of Sn_9H^{3-} were taken from the dissolved crystalline sample in en solutions. The spectrum has a single resonance at -1271 ppm with a coupling constant of $J(^{119}\text{Sn}-^{117}\text{Sn})= 398$ Hz (Figure 2.4a). In addition, it also has $J(^{119}\text{Sn}-^1\text{H})$ coupling of 21 Hz. The ^{119}Sn spectrum decoupled to ^1H is shown in Figure 2.4b. The ^1H NMR signal is at 6.1 ppm with a coupling constant of $J(^{119}\text{Sn}-^1\text{H})= 21$ Hz (Figure 2.4c). For comparison the ^1H resonance of the P_7H^{2-} ion is at 7.2 ppm.^[149]

The ^{117}Sn satellites on the ^{119}Sn signal at -1270 ppm, with integrated intensity ratios of 0.04 : 0.31 : 1.0 : 0.31 : 0.04, arise from coupling to the 9-equivalent Sn atoms. The proton resonance at 6.1 ppm is a seven-line multiplet in a ratio of 0.04: 0.24 : 0.65 : 1.0 : 0.65 : 0.25 : 0.04 and is consistent with the calculated multiplet intensity ratios 0.22 : 0.64 : 1.0 : 0.64 : 0.22, which indicates coupling to 9-equivalent Sn atoms.

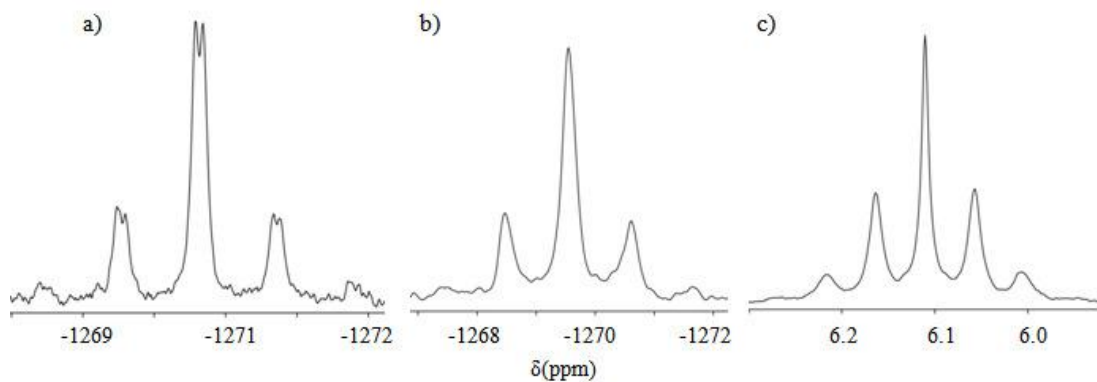


Figure 2.4. NMR spectra of the Sn_9H^{3-} taken from the crystalline sample in en at room temperature at 186 MHz and 400 MHz operating frequencies for the ^{119}Sn and ^1H spectra, respectively. a) ^{119}Sn , b) $^{119}\text{Sn}^{[160]}$, and c) ^1H NMR.

The presence of ^{117}Sn satellites on the ^{119}Sn resonance and the mutual couplings of the ^1H - ^{119}Sn indicate an intramolecular exchange mechanism. Moreover, the data suggest that the hydride is scrambling around the cluster, while the Sn vertices of the cluster are in fast exchange on the NMR time scale. A similar mechanism is also proposed for the $\text{Sn}_9\text{SnCy}_3^{3-}$ ion in Chapter 3.

As discussed in Chapter 3, a scrambling group on the clusters does not affect the square-diamond-square transformation of the Sn_9 cluster core,^[136] and results in a large coupling constant of ^{119}Sn - ^{117}Sn for a fluxional cluster. The intra-vertex ^{119}Sn - ^{117}Sn coupling constant of Sn_9H^{3-} (398 Hz) has a larger magnitude than the 263 Hz coupling constant of the Sn_9^{4-} ion, suggesting shorter interatomic distances for the Sn_9H^{3-} ion considering a positive value for the J coupling for these clusters.

The Sn-H coupling constant of the Sn_9H^{3-} ion is very small compared to the organotin hydride molecules having typical values of 2000 Hz.^[161] A possible reason for this small coupling constant $J(^1\text{H}$ - $^{119}\text{Sn})=21$ Hz is that the Sn-H interactions are averaged over 9-equivalent Sn atoms due to the mobility of the hydride ligand. Recently, Sn-Sn compounds with bridged hydrides have been reported by Power et al. Similar to our study, they reported a small Sn-H coupling constant for these compounds (89 Hz).^[162]

The ^{119}Sn NMR spectrum of $\text{Sn}_9\text{-Sn}_9^{6-}$ ion taken at room temperature in dmf solution is shown in Figure 2.5. The ^{119}Sn NMR spectrum has two resonance signals at -1386 ppm and -3 ppm with an approximate intensity ratio of 8:1.

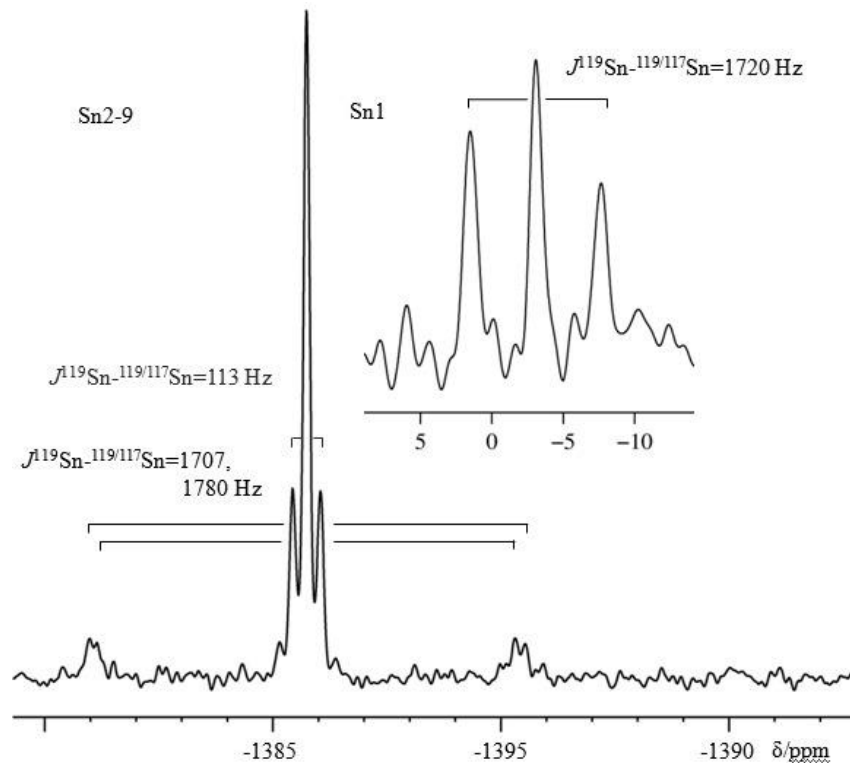


Figure 2.5. ^{119}Sn NMR spectrum of the $\text{Sn}_9\text{-Sn}_9^{6-}$ anion taken from the reaction mixture of Sn_9H^{3-} and CsCl in dmf at room temperature and 186 MHz. The signal at -1386 ppm is assigned to the cluster atoms of Sn2-9 of each cluster. The signal at -3 ppm (inset) is assigned to the *exo*-bonded Sn atoms (Sn1 and Sn1'). For the numbering scheme see the Figure 2.3.

The upfield signal (-1386 ppm) couples to the other signal at -3 ppm with coupling constants of $J(^{119}\text{Sn}-^{117}\text{Sn}) = 1707 \text{ Hz}$ and $J(^{119}\text{Sn}-^{119}\text{Sn}) = 1780 \text{ Hz}$. The intensity ratio (0.84:0.16) due to this coupling pattern signal indicates that the ratio of magnetically inequivalent Sn atoms is 8:1. This signal has a smaller coupling constant of $J(^{119}\text{Sn}-^{117}\text{Sn}) = 113 \text{ Hz}$, due to 8 magnetically equivalent Sn atoms. The ^{119}Sn signal at -3 ppm also has an average of 1720 Hz ($^{119}\text{Sn}-^{117/119}\text{Sn}$) coupling due to the upfield signal.

The chemical shifts and J couplings of resonances are very similar to the substituted Sn_9R^{3-} type clusters, where R is an alkyl group. The multiplet pattern of

the signal at -3 ppm is consistent with a calculated pattern of 1 Sn atom coupling to 8 magnetically equivalent Sn atoms (0.18 : 0.60 : 1.0 : 0.60 : 0.18). The multiplet pattern of the signal at -1385 ppm is also consistent with a calculated pattern of 8 magnetically equivalent Sn atoms (0.03 : 0.28 : 1.0 : 0.28 : 0.03). Similar signals were also obtained by using Cs⁺ cation and no discernable changes were observed in chemical shift and coupling constants. As a result of the existence of the ion in both en and dmf solutions and slight changes of the signals with different counter cations, the compound is proposed to be a coupled cluster of Sn₉-Sn₉⁶⁻.

The presence of the *J* couplings shows that the exchange mechanism is intramolecular. Furthermore, the signals corresponding to Sn1 and Sn2-9 in 1:8 ratio suggest that, two Sn atoms bound together are not involved in the exchange with the remaining 8 atoms of each cluster, while the 8 remaining Sn atoms of the cluster units on both side are in fast exchange on the NMR time scale. This observation is similar to the exchange mechanism of Sn₉-alkyl³⁻ which will be discussed in Chapter 3. Furthermore, a small coupling constant for the fast exchanging cluster units is also recorded for the Sn₉-alkyl³⁻ anions. Therefore, this type of exchange mechanism also supports the structure of Sn₉-Sn₉⁶⁻ to be an *exo*-bonded cluster.

2.2.4. Acid-base Chemistry and Alkali Metal Sequestering

Intermetallic melts of nominal composition K₄Sn₉ dissolve congruently in en solvents to give solutions of K_xSn₉^{(4-x)-} ions where x = 0, 1, 2, 3 according to eq. 2.3. Ion pairing between alkali ions and the E₉⁴⁻ ions has been well established through the ¹¹⁹Sn NMR experiments of Rudolph and co-workers.^[140] Their studies revealed that the A_xSn₉^{(4-x)-} ions (A = Na, K, Rb, Cs) give rise to single, time-averaged ¹¹⁹Sn NMR

chemical shifts that have significant alkali ion dependence due to strong ion pairing. For example the time averaged ^{119}Sn NMR chemical shifts of A_4Sn_9 salts span 108 ppm from $\delta = -1223$ ppm (Na_4Sn_9) to -1115 ppm (Cs_4Sn_9).^[140] Because the Sn_9^{4-} ion has a very large affinity for binding to alkali ions, equation 2.3 is shifted significantly to the left to give a preponderance of K_3Sn_9^- and solvated K^+ ions as the major constituent in solution.



In the presence of 2,2,2-crypt, the solution turns into darker red and become more viscous. The ^{119}Sn chemical shifts and coupling constants for the time averaged signal, after addition of 4 equivalents of 2,2,2-crypt in various solvents are given in Table 2.3. The resonance signal shifts upfield and broadens with encapsulation of K^+ cations with 2,2,2-crypt. Earlier studies attributed this broadening to the paramagnetic impurities in the solution.^[45] However, our study shows that this is the result of two competing equilibria as discussed below.

Table 2.3. ^{119}Sn NMR data of $\text{K}_x\text{Sn}_9^{(4-x)-}$ recorded at room temperature.

Cluster	Solvent	$\delta^{119}\text{Sn}$ (ppm)	$J(^{119}\text{Sn}-^{117}\text{Sn})$ (Hz)
K_3Sn_9^-	en	-1208	263
	dmf	-1146	303
	^a py-d ₅	---	---
KSn_9^{3-}	en	-1237	$\nu_{1/2}$; 605 Hz
	dmf	-1151	316
	py-d ₅	-1157	$\nu_{1/2}$; 1143 Hz

^aMelts of nominal composition K_4Sn_9 has a limited solubility in pyridine (py).

The melt of nominal composition K_4Sn_9 dissolved in en solutions was titrated with 2,2,2-crypt as shown in Figure 2.6. As the molar ratio of the 2,2,2-crypt

increases, the resonance of the $K_xSn_9^{(4-x)-}$ gradually shifts from -1208 ppm to -1236 ppm with an exception of the first molar ratio of 2,2,2-crypt (Figure 2.6 A). The 1H spectrum of uncomplexed 2,2,2-crypt has one singlet and two triplet resonance signals, however, one of the triplet signals is obscured by the en signal.

The change in $\delta^{119}Sn$ chemical shift is graphically shown in the inset of the Figure 2.6 A. The addition of 1 equivalent 2,2,2-crypt causes a slight 2 ppm downfield shift of the ^{119}Sn NMR signal for $K_xSn_9^{(4-x)-}$ with a corresponding downfield shift of 1H NMR resonances of 2,2,2-crypt (Figure 2.6). These data suggest that one equivalent of K^+ has been complexed by 2,2,2-crypt to give a solution of $[K(2,2,2-crypt)]^+ / K_3Sn_9^-$ that displays a ^{119}Sn NMR chemical shift very similar to that of the parent of $[K(en)_x]^+ / K_3Sn_9^-$ solution.

The addition of 2 to 3 equivalent 2,2,2 crypt monotonically shifts the resonance upfield with the removal of ion-pair interactions. Addition of the 4 to 8 equivalents of 2,2,2-crypt does not affect the chemical shift, however it causes broadening of the signal at the limiting chemical shift of -1237 ppm. $Rb_xSn_9^{(4-x)-}$ solutions also show similar trends of the ^{119}Sn chemical shifts from -1185 ppm to a limiting ^{119}Sn NMR chemical shift of -1232 ppm with after 3 equivalents of 2,2,2-crypt. However, the limiting chemical shift for $K_xSn_9^{(4-x)-}$ and $Rb_xSn_9^{(4-x)-}$ do not coincide at the same value, which suggests there are still an ion-pair interactions between cluster ion and alkali metals. The $A(2,2,2-crypt)^+$ signals show that 1H signals shift (Figure 2.6B) back toward uncomplexed 2,2,2-crypt and broaden with addition of 3 or more equivalents of 2,2,2-crypt to the solutions of K_4Sn_9 and Rb_4Sn_9 .

These data suggest that the prominent $K_xSn_9^{(4-x)-}$ species in equation 2.3 is KSn_9^{3-} when 3 or more equiv. of 2,2,2-crypt are present.

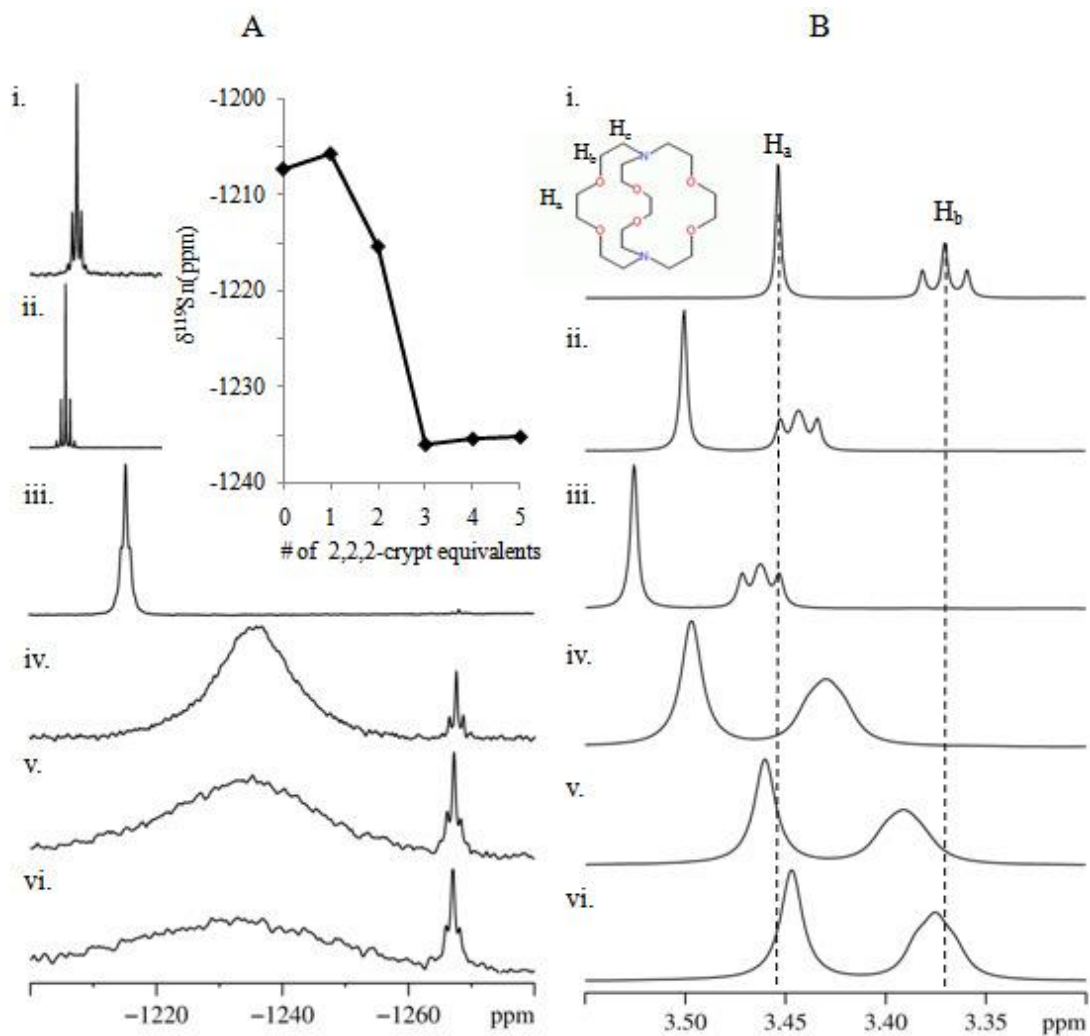
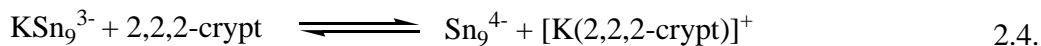


Figure 2.6. ^{119}Sn and ^1H NMR spectra for the titration of the ethylenediamine solution of $K_4\text{Sn}_9$ with molar equivalents of 2,2,2-crypt. A) ^{119}Sn NMR with increasing number of equivalents of 2,2,2-crypt; i) no 2,2,2-crypt, ii) 1 equiv., iii) 2 equiv. iv) 3 eq., v) 4 equiv., vi) 5 equiv., and the inset (upper right) graphically shows the change in $\delta^{119}\text{Sn}$ (ppm) with addition of 2,2,2-crypt equivalents. B) ^1H NMR spectra of 2,2,2-crypt in (i) and $[\text{K}-2,2,2\text{-crypt}]^+$ resonances with increasing molar equivalents of 2,2,2-crypt; ii) 1 equiv., iii) 2 equiv. iv) 3 equiv., v) 4 equiv., vi) 5 equiv., and inset (on the upper left) is the structure of the 2,2,2-crypt.

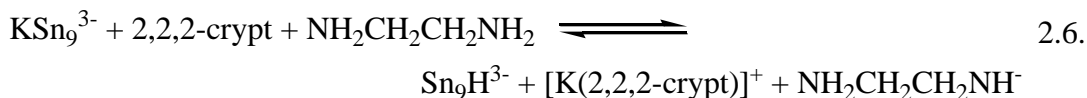
Besides the decrease in ion-pairing with increasing 2,2,2-crypt, a new signal grows in at -1268 ppm as shown in Figure 2.6A, which is due to the Sn_9H^{3-} ion with a $J(^1\text{H}-^{119}\text{Sn}) = 21$ Hz coupling constant. The simplified equilibrium relationship between these species is shown in equations 2.4 and 2.5.



Further solution studies showed that addition of NH_4Cl salt to the solution in the presence of excess 2,2,2-crypt causes the resonance of KSn_9^{3-} to broaden into baseline, and it also enhances the signal intensity of the Sn_9H^{3-} ion. The solution color also turns into the characteristic green color of the Sn_9H^{3-} solutions after addition of the NH_4Cl salt. On the contrary, addition of the KCl or K^tBuO salts retrieves the K_3Sn_9^- signal; and the Sn_9H^{3-} ions convert into K_3Sn_9^- ions. The CsCl and NaCl salts also have similar effects on the spectrum, but form ion-pairing with the mixed alkali metals $\text{Cs}_{2-x}\text{K}_x\text{Sn}_9^-$ and $\text{Na}_x\text{K}_{2-x}\text{Sn}_9^-$ ions with $\delta^{119}\text{Sn}$ chemical shift at -1141 ppm and -1212 ppm, respectively.

The solution studies with 2,2,2-crypt sequestering agents show the *in-situ* formation of the Sn_9H^{3-} anion by sequestering of the K^+ ion, suggesting that Sn_9^{4-} is a stronger base than the $\text{NH}_2\text{CH}_2\text{CH}_2\text{NH}^-$. However, due to two competing equilibria, both KSn_9^{3-} and Sn_9H^{3-} ions are present in ethylenediamine solvent, even with excess 2,2,2-crypt. Although an exact binding constant cannot be calculated due to the competing equilibrium, the observations suggest that Sn_9^{4-} has a K^+ binding constant greater than or equal to that of 2,2,2-crypt in en. The overall equilibrium is

summarized in eq. 2.6, where KSn_9^{3-} and Sn_9H^{3-} ions are in equilibrium in the presence of the $\text{NH}_2\text{CH}_2\text{CH}_2\text{NH}^-$ in ethylenediamine solvent.

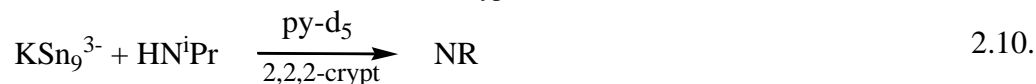
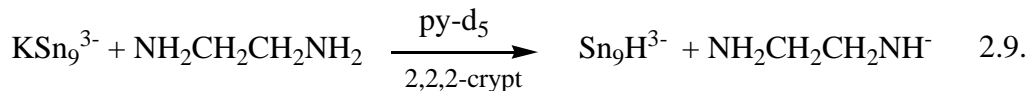


While Sn_9H^{3-} is the minor component in the equilibrium mixture with 4 equiv. 2,2,2-crypt ($\text{Sn}_9\text{H}^{3-} / \text{KSn}_9^{3-} = 1:10$ by NMR integration ratio), it crystallizes as the $[\text{K}(2,2,2\text{-crypt})]^+$ salt in high yields due to its lower solubility relative to the other species in solution and its continual replenishment due to a Le Châtelier type equilibrium shift.

Although ^1H and ^{119}Sn signals of the Sn_9H^{3-} ion are present in the en solution, dmf and pyridine solutions prepared from crystalline samples of $[\text{K}(2,2,2\text{-crypt})]_3\text{Sn}_9\text{H}$ do not show a ^{119}Sn NMR signal, even at low temperatures. It is possible that the acid/base and dynamic exchange processes may be fast on the NMR time scale in these solvents, which, in combination with eq. 2.4, broadens the ^{119}Sn NMR signals beyond detection. On the other hand, the outcome of protonation/deprotonation experiments confirm the presence of Sn_9H^{3-} ion in these solutions.

For the experiments in dmf solutions crystalline Sn_9H^{3-} samples were used. These studies showed that excess amount of K^tBuO can convert Sn_9H^{3-} ions into ion paired clusters, K_3Sn_9^- (eq. 2.7). However, the conversion to K_3Sn_9^- did not take place with $[\text{K}(2,2,2\text{-crypt})][^t\text{BuO}]$ (eq. 2.8). This also shows that the acidity of Sn_9H^{3-} ions increases in the presence of coordinating alkali metals. This is a well known

phenomenon, where coordinating alkali metals decrease the pK_a of weak organic acids.^[163]



The studies in pyridine showed that the signal of KSn_9^- at -1155 ppm disappears by addition of ethylenediamine (eq. 2.9). However, the same solution cannot deprotonate a weaker acid of diisopropyl amine, as evidenced by the persisting ^{119}Sn signal of KSn_9^- and proton signals of diisopropylamine (eq. 2.10)

As a result, Sn_9H^{3-} is a stronger acid than diisopropylamine and a weaker acid than ${}^t\text{BuOH}$. The pK_a values in dmsO solvent are given in the Table 2.4. Thus the Brønsted acidity constant of the Sn_9H^{3-} ion is expected to be in range of 32.2 - 44 in dmsO in the absence of coordinating cation. However, it decreases significantly with alkali metal coordination. For comparison, Sn_9^{4-} ion is relatively more basic than P_7^{3-} ions. The P_7H^{3-} ion has a Brønsted acidity constant between 12 - 29, and metallated $\text{HP}_7\text{M}(\text{CO})_3^{3-}$ ions (M=Cr, W) have a Brønsted acidity constant between 18.9 - 22.6.^[164, 165]

Table 2.4. Acidities of related weak acids in dmsO solution at 25°C.

	pK _a values in dmsO	ref
water	31.4	[166]
^t BuOH	32.2	[166]
dmsO	35	[166]
Ammonia	~41	[167]
Diisopropyl amine	~44	[167]

2.2.5. Coupling of Sn₉H³⁻ ions

When a stoichiometric amount of NH₄Cl salt is added to the en solution of K₄Sn₉ and 8 equivalents of 2,2,2-crypt, a single resonance of Sn₉H³⁻ at -1268 ppm is obtained (Figure 2.7a). In addition to the corresponding Sn₉H³⁻ signal, the spectrum also contains another a weak signal at -1448 ppm with a $J(^{119}\text{Sn}-^{117}\text{Sn})= 113$ Hz. This cluster species is proposed to be an oxidatively coupled Sn₉-Sn₉⁶⁻ ion. After obtaining the spectrum, the solution was split into two portions for the alkali metal halide salts experiments. Addition of the KCl salt to the first portion results in formation of the weak signal of K₃Sn₉⁻, and increases the intensity of the Sn₉-Sn₉⁶⁻ signal at -1448 ppm (Figure 2.7b). As shown in Figure 2.7c, addition of the CsCl salts to the second portion results in the formation of Cs_{2-x}K_xSn₉⁻ (-1141 ppm, $J(^{119}\text{Sn}-^{117}\text{Sn})= 293$ Hz) in the solution but does not affect the weak signal significantly at -1447 ppm.

The Sn₉-Sn₉⁶⁻ ions are also synthesized in dmf solution in a similar manner. The dmf solutions of Sn₉H³⁻ ion react with KCl salt to give oxidatively coupled cluster ion Sn₉-Sn₉⁶⁻. In this solvent, the addition of CsCl also results in the formation of coupled clusters as shown in Figure 2.5.

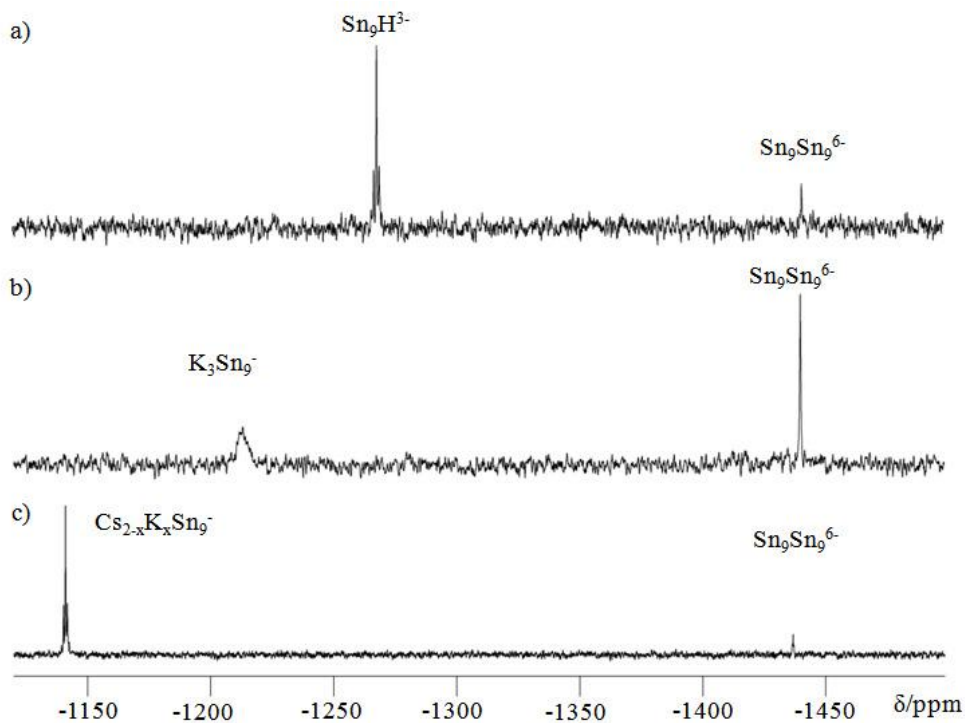


Figure 2.7. ^{119}Sn NMR spectrum of the reactions of Sn_9H^{3-} with KCl and CsCl salts in the absence of a base. a) reaction mixture of K_4Sn_9 , 8 equiv. of 2,2,2-crypt, and NH_4Cl , b) addition of KCl to the solution in (a), and c) addition of CsCl to the solution in (a).

In the proposed mechanism shown in eq.2.2, the oxidatively coupled $\text{Sn}_9\text{-Sn}_9^{6-}$ ions are formed from Sn_9H^{3-} ions in the absence of a base after addition excess alkali metal salts. As discussed earlier, alkali metal coordinations to the Sn_9H^{3-} ion polarize the Sn-H bond and cause dissociation of H^+ . In the presence of a base in the solution, this process retrieves the ^{119}Sn signal for the $\text{A}_x\text{Sn}_9^{(4-x)-}$ ions. However, in the absence of a base oxidatively coupled $\text{Sn}_9\text{-Sn}_9^{6-}$ ions forms with a possible H_2 gas evolution.

2.3. Conclusion

In this study, the previously reported Sn_9^{3-} ion has been found to be a diamagnetic Sn_9H^{3-} cluster. The true nature of this ion has been shown by NMR studies. Furthermore, the structural analysis showed that distortions of the Sn_9H^{3-} ion is similar to the reported Sn_9R^{3-} ($\text{R} = \text{}^i\text{Pr}, \text{SnCy}_3$) cluster ions, and is a result of the *exo*-substituent group. Solution dynamics of Sn_9H^{3-} have been studied and the exchange mechanism involves the mobility of the hydride substituent around the cluster while, all 9 atoms of the cluster is in a fast exchange. Similar exchange mechanisms and ^{119}Sn NMR features will be discussed for the $\text{Sn}_9\text{SnCy}_3^{3-}$ ion in Chapter 3.

In-situ studies showed that Sn_9^{4-} exists in equilibrium between KSn_9^{3-} and Sn_9H^{3-} ions in solution. 2,2,2-crypt is not only sequestering the alkali cations for better crystallization, but it also dramatically increases the basicity of the anion and creates protonated clusters in solution. Owing to strong affinity between the Sn_9^{4-} and K^+ ions, KSn_9^{3-} ions persist in the solution even with 5 equivalents of 2,2,2-crypt. This fact should be considered for all of the reactions of the K_4Sn_9 in en solvent, which will be discussed in the following chapters in this thesis.

The Brønsted acidity range of Sn_9H^{3-} was found by protonation-deprotonation studies. Our results show that Sn_9^{4-} is more basic than an amide ion. Moreover, coordinating alkali metals have been shown to decrease the acidity of this protonated cluster ion, which creates a competition of KSn_9^{3-} and Sn_9H^{3-} ions. However, due to low solubility of the Sn_9H^{3-} ion relative to the alkali metal components, Sn_9H^{3-} ion crystallizes from the solution. The similarities in electronegativities of Ge, Si and Sn

suggest that Ge_9H^{3-} and Si_9H^{3-} clusters may also exist but the NMR studies involving these nuclei are more challenging. Further experimental and theoretical studies including other group 14 members can reveal the general Brønsted acidity trends of these ions.

The coupled cluster, $\text{Sn}_9\text{-Sn}_9^{6-}$ ion, was synthesized and characterized by NMR spectroscopy. It forms with excess alkali metal ions in the absence of a base, in both en and dmf solutions. Preliminary the synthesis of $\text{Sn}_9\text{-Sn}_9^{6-}$ ion appears to provide a facile synthetic method to obtain coupled clusters. The $\text{Sn}_9\text{-Sn}_9^{6-}$ ion has a different exchange mechanism than the Sn_9H^{3-} ion and have similar spectral features to the Sn_9R^{3-} ions with an alkyl substituent. In this mechanism, the *exo*-bonded Sn nuclei of the two cluster units are not involved with the remaining fast exchanging 8 Sn atoms of each cluster. This type of exchange mechanism is also reported for the $\text{Sn}_9\text{-}^i\text{Pr}^{3-}$ ion (Chapter 3).

2.4. Experimental Section

2.4.1. General Data

All reactions were performed in a nitrogen atmosphere drybox. The ^{119}Sn NMR spectra were recorded on a Bruker DRX500 AVANCE spectrometer at 186.5 MHz. The pulse sequence used for the ^{119}Sn NMR studies was the standard Bruker pulse program with 90 ° pulse strength and 0.3 s relaxation delays were used. The signals were confirmed and verified by repeating the final measurements with different transmitter offsets. The ^{119}Sn chemical shifts were referenced to the external Me_4Sn standard in C_6D_6 (0 ppm) at room temperature. The ^1H spectrum of Sn_9H^{3-} was

recorded on AM400 spectrometer at 400 MHz with BBI probe. In this experiment, Gaussian shaped pulse with 180° pulse duration was applied resulting in selective excitation of the proton signal of Sn_9H^{3-} and slight suppression of the other signals. The ^1H chemical shifts referenced to the residual toluene signal at 7 ppm (relative to TMS at 0 ppm). The percentage yields were calculated by considering the amount of alloy precursor K_4Sn_9 that was used.

2.4.2. Chemicals

Melts of nominal composition K_4Sn_9 were made by fusion of stoichiometric ratios of the elements at high temperature. The chemicals were sealed in evacuated silica tubes and heated carefully with a natural gas/oxygen flame. *Caution: molten alloy synthesis can result in serious explosion and reactions should be conducted with great caution behind blast shields.* 4,7,13,16,21,24-Hexaoxa-1,10-diazobicyclo[8,8,8]hexacosane (2,2,2-crypt) were purchased from Fisher Scientific. Anhydrous ethylenediamine (en) was purchased from Fisher, vacuum distilled from K_4Sn_9 , and stored under dinitrogen. Toluene was distilled from sodium/benzophenone under dinitrogen and stored under dinitrogen. NH_4Cl and CsCl were purchased from Sigma Aldrich and vacuum dried overnight. KCl was purchased from J.T.Baker and dried in vacuum.

2.4.3. Synthesis

Synthesis of $[\text{K}(2,2,2\text{-crypt})]_3[\text{Sn}_9\text{H}]\cdot\text{en}$

In a glass vial 1, K_4Sn_9 (80 mg, 0.065 mmol) and 2,2,2-crypt (98 mg, 0.26 mmol) were dissolved in 2 mL of ethylenediamine. The solution was stirred for ½ hr. and filtered through tightly packed glass wool. After 2 days, the black-green large

needle crystals of $[\text{K}(2,2,2\text{-crypt})]_3[\text{Sn}_9\text{H}]\cdot\text{en}_{0.5}$ (97 mg, % 65) were obtained. $\delta^{119}\text{Sn}$ / ppm (en, 25 °C) -1270 (9 Sn, $J(^{119}\text{Sn}-^{117}\text{Sn})$; 398 Hz, $J(^{119}\text{Sn}-^1\text{H})$; 21 Hz) $\delta^1\text{H}$ / ppm (en, 25 °C) 6.1 (1 H, $J(^1\text{H}-^{119/117}\text{Sn})$; 21Hz).

Synthesis of $[\text{Sn}_9\text{-Sn}_9]^{6-}$ ion

In 1 glass vial 1, K_4Sn_9 (80 mg, 0.065 mmol) and 2,2,2-crypt (98 mg, 0.26 mmol) were dissolved in 2 mL of ethylenediamine and stirred for 10 minutes. NH_4Cl salt (3.5 mg, 0.065 mmol) was added as a solid. The green solution was stirred for ½ hr. Excess amount of KCl salt was added to vial 1 as solid, resulting in red solution. Solution was filtrated through tightly packed glass wool.

In an alternative method, $[\text{K}(2,2,2\text{-crypt})[\text{Sn}_9\text{H}]\cdot\text{en}_{0.5}$ crystals and excess KCl salt was dissolved in 1 ml of dmf at room temperature. Solution was filtrated through tightly packed glass wool. $\delta^{119}\text{Sn}$ / ppm (186.4 MHz; dmf; Me_4Sn ; 25 °C) -1386 (16 Sn, $J(^{119}\text{Sn}-^{117}\text{Sn})$; 113 Hz, $J(^{119}\text{Sn}-^{119}\text{Sn})$; 1780 Hz, $J(^{119}\text{Sn}-^{119}\text{Sn})$; 1707 Hz), -3 (2 Sn, $J(^{119}\text{Sn}-^{119/117}\text{Sn})$; 1720.

Chapter 3: Sn_9R^{3-} ($\text{R} = {}^i\text{Pr}, \text{SnCy}_3, \text{Sn}({}^n\text{Bu})_3$) clusters and their solution dynamics Introduction

In solution, a single time-averaged ^{119}Sn NMR signal is observed for the K_4Sn_9 ions even though the cluster has a C_{4v} monocapped square antiprismatic structure with a 4:4:1 ratio of chemically distinct Sn atoms in the solid state.^[134] The ^{119}Sn resonance of the K_4Sn_9 ions show $J(^{119}\text{Sn}-^{117}\text{Sn})$ coupling constants in the range of 256-310 Hz that are solvent and counter cation dependent.^[38] The intensity and pattern of the ^{117}Sn satellites (^{117}Sn , $I = 1/2$, 7.6 % abund.) shows that the cluster maintains its 9-atom nuclearity in an intramolecular exchange process. In static clusters, such as Sn_4^{4-} , $\text{Sn}_9\text{Cr}(\text{CO})_3^{4-}$ and $\text{Sn}_6\text{Nb}_2(\text{tol})_2$, the $J(^{119}\text{Sn}-^{117}\text{Sn})$ couplings are significantly larger with values between 1975 and 1043 Hz.^[38, 97, 98, 110] This suggests that the observed J values represent the weighted average couplings of the various Sn-Sn interactions during the exchange process. The proposed exchange mechanism involves the interconversion between the two lowest energy structures of C_{4v} and D_{3h} symmetry, which requires making a bond across the square face and breaking a bond at a triangular face as shown in the Figure 3.1.^[136] The energy barrier between the two symmetries has been calculated as 0.01 eV.^[137]

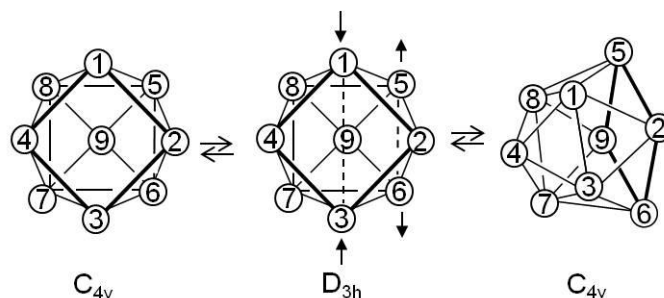


Figure 3.1. Exchange mechanism of the Sn_9^{4-} ion between the two lowest energy structures.

Sevov and coworkers have shown that a variety of substituents such as ^tBu , vinyl, styrene, and post transition metal groups can be attached to the exterior of the group 14 Zintl ion clusters in *exo* positions (*i.e.* not vertex or interstitial positions).^[76-79, 81, 158] The number substituents do not exceed 2 for the Ge_9 analog, whereas only mono-substituted Sn_9 clusters have been reported to date. The structures of these clusters are similar to highly substituted organostannane clusters prepared via different synthetic routes.^[168-170]

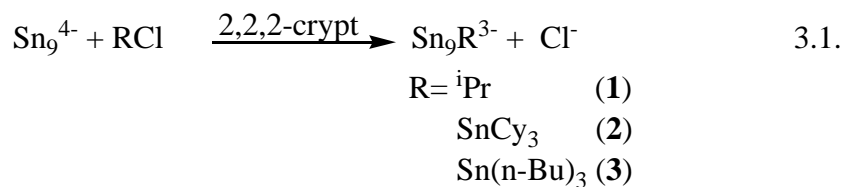
Although the formation mechanism was thought to involve an electron transfer mechanism, it was later proposed to be nucleophilic substitution reaction mechanism without the involvement of radical or carbocation alkyl group intermediates. Such that, the cyclo-propane group does not rearrange in the $\text{Ge}_9(\text{CH}_2\text{CH}(\text{CH}_2))_2^{2-}$ cluster.^[80]

In this chapter, the solution dynamics of the substituted Sn_9 clusters has been studied in detail for the first time and they have been found to have different exchange mechanisms for different types of substituent groups.^[152]

3.2. Results and Discussion

3.2.1. Synthesis

The Sn_9R^{3-} ions ($\text{R} = \text{}^i\text{Pr}$, SnCy_3 , $\text{Sn}(\text{}^n\text{Bu})_3$) were prepared using slight modifications of previously reported methods.^[81] Ethylenediamine (en) solutions of K_4Sn_9 and 4 equivalents of 2,2,2-crypt react with en solutions of ${}^i\text{PrCl}$ to give $\text{Sn}_9\text{-}{}^i\text{Pr}^{3-}$ cluster ions according to eq.3.1. Evaporation of the ethylenediamine and extraction of the product into pyridine gives the $\text{Sn}_9\text{-}{}^i\text{Pr}^{3-}$ cluster anion, **1**, in ca. 80% crystalline yield as the $[\text{K}(2,2,2\text{-crypt})]^+$ salt. The $[\text{K}(2,2,2\text{-crypt})]_3[\text{Sn}_9\text{-}{}^i\text{Pr}]$ salt has been characterized by single crystal XRD and ${}^1\text{H}$, ${}^{13}\text{C}$, ${}^{119}\text{Sn}$ NMR spectroscopy.



The pyridine extract of the evaporated en solution of K_4Sn_9 and 4 equivalents of 2,2,2-crypt react with a toluene solution of Cy_3SnCl to give the $\text{Sn}_9\text{SnCy}_3^{3-}$ (**2**) cluster anion, in ca. 72% crystalline yield as $[\text{K}(2,2,2\text{-crypt})]^+$ salts. The crystalline salt has been characterized by single crystal XRD, ${}^1\text{H}$, ${}^{13}\text{C}$, ${}^{119}\text{Sn}$ and one dimensional gradient enhanced heteronuclear multiple bond correlation (1D ge-HMBC) NMR spectroscopy. The reaction of the en solutions of K_4Sn_9 and the toluene solutions of Cy_3SnCl also gives the same anion but crystalline yield is lower compared to the pyridine reaction mixture. The balanced equation is summarized in eq.3.1. Similarly, the reaction of K_4Sn_9 with $(\text{}^n\text{Bu})_3\text{SnCl}$ in a py/tol solution gives $\text{Sn}_9\text{Sn}(\text{}^n\text{Bu}_3)^{3-}$ (**3**), however a crystalline product was not been isolated.

The salts **1** and **2** have been characterized by single crystal XRD, ^1H , ^{13}C and ^{119}Sn NMR spectroscopy. The salts **3** have been characterized by ^{119}Sn NMR spectroscopy. The air and moisture sensitive salts of the cluster anions are soluble in pyridine, dmf, and en solutions.

3.2.2. Solid State Structure

Each of the crystal unit cells contains a non-interacting Sn_9R^{3-} ($\text{R} = \text{}^i\text{Pr}$ and SnCy_3) anion, 3 $[\text{K}(2,2,2\text{-crypt})]^+$ cations, and 2 pyridine molecules. The crystallographic data is given in in Table 1. Both salts are triclinic space group $\text{P}\bar{1}$.

Table 3.1. Crystallographic data for the Sn_9R^{3-} ($\text{R} = \text{}^i\text{Pr}$, SnCy_3) ions.

Compound	$[\text{K}(2,2,2\text{-crypt})]_3 \cdot (1) \cdot 2\text{py}$ $[\text{Sn}_9\text{}^i\text{Pr}]$	$[\text{K}(2,2,2\text{-crypt})]_3 \cdot (2) \cdot 2\text{py}$ $[\text{Sn}_9\text{SnCy}_3]$
formula weight	2516.26	2841.31
temperature (K)	150(2)	150(2)
Wavelength (\AA)	0.7107	0.7107
crystal system	Triclinic	Triclinic
space group	P-1	P-1
unit cell dimensions		
a (\AA)	14.446(5)	14.331(6)
b (\AA)	16.342(5)	15.288(6)
c (\AA)	22.341(7)	25.554(10)
α ($^\circ$)	85.716(5)	87.639(7)
β ($^\circ$)	78.865(5)	86.052(7)
γ ($^\circ$)	65.485(5)	76.534(6)
volume (\AA^3)	4708.1(3)	5430.2(4)
Z	2	2
D_{calc} (Mg/m^3)	1.775	1.738
Abs. coeff. (mm^{-1})	2.537	2.432
final R indices(all data) ^a		
R1, $I > 2\sigma(I)$	0.0384	0.0348
wR2	0.0859	0.0799

$$^a R_1 = \frac{\sum ||F_o| - |F_c||}{\sum |F_o|}, wR_2 = \left[\frac{\sum w(F_o^2 - F_c^2)^2}{\sum w(F_o^2)^2} \right]^{1/2}$$

The summary of the selected bond lengths are given in Table 2 and Table 3 for the cluster anions **1** and **2**, respectively. The structures of both anions (Figure 3.2) are distorted from idealized C_{4v} symmetry of the Sn_9^{4-} anion and have virtual C_s symmetry. The mirror planes pass through Sn1, Sn3, and C1/Sn10. The anions have an *exo* substituent attached to one of the tin atoms on the open square face of the parent Sn_9^{4-} structure. The iPr substituent in the cluster ion **1** is slightly bent up and out of the square plane ($Sn1-Sn3-C1 = 162^\circ$). The Sn1-9 core is slightly distorted toward the tricapped trigonal prismatic D_{3h} structure. The ratio of the Sn1-Sn3/Sn2-Sn4 diagonals is 1.17. For the ideal C_{4v} geometry of Sn_9^{4-} ion, the ratio of the diagonals on the open square face is 1.0, whereas the diagonal ratio range is 1.32-1.45 for the approximate D_{3h} geometry of Sn_9^{3-} structures (see the Sn_9H^{3-} ion, Chapter 2).^[45, 108]

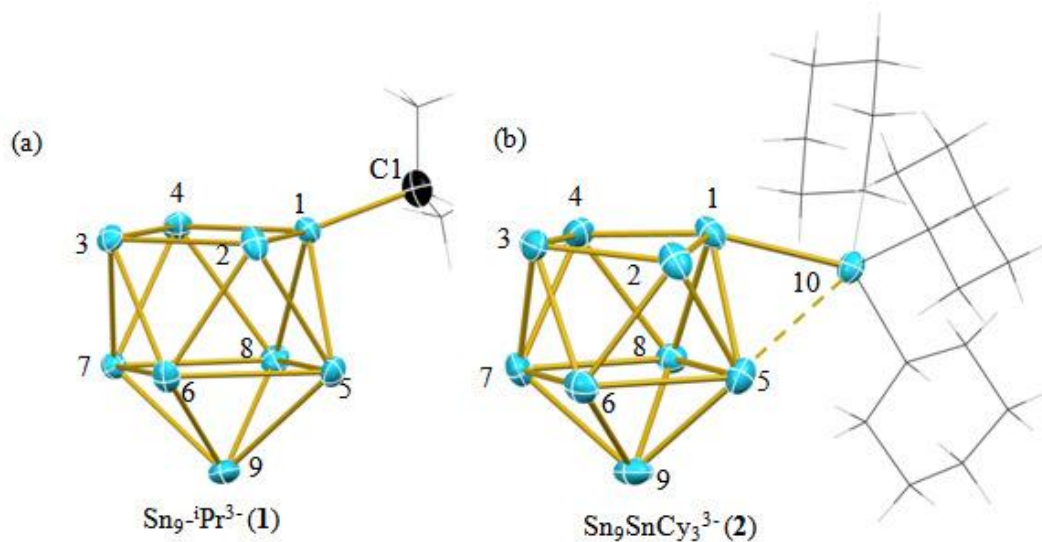


Figure 3.2. ORTEP drawing of the Sn_9R^{3-} ions, where R is iPr in (a) and $SnCy_3$ in (b). The solid lines define the bond distances smaller than 3.4 \AA , whereas the dotted line denotes the longer contact in the range $3.4 \text{ \AA} < x < 3.7 \text{ \AA}$. The iPr and $SnCy_3$ groups are shown as C1 and 10, respectively.

The SnCy₃ substituent in the Sn₉SnCy₃³⁻ cluster anion **2**, bends down toward the Sn1-Sn8-Sn5 triangular face. The Sn1-9 core is more distorted toward D_{3h} geometry than the cluster anion **1** having a Sn3-Sn1-Sn10 angle of 197° and a diagonal ratio of 1.26 (Sn1-Sn3 / Sn2-Sn4).

The structure of the Sn₉ⁱPr³⁻ anion is very similar the reported alkyl substituted Ge₉R³⁻, Sn₉R³⁻ (R= vinyl, ^tBu, styrene) clusters where the substituent groups are attached to the cluster atom on the open square, bending away from the triangular faces of the clusters.^[78, 79, 81]

The SnCy₃ moiety in cluster ion **2** can be viewed as a semi-bridging group which makes a primary bond between Sn10-Sn1 of 2.911 (4) Å and a longer contact between Sn10-Sn5 of 3.658 (5) Å. The distance of the Sn10 to Sn8 is 3.89 Å and is non-bonding. The Sn₉SnCy₃³⁻ structure is similar to the Ge₉SnMe₃³⁻ cluster having a semi-bridging -SnMe₃ substituent over the Sn1-Sn5 bond. In contrast the Ge₉SnPh₃³⁻ cluster has a symmetrically bridging substituent moiety.^[78]

The summary of the selected bond lengths are given in Table 2 and Table 3 for the cluster anions **1** and **2**, respectively. The cluster ions **1** and **2** have Sn-Sn bond lengths within the Sn₉ cluster core ranging between 2.853 (4)-3.230 (5) Å and 2.884(4)-3.260(4) Å, respectively. In both cluster anions Sn-Sn contacts are consistent with the typical bond lengths for the 9-vertex Sn₉⁴⁻ and Sn₉H³⁻ clusters.^[45] The Sn1-C1 bond length in cluster ion **1** is 2.250(5) Å, slightly greater than a typical Sn-C bond length e.g. Sn(C₆H₁₁)₃I with a Sn-C bond distances of 2.10-2.19 Å,^[171] but slightly shorter than the Sn-C bond in the Sn₉-^tBu³⁻ ion (2.265(7)). Similarly, the average Sn-C bond lengths of the SnCy₃ moiety in the cluster ion **2** is 2.222 (4) Å.

Both the cluster anions **1** and **2** are 9-vertex $22e^-$ *nido* clusters as expected from a Wade-Mingos analysis.^[36] In this analysis, vertex tin atoms contribute 2 electrons and the substituted groups' contributions are counted as 1 since both the alkyl and post-transition metal groups make 2-center $2-e^-$ bonds to the open square face of the cluster. The summation of all contributions and three electrons due to charge gives a total of 22 cluster bonding electrons, which correspond to a $2n+4$ ($n=9$) *nido* cluster when $n=9$ and are isoelectronic with the Sn_9^{4-} ion.

Table 3.2. Selected bond lengths of the Sn_9-Pr^{3-} anion in Å.

	Bond Lengths		Bond Lengths	
Sn1-Sn2	2.8584 (4)	Sn4-Sn7	2.9531 (4)	
Sn1-Sn4	2.8535 (4)	Sn4-Sn8	3.0369 (4)	
Sn1-Sn5	2.9547 (4)	Sn5-Sn6	3.2246 (5)	
Sn1-Sn8	2.9739 (4)	Sn5-Sn8	3.2302 (5)	
Sn2-Sn3	3.0322 (4)	Sn5-Sn9	2.9346 (5)	
Sn2-Sn5	3.0716 (5)	Sn6-Sn7	3.1868 (4)	
Sn2-Sn6	2.9365 (5)	Sn6-Sn9	2.9642 (5)	
Sn3-Sn4	3.0142 (4)	Sn7-Sn8	3.1279 (4)	
Sn3-Sn6	2.9671 (4)	Sn7-Sn9	2.9574 (4)	
Sn3-Sn7	2.9860 (4)	Sn8-Sn9	2.9674 (5)	

Table 3.3. Selected bond lengths of the $\text{Sn}_9\text{SnCy}_3^{3-}$ anion in Å.

Atom numbers	Bond Lengths	Atom numbers	Bond Lengths
Sn1-Sn2	2.8836 (4)	Sn5-Sn6	3.2602 (4)
Sn1-Sn4	2.8988 (5)	Sn5-Sn8	3.2380 (4)
Sn1-Sn5	3.0196 (5)	Sn5-Sn9	2.9172 (5)
Sn1-Sn8	3.0411 (4)	Sn6-Sn7	3.0802 (5)
Sn2-Sn3	3.0093 (5)	Sn6-Sn9	2.9541 (4)
Sn2-Sn5	2.9524 (5)	Sn7-Sn8	3.1936 (4)
Sn2-Sn6	2.9911 (5)	Sn7-Sn9	2.9643 (5)
Sn3-Sn4	2.9970 (5)	Sn8-Sn9	2.9404 (4)
Sn3-Sn6	2.9899 (5)	Sn1-Sn10	2.9112 (4)
Sn3-Sn7	3.0150 (5)	Sn10-C11	2.2219 (4)
Sn4-Sn7	2.9604 (5)	Sn10-C31	2.2219 (4)
Sn4-Sn8	2.9600 (4)	Sn10-C21	2.2222 (4)

3.2.3. NMR Spectroscopic Studies

The ^{119}Sn NMR data of Sn_9R^{3-} ($\text{R} = \text{}^i\text{Pr}$, SnCy_3 , $\text{Sn}(\text{}^n\text{Bu})_3$) are summarized in Table 3.4. The cluster anions are highly fluxional in the NMR time scale. Despite their low symmetry solid state structures, all four anions have only two time averaged signals in the ^{119}Sn spectra. The integrated intensity ratio of these two signals for each ion are approximate 1:8 and 1:9 for the alkyl and post transition substituents, respectively.

Table 3.4. ^{119}Sn NMR data of the clusters anions Sn_9R^{3-} .^a

Cluster Ions	$\delta^{119}\text{Sn}$	$J(^{119}\text{Sn}-^{117}\text{Sn})$	$J(^{119}\text{Sn}-^{119}\text{Sn})$	$J(^{119}\text{Sn}-^{117}\text{Sn})$
$\text{Sn}_9\text{-}^i\text{Pr}^{3-}$ (1)	-1413	170	115	1876
$\text{Sn}_9\text{SnCy}_3^{3-}$ (2)	-1172	155	295	1331
$^b\text{Sn}_9\text{Sn}(\text{}^n\text{Bu})_3^{3-}$ (3)	-1119	62	278	1330

^aThe data were recorded from dmf solutions at room temperature. ^bThe data for the Sn₉Sn(ⁿBu)₃³⁻ ion were recorded in py/tol solutions at room temperature.

All Sn₉R³⁻ are highly fluxional showing rapid exchange of the Sn atoms of the clusters' vertices. The ¹¹⁹Sn chemical shifts of the exchanging cluster vertex atoms appear at a range of -1119 ppm and -1413 ppm, respectively. Presence of the $J(^{119}\text{Sn}-^{117}\text{Sn})$ coupling constants in the resonances for the fluxional cluster core atoms shows that both mechanism are intramolecular. Although the data appear similar, the mechanisms of exchange are quite different for different type of substituents. Since similar type of substituents such as SnCy₃ or Sn(ⁿBu)₃ have similar chemical shifts and J coupling constants, a similar exchange mechanism is expected.

The ¹¹⁹Sn NMR spectra of the Sn₉SnR₃³⁻ (R= Cy, ⁿBu) clusters have similar features. The downfield signals of the Sn₉SnR₃³⁻ clusters spectra (Figure 3.3 and 3.5) were assigned to the Sn10 atoms of the SnR₃ groups and the upfield signals were assigned the nine time-averaged vertex Sn nuclei. The two signals are in a ratio of 1:9 and are coupled to each other. The Sn₉SnCy₃³⁻ anion have well resolved coupling constants of $J(^{119}\text{Sn}-^{119}\text{Sn}) = 1331$ Hz and $J(^{119}\text{Sn}-^{117}\text{Sn}) = 1272$ Hz, which can be seen for both signals (Figure 3.3). The ^{119/117}Sn satellites on the peak at -1172 ppm (16% integrated intensities, which indicates coupling of 9-Sn atoms to a chemically distinct Sn atom) arise from coupling to one Sn atom of the -SnCy₃ group. The resonance at 155 ppm is a 0.24 : 0.65 : 1.0 : 0.65 : 0.25 five-line multiplet and is consistent with the calculated 0.22 : 0.64 : 1.0 : 0.64 : 0.22 ^{119/117}Sn satellite pattern associated with coupling to nine equivalent Sn atoms. Having one time averaged ¹¹⁹Sn signal for the Sn₉ cluster core shows that the 9-equivalent Sn atoms are in fast

exchange. The time averaged signal of the Sn₉ core of **2** has the coupling constants of $J(^{119}\text{Sn}-^{117}\text{Sn}) = 295$ for cluster anion **2**.

While the ^{119}Sn spectra of the Sn₉-ⁱPr³⁻ ion are very similar to that of the Sn₉SnCy₃³⁻ ion, the origins of the signals are significantly different. The downfield signal of **1** is due to *exo*-bonded Sn vertex atom coupling to the 8 equivalent Sn nuclei of the cluster. However, the downfield signal of the **2** is due to the SnCy₃ substituent group. Moreover, both ^{119}Sn signals of **2** do not show a coupling pattern due to *exo*-bonded Sn atom of the cluster, which excludes the possibility of a missing signal. Furthermore, a 1D gradient enhanced heteronuclear multiple bond correlation experiment (1D ge-HMBC) was conducted to support the validity of assignment of the resonances for the cluster anion **2** (Figure 3.4). In this experiment, ^1H NMR was collected by setting the frequency of the decoupler channel (^{119}Sn) was firstly set at the chemical shift 155 ppm and proton signals of the cyclohexyl groups were recorded. Later, this frequency was set at chemical shift -1172 ppm for the control experiment and no proton signal was recorded. Thus, the down field ^{119}Sn chemical shift was proved to be Sn10 of the SnCy₃ group by the recorded correlation of the ^{119}Sn signal to the proton signals of the SnCy₃ group.

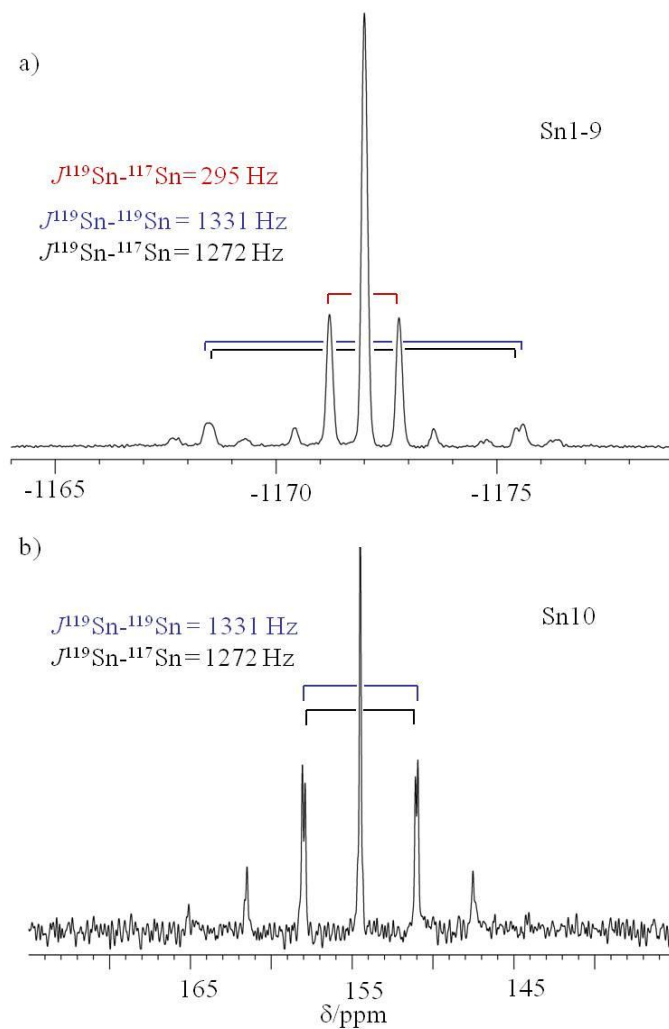


Figure 3.3. ^{119}Sn NMR spectrum of the $\text{Sn}_9\text{SnCy}_3^{3-}$ anion taken at RT in dmf and 186.5 MHz; signal assigned for the Sn_9 cluster core (a), signal assigned for the SnCy_3 (b).

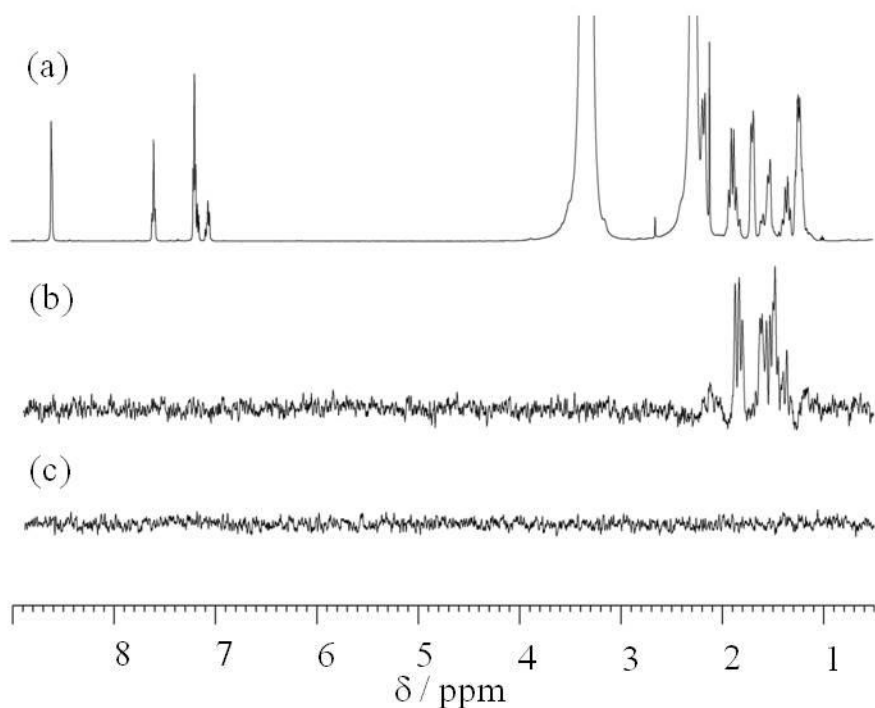


Figure 3.4. ^1H spectrum of $[\text{K}(2,2,2\text{-crypt})]_3[\text{Sn}_9\text{Sn}(\text{Cy})_3]\cdot 2\text{py}$ in $\text{py}\text{-d}_5$ solution at RT at 600 MHz; (a) ^1H spectra, (b) 1D ge-HMBC with decoupler offset = 155 ppm, (c) 1D ge-HMBC with decoupler offset = -1172 ppm.

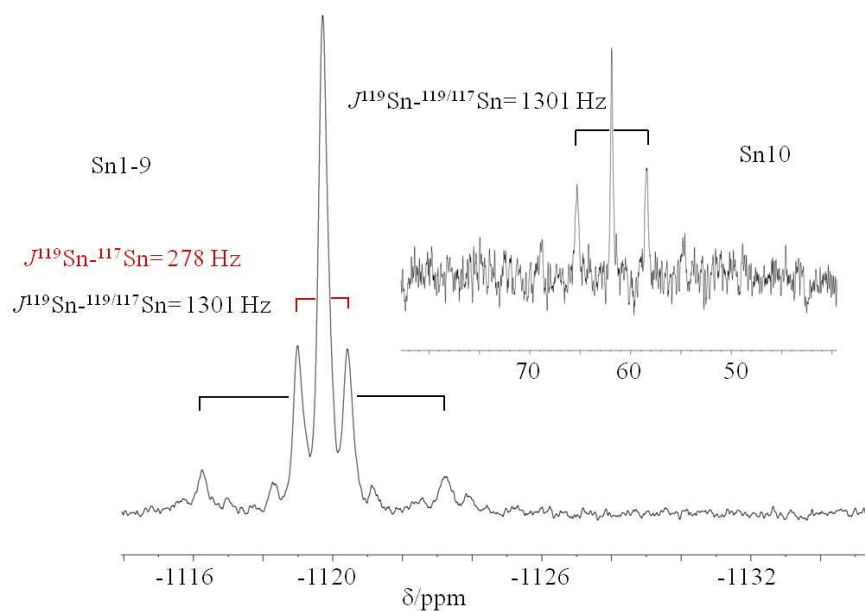


Figure 3.5. ^{119}Sn NMR spectrum of the $\text{Sn}_9\text{Sn}(\text{nBu})_3^{3-}$ anion taken at RT in py/tol and 186.5 MHz. The signal at -1120 ppm assigned for the Sn_9 cluster core. The signal at 62 ppm (inset) is assigned to the SnCy_3 group.

Although the $\text{Sn}_9\text{Pr}^{3-}$ ion, **1**, have similar spectral features similar to those of **2** and **3**, the origins of the signals are quite different (Figure 3.6). The down field chemical signal at 170 ppm for the $\text{Sn}_9\text{-Pr}^{3-}$ anion is assigned to the Sn1 atom, which is the Sn atom with the *exo*-bonded alkyl substituent. The signal at -1414 ppm with an intensity 8 times that of the other signal is assigned to the time averaged Sn2-9 nuclei of the cluster. The Sn2-9 and the Sn1 resonances are mutually coupled with $J(^{119}\text{Sn}-^{119}\text{Sn}) = 1876$ Hz and $J(^{119}\text{Sn}-^{117}\text{Sn}) = 1793$ Hz with a 16% integrated intensity due to coupling to a chemically distinct Sn atom. An average $J(^{119}\text{Sn}-^{119/117}\text{Sn}) = 1844$ Hz was observed on the Sn1 signal (170 ppm) and integrated intensities of the 0.18 : 0.60 : 1.0 : 0.60 : 0.18 five-line multiplet is consistent with the calculated $^{119/117}\text{Sn}$ satellite pattern (0.18 : 0.60 : 1.0 : 0.60 : 0.18) associated with coupling to eight equivalent Sn atoms. Presence of a single time-averaged signal for the 8 Sn nuclei shows that they are in fast exchange in the NMR time scale. The $J(^{119}\text{Sn}-^{117}\text{Sn})$ coupling constant of the exchanging Sn2-8 nuclei is 115 Hz which is less than half magnitude of the $J(^{119}\text{Sn}-^{117}\text{Sn})$ coupling constant of fast-exchanging Sn1-9 on the $\text{Sn}_9\text{SnR}_3^{3-}$ and the Sn_9^{4-} cluster anions, suggesting a different exchange mechanism.

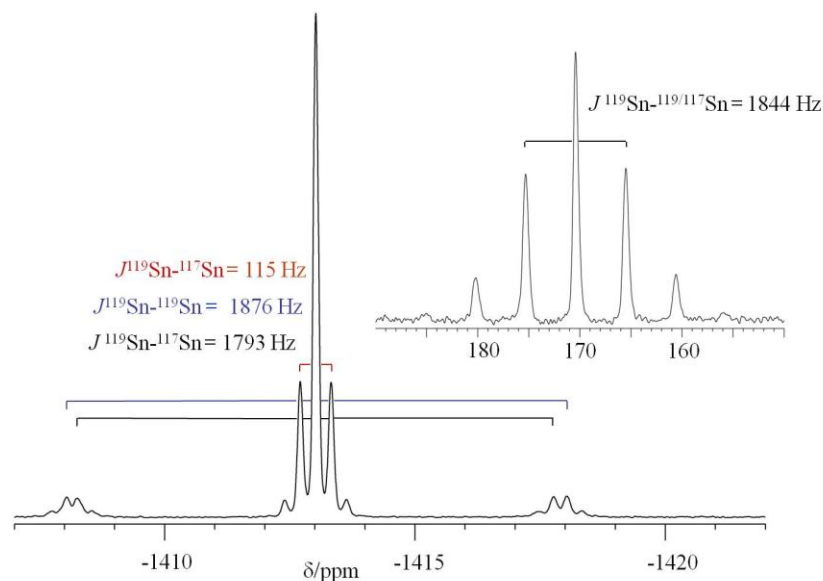


Figure 3.6. ^{119}Sn NMR spectrum of the $\text{Sn}_9\text{-}^i\text{Pr}^{3-}$ anion taken at RT in dmf at 186.5 MHz transmitter frequency. The signal at -1413 ppm is assigned to the Sn2-9 nuclei and the signal at 170 ppm (inset) is assigned to Sn1. See the Figure 3.1 for the numbering scheme of the nuclei.

Variable temperature ^{119}Sn NMR spectra were recorded for the Sn_9R^{3-} ions ($\text{R} = ^i\text{Pr}, \text{SnCy}_3$). In the limiting spectra for the $\text{Sn}_9\text{-}^i\text{Pr}^{3-}$ ion, 6 ^{119}Sn resonances are expected in a 1:2:2:2:1:1 integral ratio due to C_s structure of the cluster in the solid state with six different Sn environments. In the limiting spectra of the $\text{Sn}_9\text{SnCy}_3^{3-}$, six resonances are expected for the Sn_9 cluster core in ratio similar to that of ^iPr substituted ion and the SnCy_3 resonance is expected to remain distinct due to intact cyclohexyl groups on this Sn atom. Signals of both ions **1** and **2** gradually broaden in lower temperatures up to $-55\text{ }^\circ\text{C}$, however the limiting spectrum could not be reached (Figure 3.7). The downfield resonances of ions show slight broadening in lower temperatures because of tumbling effect. On the other hand, significant broadening of the upfield signal is due to decrease in the exchange rate.

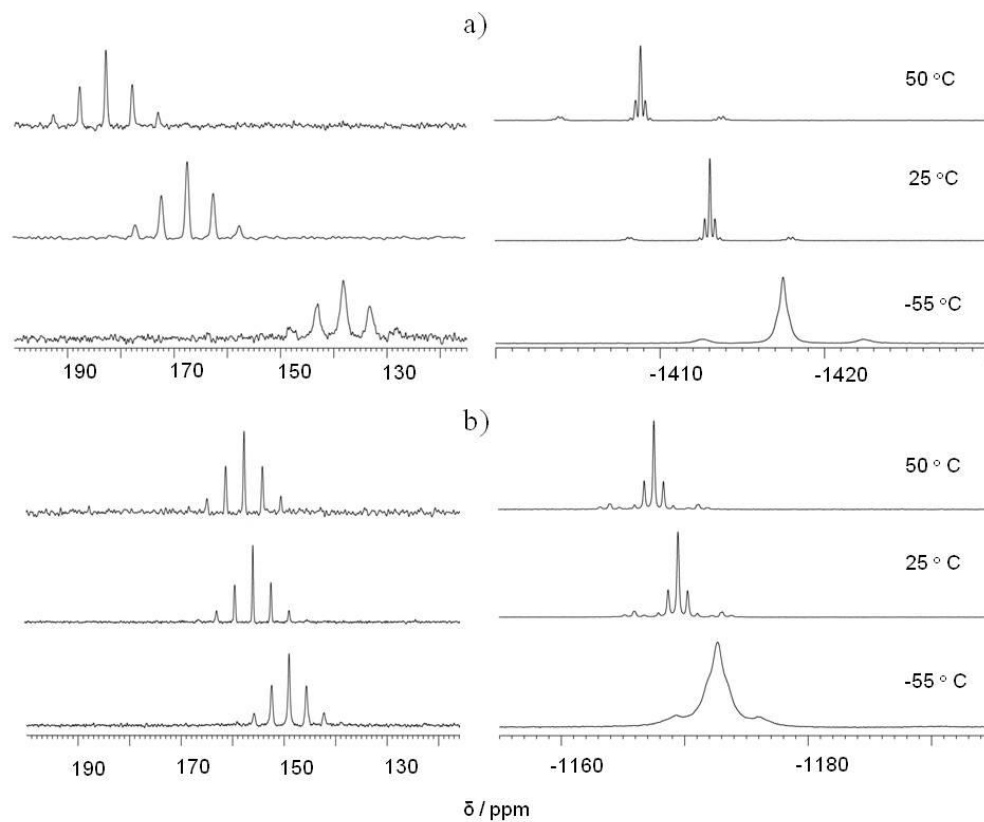


Figure 3.7. Variable temperature ^{119}Sn NMR spectra for the Sn_9R^{3-} ion. The data were recorded from dmf solutions and 186 MHz; a) $\text{R} = \text{}^i\text{Pr}$, b) SnCy_3

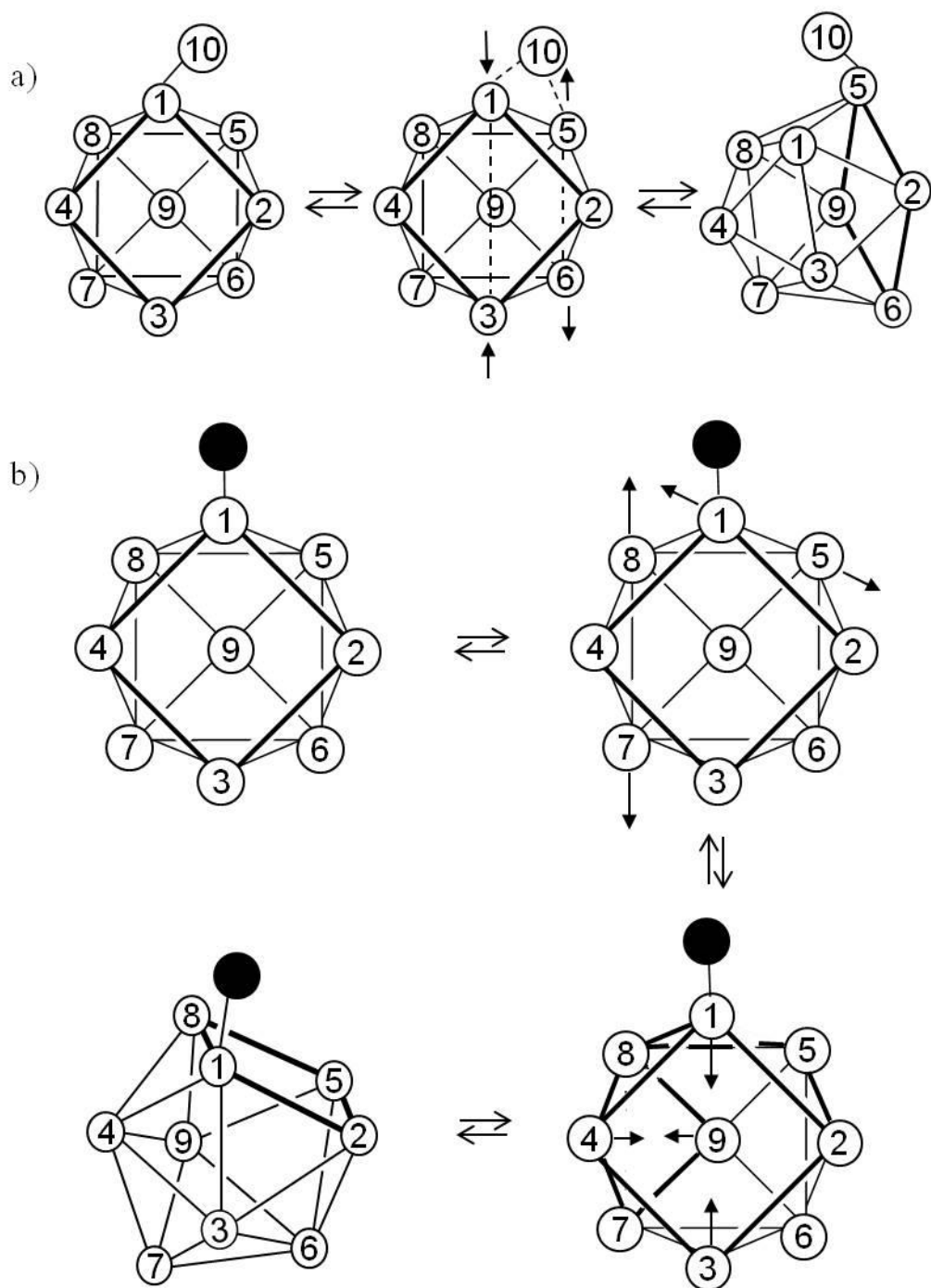


Figure 3.8. Proposed exchange mechanisms for the Sn_9R^{3-} ions; a) $\text{R} = \text{SnCy}_3$, $\text{Sn}(\text{}^n\text{Bu})_3$ and b) $\text{R} = \text{}^i\text{Pr}$.

In the proposed exchange mechanism for the $\text{Sn}_9\text{-}^i\text{Pr}^{3-}$ ion, (Figure 3.8 b), the Sn-C bond is not labile, which precludes chemical exchange of the Sn1 vertex with the other 8 vertex Sn atoms. Therefore, the exchange process results in two signals in a ratio of 1:8 and the chemical shift of Sn1 remains unique ($\delta^{119}\text{Sn} = 119$ ppm) and shows large $J(^{119}\text{Sn}\text{-}^{119}\text{Sn})$ and $J(^{119}\text{Sn}\text{-}^{117}\text{Sn})$ couplings of 1876 and 1793 Hz, respectively. The small 115 Hz $^{119}\text{Sn}\text{-}^{117}\text{Sn}$ satellites on the -1413 ppm central resonance suggest that the exchange mechanism goes through a more open transition state due to the presence of the alkyl group. As a result, Sn1 cannot exchange with the other vertices and gives rise to the chemically distinct 170 ppm resonance. While the Sn2-9 core of $\text{Sn}_9\text{-}^i\text{Pr}^{3-}$ is clearly highly fluxional, it does not appear to go through the same $C_{4v} - D_{3h} - C_{4v}$ multiple exchange process. Such a mechanism would periodically move the ^iPr substituent off of the square face (the preferred site in the solid state structure, which prevents any of the vertex Sn atoms from exceeding a 5-coordinate environment). To avoid these unfavorable coordination environments, in a proposed mechanism, Sn1 most likely remains attached to the open square plane at all the exchange steps. However, invoking the $C_{4v} - D_{3h} - C_{4v}$ mechanism similar to the proposed mechanism for the bare Sn_9^{4-} (Figure 3.1)^[136] while keeping Sn1 on the square face would not exchange all 8 remaining atoms. An alternate mechanism involving a more open transition state would be required to exchange all remaining 8 tin atoms (Figure 3.8 b). A more open transition state would lengthen the average Sn-Sn contact during the exchange process and is consistent with the smaller $J(^{119}\text{Sn}\text{-}^{117}\text{Sn})$ coupling constant observed for the $\text{Sn}_9\text{-}^i\text{Pr}^{3-}$ complex. The coupling constant is also reminiscent of the small coupling constant in the endohedral clusters such as

Cu@Sn_9^{3-} , $\text{Pt@Sn}_9\text{Pt}(\text{PPh}_3)^{2-}$, $J(^{119}\text{Sn}-^{117}\text{Sn})$ couplings constants (≤ 85 Hz) due to the result of an elongated Sn_9 framework having endohedral transition metal atoms.^[116, 117]

The dynamic exchange of the Sn_9 core of the $\text{Sn}_9\text{SnCy}_3^{3-}$ ion appears to go through the traditional "diamond-square-diamond" exchange mechanism as evidenced by the typical 295 Hz $^{119}\text{Sn}-^{117}\text{Sn}$ satellites on the -1172 ppm central resonance. In addition to the dynamic exchange of the core, the Cy_3Sn substituent rapidly scrambles around the outside of the Sn_9 cluster in sharp contrast to the alkyl ligand. The proposed mechanism is shown in Figure 3.8 a. The *exo*-bonded SnCy_3 group must undergo an intramolecular "walk" around the Sn_{1-9} core to exchange all 9 vertex atoms. The first step in this process involves a migration of the SnCy_3 group from Sn_1 to Sn_5 . As the SnCy_3 group migrates and forms a bond between Sn_5 and Sn_{10} , the bond between Sn_5 and Sn_6 is broken. Concurrently, a bond is made between Sn_1 and Sn_3 . The transition state in this process involves a pseudo- D_{3h} like structure defined by tricapped trigonal prismatic Sn_9 core with the SnCy_3 group symmetrically bridging the Sn_1 - Sn_5 edge (e.g. $\text{Ph}_3\text{SnGe}_9^{3-}$). The $\text{C}_{4v} - \text{D}_{3h} - \text{C}_{4v}$ exchange process of the Sn_9 core is identical to that proposed for Sn_9^{4-} by Corbett.^[136] Continuing this process will exchange all atoms within the Sn_{1-9} core. Moreover, the crystal structure shows the cluster is distorted towards this transition-state geometry. Importantly, this concerted process prevents any of the vertex Sn atoms from exceeding a 5-coordinate environment and always leaves the SnCy_3 group on the open square face (the preferred site). The observation of the difference in the J couplings for the fluxional clusters can be generalized for the type of the substituent groups. When the

substituent group can scramble around the cluster, which also been observed for the Sn_9H^{3-} ion (Chapter 2), the J coupling for the fluxional cluster remains large, whereas it decreases for a non-mobile substituent group as in the Sn_9R^{3-} ions ($\text{R} = \text{}^t\text{Bu}, \text{}^i\text{Pr}$).

3.3. Conclusion

The three new substituted Sn_9R^{3-} clusters in this study have been synthesized and the effect of the different substituent groups on the exchange mechanism of the Sn_9 cluster has been studied in detail.

^{119}Sn NMR studies show that the Sn_9R^{3-} ions ($\text{R} = \text{}^i\text{Pr}, \text{SnCy}_3, \text{Sn}(\text{}^n\text{Bu})_3$) are highly fluxional in solution even at $-50\text{ }^\circ\text{C}$. They exhibit substituent dependent exchange mechanisms. The exchange mechanism of $\text{Sn}_9\text{SnR}_3^{3-}$ ions ($\text{R} = \text{Cy}, \text{}^n\text{Bu}$) exhibits rapid migration of the SnCy_3 and Sn^nBu_3 groups around the cluster, while all 9-Sn atoms of the cluster core have an intramolecular square-diamond-square exchange mechanism. The $\text{Sn}_9\text{-}^i\text{Pr}^{3-}$ ion have a non-mobile substituents group, which removes the *exo*-bonded Sn atom from exchanging with the remaining 8-Sn atoms of the cluster. The $J(^{119}\text{Sn}\text{-}^{117}\text{Sn})$ coupling constants for the equivalent Sn atoms of the cluster atoms are also specific for the different type of the substituent, which also supports different exchange mechanisms. While this coupling constant is very similar to the parent Sn_9^{4-} ion for the SnCy_3 substituents, the ^iPr substituted cluster has smaller coupling constants.

3.4. Experimental Section

3.4.1. General Data

The ^{119}Sn NMR spectra were recorded on a Bruker DRX500 AVANCE spectrometer at 186.5 MHz. In all measurements, to avoid RF heating, a high nitrogen flow rate was used in combination with a temperature controller. A standard Bruker pulse sequence was used. A 30 degree pulse strength and 1.0 s relaxation delays were used. An approximate 200 dummy scans prior recording data were used. A macro automation program was written so that multiple block searches of 300 ppm were used in locating the ^{119}Sn signal. The spectral window -2500 to +3000 ppm was searched by this method. The signals were confirmed and verified by repeating the final measurements with different transmitter offsets. The ^{119}Sn chemical shifts were calibrated to Me_4Sn , external standard in C_6D_6 (0 ppm) at room temperature. Temperature calibration was done by using methanol for variable temperature ^{119}Sn NMR experiments. Both the ^1H and $^{13}\text{C}^{[160]}$ spectra of $[\text{K}(2,2,2\text{-crypt})]_3[\text{Sn}_9\text{-SnCy}_3]_2\text{py}$ were recorded on a Bruker DRX500 AVANCE spectrometer at 500.13 MHz and 125 MHz, respectively, and chemical shifts were referenced to TMS. The ^1H spectra of $[\text{K}(2,2,2\text{-crypt})]_3[\text{Sn}_9\text{-}^i\text{Pr}]_2\text{py}$ were recorded on a Bruker AVIII-600 MHz spectrometer at 600.13 MHz and chemical shifts were referenced to TMS. 1D gradient selective HMBC experiment was carried out with the standard Bruker pulse program. A 90° pulse durations were applied for the ^{119}Sn channel and offsets are set to the previously recorded ^{119}Sn resonances. The “constant 2” ($d_2 = 1/2J(^{119}\text{Sn}\text{-}^1\text{H})$) was calculated by using a typical $^2J(^1\text{H}\text{-}^{119}\text{Sn}) = 54$ Hz coupling constant. The frequencies for ^1H and ^{119}Sn are 500.13 MHz and 186.5 MHz correspondingly. The

^1H FID resolution used was 0.27 Hz per data point and 1000 scans were used. The ^{119}Sn offset was sequentially set to the observed ^{119}Sn signals for $\text{Sn}_9\text{SnCy}_3^{3-}$; 155 ppm and -1172 ppm correspondingly. The percentage yields were calculated by considering the amount of alloy precursor K_4Sn_9 that was used.

3.4.2. Chemicals

Melts of nominal composition K_4Sn_9 were made by fusion of stoichiometric ratios of the elements at high temperature under N_2 atmosphere. The chemicals were loaded in silica tubes and heated carefully with a natural gas/oxygen flame. **Caution:** *molten alloy synthesis can result in serious explosion and reactions should be conducted with great caution behind blast shields.* 4,7,13,16,21,24-Hexaoxa-1,10-diazobicyclo[8,8,8]hexacosane (2,2,2-crypt) was purchased from Fisher Scientific. Tricyclohexyl tin chloride and tributyl tin chloride were purchased from Aldrich. 2-chloropropane ($^i\text{PrCl}$) was purchased from Across Organics and vacuum distilled from CaCl_2 . Anhydrous ethylenediamine (en) and dimethylformamide (dmf) were purchased from Fisher, vacuum distilled from K_4Sn_9 , and stored under dinitrogen. Toluene was distilled from sodium/benzophenone under dinitrogen and stored under dinitrogen. Pyridine (py) was distilled from KOH under dinitrogen and stored under dinitrogen. All reactions were performed in a nitrogen atmosphere drybox.

3.4.3. Synthesis

Synthesis of $[\text{K}(2,2,2\text{-crypt})]_3[\text{Sn}_9\text{-}^i\text{Pr}]\cdot 2\text{py}$

In a glass vial 1, K_4Sn_9 (60 mg, 0.049 mmol) and 2,2,2-crypt (110 mg, 0.292 mmol) were dissolved in 3 mL of ethylenediamine. In glass vial 2, 1ml of ethylenediamine was added to 7 μl of $^i\text{PrCl}$ (0.011 M, 0.077 mmol). Solution from

vial 2 was added dropwise to vial 1, and the reaction mixture was stirred for a 30 minutes. The ethylenediamine was removed under vacuum. The remaining solid material was redissolved in 2.5 mL of pyridine. After filtration through tightly packed glass wool, solution was layered with 4 mL of toluene. After 24 hours, the black crystals of $[\text{K}(2,2,2\text{-crypt})]_3[\text{Sn}_9\text{.}^i\text{Pr}]\cdot 2\text{py}$ (45 mg, 82%) were obtained. $\delta^{119}\text{Sn}$ / ppm (186.4 MHz; dmf; Me_4Sn ; 25 °C) -1413 (8 Sn, $J(^{119}\text{Sn}\text{-}^{117}\text{Sn})$; 1793 Hz, $J(^{119}\text{Sn}\text{-}^{119}\text{Sn})$; 1876 Hz, $J(^{119}\text{Sn}\text{-}^{117}\text{Sn})$; 115 Hz, Sn(2-9)). 170 (1 Sn, $J(^{119}\text{Sn}\text{-}^{119/117}\text{Sn})$) 1844 Hz, Sn(1)). $\delta^1\text{H}$ / ppm (600 MHz, pyridine- d_5 , 25 °C) 3.44 (s, 2,2,2-crypt), 3.37 (t, 2,2,2-crypt), 2.36 (t, 2,2,2-crypt), 2.20 (d, $J = 7.19$ Hz, $-\text{CHMe}_2$), 2.41 (septet, $J = 7.19$, CHMe_2). $\delta^{13}\text{C}$ / ppm (pyridine- d_5 , 25 °C) 70.7 (2,2,2-crypt), 67.91 (2,2,2-crypt), 54.16 (2,2,2-crypt), 32.16 ($-\text{CHMe}_2$), and 29.79 ($-\text{CHMe}_2$ of ^iPr)

Synthesis of $[\text{K}(2,2,2\text{-crypt})]_3[\text{Sn}_9\text{SnCy}_3]\cdot 2\text{py}$

In glass vial 1, a solution of K_4Sn_9 (80 mg, 0.065 mmol) and 2,2,2-crypt (82 mg, 0.22 mmol) in 1 mL of ethylenediamine was stirred for 30 minutes. The ethylenediamine was removed under vacuum. The remaining solid material was redissolved in 2.5 mL of pyridine. In glass vial 2, Cy_3SnCl (29 mg, 0.072) was dissolved in 1 ml of toluene. Solution from vial 2 was added dropwise to vial 1, and the reaction mixture was stirred for a 30 min. After filtration through tightly packed glass wool, solution was layered with 2 mL of toluene. After two days, purple-red crystals of the $[\text{K}(2,2,2\text{-crypt})]_3[\text{Sn}_9\text{SnCy}_3]\cdot 2\text{py}$ (67 mg, 72%) were formed. $\delta^{119}\text{Sn}$ / ppm (dmf, 25 °C) -1172 (9 Sn, $J(^{119}\text{Sn}\text{-}^{117}\text{Sn})$; 1272 Hz , $J(^{119}\text{Sn}\text{-}^{119}\text{Sn})$; 1331 Hz, $J(^{119}\text{Sn}\text{-}^{117}\text{Sn})$; 295 Hz , Sn(1-9)). 155 (1 Sn, $J(^{119}\text{Sn}\text{-}^{117}\text{Sn})$; 1272 Hz , $J(^{119}\text{Sn}\text{-}^{119}\text{Sn})$; 1331 Hz, Sn(10)). $\delta^1\text{H}$ / ppm (pyridine- d_5 , 25 °C) 4.59 (s, 2,2,2-crypt), 4.52 (t, 2,2,2-

crypt), 3.51 (t, 2,2,2-crypt), 3.23 (m, -Cy), 2.97 (m, -Cy), 2.78 (m, -Cy), 2.52 (m, -Cy). $\delta^{13}\text{C}$ / ppm (pyridine- d_5 , 25 °C) 70.70 (2,2,2-crypt), 67.90 (2,2,2-crypt), 54.20 (2,2,2-crypt), 34.43 (-Cy), 30.82 (-Cy), 30.67 (-Cy), 28.40 (-Cy).

Synthesis of $[\text{K}(2,2,2\text{-crypt})]_3[\text{Sn}_9\text{Sn}(\text{}^n\text{Bu})_3]$

In vial 1, a solution of K_4Sn_9 (80 mg, 0.065 mmol) and 2,2,2-crypt (82 mg, 0.22 mmol) in 1 mL of ethylenediamine was stirred for 30 min. The ethylenediamine was removed under vacuum. The remaining solid material was redissolved in 2.5 mL of pyridine. In vial 2, the $(\text{}^n\text{Bu})_3\text{SnCl}$ (23 mg, 0.072) was dissolved in 1 ml of toluene. Solution from vial 2 was added dropwise to vial 1, and the reaction mixture was stirred for a 30 min. After filtration through tightly packed glass wool, solution was layered with 2 mL of toluene. $\delta^{119}\text{Sn}$ / ppm (py/tol, 25 °C) -1119 (9 Sn, $J_{119\text{Sn}-117\text{Sn}}$; 1330 Hz $J(^{119}\text{Sn}-^{117}\text{Sn})$; 278 Hz, Sn1-9). 62 (1 Sn, $J(^{119}\text{Sn}-^{119/117}\text{Sn})$; 1330 Hz, Sn10).

Crystallographic Studies

The crystal structures of the $\text{Sn}_9\text{-}^i\text{Pr}^{3-}$ and $\text{Sn}_9\text{SnCy}_3^{3-}$ anions were determined at single crystal X-ray facility at Chemistry and Biochemistry Department, University of Maryland, by Dr. Peter Zavalij.

Chapter 4: Endohedral Derivatives of Exo-substituted Zintl

Clusters

4.1. Introduction

Many group 14 clusters with transition metals have been prepared from reactions between E_9^{4-} Zintl ions ($E = \text{Si, Ge, Sn, Pb}$) and transition metal complexes since Rudolph first described the reactions of Sn_9^{4-} with $\text{Pt}(\text{PPh}_3)_4$.^[93, 172] Using low valent transition metal complexes that have labile ligands (*e.g.* $\text{Pt}(\text{PPh}_3)_4$), ligand-free naked metal atoms can be inserted inside the E_9^{4-} ions to form endohedral clusters. For example, Cu^+ reacts with Sn_9^{4-} to give $\text{Cu}@\text{Sn}_9^{3-}$ in a well-defined reaction, exhibiting both mass and charge balance.^[116] Isoelectronic to this cluster, the $\text{Pt}@\text{Sn}_9\text{H}^{3-}$ ion has been synthesized and characterized by NMR studies although it was not been isolated.^[115] Most other reactions appear to involve partial oxidation of the E_9^{4-} ions with sacrificial reduction of ligands or solvent. For example, Sn_9^{4-} and $\text{Pt}(\text{PPh}_3)_4$ react in a 1:2 ratio to give $\text{Pt}@\text{Sn}_9\text{Pt}(\text{PPh}_3)^{2-}$ and H_2 gas resulting from the reduction of the ethylenediamine (en) solvent.^[117] Other reactions give oxidized clusters for which the fate of "lost electrons" is not so clear, such as in the formation of the paramagnetic $\text{Ni}@\text{Sn}_9\text{Ni}(\text{CO})^{3-}$ cluster.^[117] The disproportionation reactions to give $\text{M}@\text{E}_{10}^{2-}$ and $\text{M}@\text{E}_{12}^{n-}$ clusters ($\text{M} = \text{Ni, Pd, Pt, Ir}$; $\text{E} = \text{Pb, Sn}$ and $n = 2, 3$) are even more complicated and their mechanism of formation is not clear.^[121, 122]

Stepwise reactions of converting one cluster ion into another can provide valuable mechanistic insight into endohedral cluster formation, yet examples of such transformations are few in number.^[99, 100, 103, 119, 121] The conversion $\text{Ge}_9^{4-} \rightarrow$

$\text{Ni@Ge}_9^{3-} \rightarrow \text{Ni@Ge}_9\text{Ni(CO)}^{2-}$ is one example of a sequential reaction, and except for the two electrons lost from the Ge_9^{4-} precursor, it represents a balanced transformation.^[99] However, the mechanisms of other transformations are not as straight forward, such as the reaction of $\text{Ge}_9\text{Pd(PPh}_3\text{)}^{3-}$ with $\text{Ni(PPh}_3\text{)}_4$ to give $\text{Ni@Ge}_9\text{Pd(PPh}_3\text{)}^{2-}$.^[100] In addition, a variety of ligands can coordinate to the vertex metal atoms, as illustrated in the complexes $\text{Ni@Ge}_9\text{Ni(CO)}^{2-}$, $\text{Ni@Ge}_9\text{Ni(PPh}_3\text{)}^{2-}$, $\text{Ni@Ge}_9\text{Ni(en)}^{3-}$ and $\text{Ni@Ge}_9\text{Ni(CCPh)}^{3-}$.^[4]

More recent studies have shown that the E_9^{4-} ions can form *exo*-functionalized derivatives containing covalently-bonded substituents on the exterior of the clusters. In particular, the RGe_9^{3-} , $\text{R}_2\text{Ge}_9^{2-}$, $\text{RGe}_9\text{-Ge}_9\text{R}^{4-}$ and RSn_9^{3-} clusters where R is an *exo*-bonded alkyl or post-transition metal group (*e.g.* R = ^tBu, SbPh₃) have been prepared from nucleophilic substitution reactions.^[78, 79, 81] Unlike the multi-center two-electron bonding within the E_9 clusters, the *exo* substituents are attached to the clusters through two-center, two-electron bonds. The substituents are known to affect the solubility and dynamic properties of the clusters, however, the reactivity of these ions have not been studied in detail.

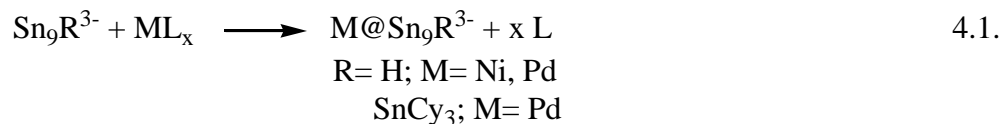
In this chapter, we describe synthesis and characterization of *exo*-substituted endohedral Zintl clusters, $\text{M@Sn}_9\text{R}^{3-}$ (M = Pd, Ni, R = H, SnCy₃). Stepwise conversions of $\text{Sn}_9\text{H}^{3-} \rightarrow \text{Ni@Sn}_9\text{H}^{3-} \rightarrow \text{Ni@Sn}_9\text{SnCy}_3^{3-}$ and $\text{Sn}_9\text{SnCy}_3^{3-} \rightarrow \text{Pd@Sn}_9\text{SnCy}_3^{3-} \rightarrow \text{Pd@Sn}_9\text{PdSnCy}_3^{3-}$ will be discussed. To our knowledge, these are the first reactivity studies of *exo*-compounds of the group 14 Zintl ions. The synthesis and characterization of the $\text{Ni@Ge}_9\text{H}^{3-}$ ion will also be discussed in this chapter. Effects of endohedral transition metals on structures of the *exo*-substituted clusters

and their solution dynamics compared to the parent non-endohedral clusters will be discussed.^[173]

4.2. Results and Discussion

4.2.1. Synthesis

Reactions of the Sn_9R^{3-} (R= H, SnCy_3) ions with transition metal precursors having labile PPh_3 and cod ligands gives the endohedral derivatives of these *exo*-substituted $\text{M@Sn}_9\text{R}^{3-}$ according to eq.4.1. Formation of the endohedral $\text{M@Sn}_9\text{H}^{3-}$ $\text{Pd@Sn}_9\text{SnCy}_3^{3-}$ ions are inclusion reactions of the transition metal atoms into the parent substituted clusters of Sn_9H^{3-} and $\text{Sn}_9\text{SnCy}_3^{3-}$.

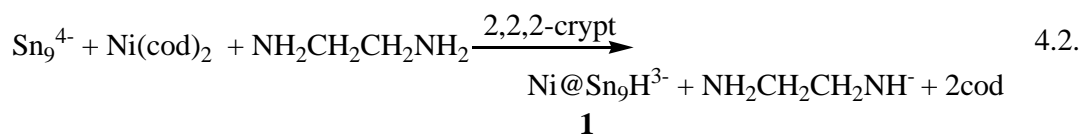


Further reactivities of the $\text{M@Sn}_9\text{R}^{3-}$ ions (M=Pd; R= SnCy_3 and M= Ni; R= H) have been investigated. The $\text{Ni@Sn}_9\text{SnCy}_3^{3-}$ ion forms via the intermediate cluster of $\text{Ni@Sn}_9\text{H}^{3-}$ by exchanging the hydride substituent by the SnCy_3 group. In this conversion reaction, *in-situ* formed amide ions are anticipated to accept H^+ ions to form ethylenediamine. Synthetic protocol for the $\text{Ni@Sn}_9\text{SnCy}_3^{3-}$ ion is different than its Pd analog, obtained by inclusion of Pd metal into $\text{Sn}_9\text{SnCy}_3^{3-}$ cluster. The $\text{Pd@Sn}_9\text{SnCy}_3^{3-}$ ion further reacts with the Pd metal precursor to give the $\text{Pd@Sn}_9\text{PdSnCy}_3^{3-}$ cluster through an oxidative insertion of a Pd atom into the *exo* $\text{Pd@Sn}_9\text{—SnCy}_3$ bond.

The studies to obtain similar Pt metal derivatives were unsuccessful. The reaction of $\text{Sn}_9\text{SnCy}_3^{3-}$ with the $\text{Pt}(\text{PPh}_3)_4$ complex resulted in a ^{119}Sn NMR signal at -480 ppm, which has not been reported for any Pt-Sn Zintl cluster. However, under different reaction conditions, the coordination complex of $\text{PtH}(\text{PPh}_3)(\text{Cy}_3\text{Sn})_2^-$ and $\text{Pd}@\text{Sn}_9\text{PtSnCy}_3^{3-}$ ion were obtained. The synthesis and XRD structures of these two ions will be given in the Appendices of this thesis.

In the following paragraphs the detailed syntheses of the Ni and Pd derivatives of the substituted clusters are discussed. Isolation of crystalline product from the reaction mixtures containing multiple constituents showed that when the two cluster ions have similar crystallographic structures, it can result in co-crystallization of the ions. Although, it is not common in this field, some rare cases have also reported similar occupation of the two different clusters in the same unit cell such as, the $\text{Ni}@\text{Ge}_9^{3-}/\text{Ge}_9^{3-}$ ions.^[126]

Ni@Sn₉H³⁻: En solutions of K_4Sn_9 and 4 equivalents of 2,2,2-crypt react with solid $\text{Ni}(\text{cod})_2$ to give the $\text{Ni}@\text{Sn}_9\text{H}^{3-}$ (**1**) cluster ion (eq.4.2.).

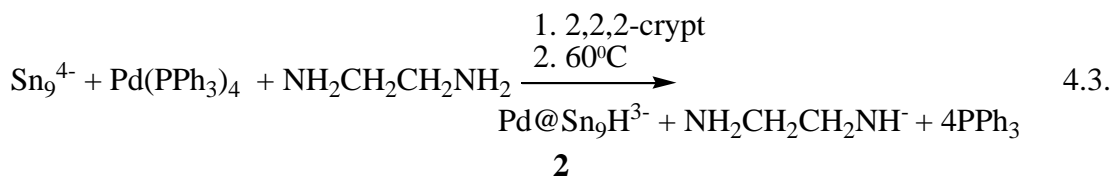


Crystal growth from the reaction mixture results in co-crystallization of the two clusters, the Ni centered and empty Sn_9H^{3-} clusters with a ratio of 0.4:0.6, respectively as $[\text{K}(2,2,2\text{-crypt})]^+$ salt, in ca. 32% yield of the $\text{Ni}@\text{Sn}_9\text{H}^{3-}$ component. Starting with two equivalents of $\text{Ni}(\text{cod})_2$ also results in the same two ions in the

crystalline product, but with a higher occupancy of the Ni@Sn₉H³⁻ (**1**) ion in the unit cell and a ratio of 0.9:0.1, relative to the empty Sn₉H³⁻ cluster. Since the latter crystalline product has a higher occupation factor of Ni centered ion, for the detailed single crystal XRD analysis of these crystals were used. The air and moisture sensitive red crystals were also characterized by ¹¹⁹Sn, and ¹H NMR spectroscopy.

In earlier studies by Esenturk et al. showed that en solutions of K₄Sn₉ react with and toluene solutions of the Ni(cod)₂ to give the fused cluster ion Ni₂@Sn₁₇⁴⁻.^[128] However, controlling the dissolution of the Ni(cod)₂ precursor by adding it as solid results in Ni@Sn₉H³⁻ cluster (**1**) as the only metallated product in a good yield.

Pd@Sn₉H³⁻: Ethylenediamine (en) solutions of K₄Sn₉ and 4 equivalents of 2,2,2-crypt react with solid Pd(PPh₃)₄ at 60 °C, to give the Pd@Sn₉H³⁻ cluster ion (**2**). The balanced equation is summarized in eq.4.3., and en is also the proton source.

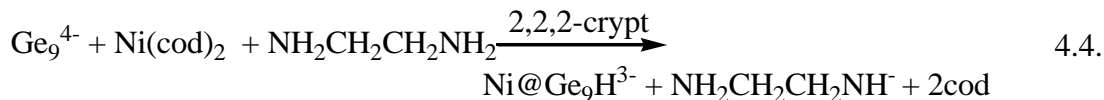


Air and moisture sensitive red-orange crystals of **2** are obtained as [K(2,2,2-crypt)]⁺ salts in 10% crystalline. These salts have been characterized by ¹¹⁹Sn and ¹H NMR spectroscopy. In earlier studies, the Pd@Sn₉H³⁻ ions were also synthesized by Dr. Melani Moses as a [Na(2,2,2-crypt)]⁺ salt, and the single crystal XRD analysis was determined by Dr. James Fettingner.

The yield of crystalline salt Pd@Sn₉H³⁻ is low due to other competing reactions yielding Pd₂@Sn₁₈⁴⁻ ion in the same reaction mixture, which will be

discussed in Chapter 6. Reaction of solid Pd(PPh₃)₄ with K₄Sn₉ favors formation of Pd@Sn₉H³⁻ in a higher yield, but still it forms along with Pd₂@Sn₁₈⁴⁻ cluster. Heating the solutions resulted in precipitation of the thermally unstable Pd₂@Sn₁₈⁴⁻ cluster, and resulted in isolation of the Pd@Sn₉H³⁻ cluster.

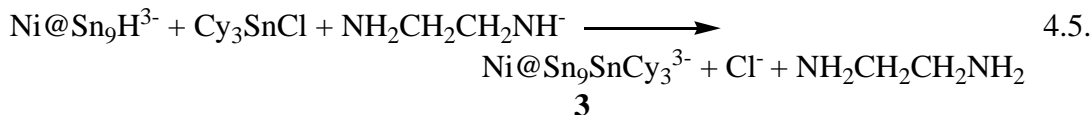
Ni@Ge₉H³⁻: K₄Ge₉ and 2,2,2-crypt in en solution react with two equivalents of solid Ni(cod)₂ to give Ni@Ge₉H³⁻ according to eq.4.4. The synthesis of the Ni@Ge₉H³⁻ cluster was described in earlier studies and was characterized by single crystal XRD and Mass spectrometry.^[126] However, the cluster was incorrectly reported to be a paramagnetic Ni@Ge₉³⁻ ion. The structural similarities to the M@Sn₉H³⁻ series (M= Ni, Pd, Pt) led us to repeat the syntheses as previously described, but we have not repeated the structure analysis.



Similar to the Ni@Sn₉H³⁻ ion, the Ni@Ge₉H³⁻ ion was also reported to crystallize with 3 [K(2,2,2-crypt)]⁺ cations together with its non-interstitial analog Ge₉H³⁻, incorrectly reported to be Ge₉³⁻ ion in the crystal lattice with an occupation ratio of 0.85:0.15. In this study, we characterized Ni@Ge₉H³⁻ ion by ¹H NMR spectroscopy.

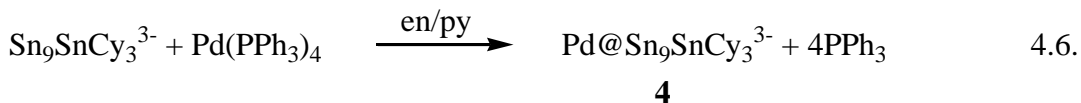
Ni@Sn₉SnCy₃³⁻: En solutions of the Ni@Sn₉H³⁻ cluster react with toluene solutions of Cy₃SnCl to give the Ni@Sn₉SnCy₃³⁻ cluster ion (**3**). The proposed equation is given in eq.4.5. The Ni@Sn₉H³⁻ cluster (**1**) product is synthesized as

described earlier in this chapter from the reaction of K_4Sn_9 and $\text{Ni}(\text{cod})_2$ in en in the presence of 2,2,2-crypt.



The red crystalline $[\text{K}(2,2,2\text{-crypt})]_3[\text{Ni@Sn}_9\text{SnCy}_3]_{0.9}[\text{Ni@Sn}_9\text{H}]_{0.1}$ salt of **3** was obtained in 20% yield. The air and moisture sensitive salt has been characterized by single crystal XRD and by ^1H , ^{13}C , and ^{119}Sn NMR spectroscopy.

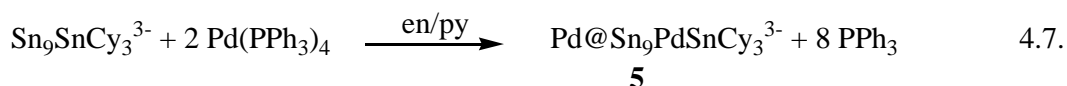
Pd@Sn₉SnCy₃³⁻: The cluster $\text{Pd@Sn}_9\text{SnCy}_3^{3-}$ (**4**) is obtained from the reaction of $\text{Sn}_9\text{SnCy}_3^{3-}$ ion (Chapter 3) and solid $\text{Pd}(\text{PPh}_3)_4$ in a 1:1 stoichiometry in en/py solutions as shown in equation 4.6.



The ion **4** co-crystallized with the empty $\text{Sn}_9\text{SnCy}_3^{3-}$ ion in a ratio of 0.68:0.32 as a $[\text{K}(2,2,2\text{-crypt})]^+$ salt, 27% crystalline yield based on the $\text{Sn}_9\text{SnCy}_3^{3-}$ precursor used for the reaction. The red crystals have been characterized by single crystal XRD and NMR spectroscopy.

Slow additions of solid $\text{Pd}(\text{PPh}_3)_4$ to en/py solutions of the $\text{Sn}_9\text{SnCy}_3^{3-}$ ion in equimolar amounts produces **4** almost exclusively, as evidenced by ^{119}Sn NMR studies. However, this process produces **4** as a polycrystalline powder product, which is not suitable for the structure analysis.

Pd@Sn₉PdSnCy₃³⁻: The Pd@Sn₉PdSnCy₃³⁻ cluster (**5**) forms as a result of the reaction between the Sn₉SnCy₃³⁻ cluster and 2 equivalents of the Pd(PPh₃)₄ complex in en/py solutions as shown in eq. 4.7. The black crystalline [K(2,2,2-crypt)]⁺ salt of **5** was obtained with a 60% crystalline yield. It was characterized by single crystal XRD, ¹¹⁹Sn, ¹³C and ¹H NMR spectroscopy. The air sensitive cluster ion is thermally stable up to 100°C in solutions under N₂ atmospheres.



4.2.2. Solid State Structure

Except the structure of the 10 vertex Pd@Sn₉PdSnCy₃³⁻ cluster (**5**), the structure of the M@Sn₉R³⁻ clusters **1-4** (M= Ni, Pd, R= H, SnCy₃) are all 9-vertex clusters with an *exo*-substituent. The M@Sn₉ cluster frameworks adopt distorted tricapped trigonal prismatic geometries as in Sn₉H³⁻ ion (Chapter 2). As described in Chapter 2, the tricapped trigonal prism is defined by the smallest ratio of average prism height (h) /average prism edge (e) among three virtual trigonal prisms. The deviation in the prism heights compared to the monocapped trigonal prismatic geometry of Sn₉⁴⁻ ion is an indication of the distortion from the ideal C_{4v} symmetry.

The crystallographic data for M@Sn₉H³⁻ (M= Ni (**1**), Pd (**2**)) are given in Table 4.1. The structure analysis of **2** was done with the crystals of the [Na(2,2,2-crypt)]⁺ salt; and cluster **1** was crystallized as [K(2,2,2-crypt)]⁺ salt. Crystal lattices of both salts of cluster ions **1** and **2** are monoclinic space group, P2₁/n. However, they are not isomorphic since the Ni occupied unit cell has two independent Ni@Sn₉H³⁻ ions.

Table 4.1. Crystallographic data for the M@Sn₉H³⁻ (M= Pd, Ni) ions.

Compound	[K(2,2,2crypt)] ₃ [1].1/2en.tol ^b [Ni@Sn ₉ H] _{0.9} [Sn ₉ H] _{0.1}	[Na(2,2,2-crypt)] ₃ [2]-en [Pd@Sn ₉ H]
formula weight		2433.2
temperature (K)		193(2)
Wavelength (Å)	0.71073	0.71073
crystal system	Monoclinic	Monoclinic
space group	P2 ₁ /c	P2 ₁ /n
unit cell dimensions		
a (Å)	28.212(3)	18.962(2)
b(Å)	23.516(3)	20.869(2)
c (Å)	27.828(3)	21.274(3)
α (°)	90	90
β (°)	93.589(1)	93.081(2)
γ (°)	90	90
volume (Å ³)	18425.6	8405.9(2)
Z		4
D _{calc} (Mg/m ³)		1.923
Abs. coeff. (mm ⁻¹)		2.91
final R indices(all data) ^a		
R1, I>2σ(I)		0.0372
wR2,		0.0783

^a $R_1 = \sum ||F_o| - |F_c|| / \sum |F_o|$, $wR_2 = [\sum w(F_o^2 - F_c^2)^2 / \sum w(F_o^2)^2]^{1/2}$ ^b Preliminary data

As shown in Figure 4.1a and 4.1c, both structures are 9-vertex clusters with endohedral Ni and Pd metal atoms, respectively. Since the electron density of a hydrogen atom is small and difficult to discern within the close proximity to the cluster, the hydride ligands could not be crystallographically located. The theoretical DFT calculations of the minimized energy structure of the Ni@Sn₉H³⁻ ion have been done by Prof. Andrei Vedernikov. In the optimized structure, the hydride substituent is located as a bridging ligand with two bonding contacts to the Sn3 and Sn6 atoms as shown in Figure 4.1b. The structure of the ions and calculated location of the hydride ligand are similar to the M@Sn₉SnCy₃³⁻ ions (M= Ni, Pd).

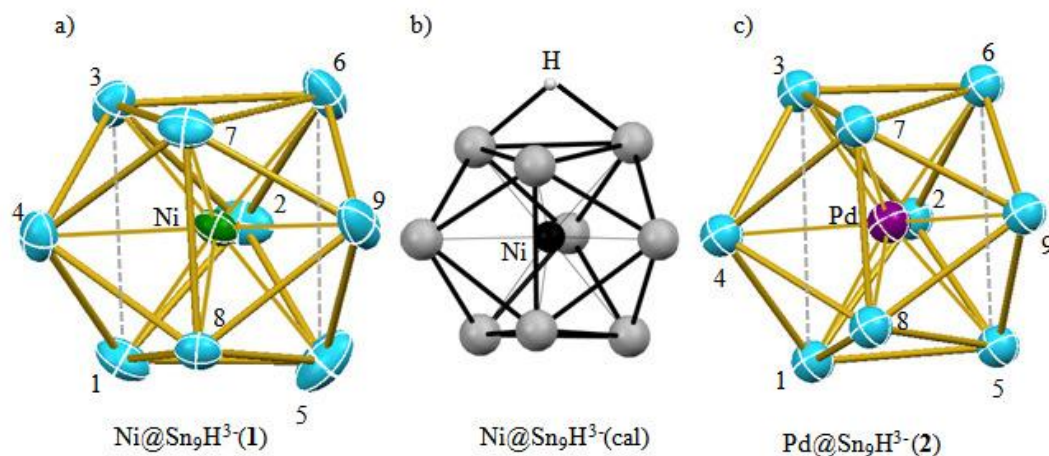


Figure 4.1. ORTEP drawing of the $M@Sn_9H^3-$ ions; a) $M= Ni$ **1**, b) energy optimized structure of $Ni@Sn_9H^3-$ ion, and c) $M= Pd$ **2**. Thermal ellipsoids are set at the 50% probability level. The dotted lines represent the contacts between $3.4 < x < 3.7$ Å, whereas solid lines denotes the bond lengths less than 3.4 Å.

The summary of the selected bond lengths of ions **1** and **2** are given in the Table 4.2. Ignoring the hydride ligands, structures of both anions (Figure 4.1) have virtual C_{2v} symmetry with a two-fold rotation axes passing through the endohedral transition metal atoms and the capping Sn2 atom. However, considering a bridging hydride, located by the theoretical calculations of the energy optimized structure shown in Figure 4.1c, the symmetry of the ions reduce to C_s with a mirror plane defined by Sn2, Sn7, Sn8, and the endohedral transition metals. The geometry of the clusters is distorted from a mono capped square anti-prism towards a tricapped trigonal prism. Both structures have 1 short and two elongated prism heights. For the $Pd@Sn_9H^3-$ ion, one of the prism heights is 3.192 Å (Sn7-8); and two prism heights of the virtual prism are elongated and non-bonding (Sn5-Sn6 4.289 Å, Sn1-Sn3 4.140 Å). Compared to the prism heights of the Sn_9H^3- ion, in the **2** the Sn7-8 is shortened by 0.8%, whereas other prism heights Sn5-6 and Sn7-8 are elongated by 21% and

28%, respectively. Similarly, one of the prism heights of the $\text{Ni@Sn}_9\text{H}^{3-}$ ion, Sn7-8, is shortened by 18%, whereas the Sn5-6 and Sn1-3 are elongated by 21% and 6% compared to the Sn_9H^{3-} ion respectively. However, the co-crystallization of the Sn_9H^{3-} ion hinders this comparison.

The reported structure for the Ni@Ge_9^{3-} ion is also very similar in elongation of the specific trigonal prism heights of the cluster (Figure 4.7a).^[126] Including a hydride ligand on the cluster ion gives it a molecular formula of $\text{Ni@Ge}_9\text{H}^{3-}$, and it is isoelectronic to the $\text{M@Sn}_9\text{H}^{3-}$ ions **1** and **2**. On the other hand, the idealized D_{3h} symmetric Cu@Sn_9^{3-} cluster,^[116] which is also isoelectronic with the $\text{M@E}_9\text{H}^{3-}$ clusters (E= Ge, Sn), has 3 prism heights that are symmetrically elongated. The distortions in the $\text{M@E}_9\text{H}^{3-}$ ions (E= Ge, Sn, M= Ni) are quite distinct and are presumably a result of the $\mu\text{-H}$ ligand.

The Ni centered cluster **1**, has Sn-Sn bond lengths ranging between 2.923 (3) Å - 3.429(4) Å. The Pd centered cluster **2** has Sn-Sn bond lengths ranging between 2.914 (2) Å - 3.402 (3) Å. Both of the cluster anions have Sn-Sn contacts consistent with the typical bond lengths of the 9-vertex Sn_9^{4-} cluster. However, Sn-Sn bonds are typically elongated in the presence of an endohedral transition metal atom. For the true comparison of the elongation, all 21 Sn-Sn contacts that are present for the Sn_9H^{3-} cluster were taken as a reference. While the non-interstitial Sn_9H^{3-} ion (Chapter 2) has an average Sn-Sn bond length of 3.035 ± 0.120 , the average Sn-Sn contacts are 3.123 ± 0.26 Å and 3.248 ± 0.34 Å for the clusters **1** and **2**, respectively. The M-Sn average bond lengths are 2.597 ± 0.14 Å for cluster **1** and 2.693 ± 0.03 Å for

2 in agreement with the covalent radii of the parent transition metals: Ni, 1.15 Å; Pd, 1.28 Å.

The cluster anions **1** and **2** are 9-vertex 22 e⁻ *nido* clusters, in a Wade-Mingos description. In this analysis, there are 18 electrons from the 9-atom Sn cluster (2x9); 1 electron for the hydrogen substituent; and 3 electrons due to charge, giving a total of 22 cluster bonding electrons (c.b.e.). This situation corresponds to a 2n+4 *nido* cluster when n=9 and are isoelectronic with the Sn₉⁴⁻ ion. A zero valent d¹⁰ transition metal does not contribute any electrons to the c.b.e.

Table 4.2. Selected Bond Lengths [Å] for the M@Sn₉H³⁻ (M= Ni, Pd) clusters

Distances	Ni@Sn ₉ H ³⁻	Pd@Sn ₉ H ³⁻	Distances	Ni@Sn ₉ H ³⁻	Pd@Sn ₉ H ³⁻
Sn1-5	3.137(2)	2.914(2)	Sn1-M	2.601(3)	2.679(2)
Sn1-2	2.967(3)	3.160(2)	Sn2-M	2.640(2)	2.667(7)
Sn2-5	2.996(2)	3.214(2)	Sn3-M	2.590(2)	2.661(2)
Sn2-6	3.055(4)	3.191(2)	Sn4-M	2.649(2)	2.716(2)
Sn2-3	3.087(2)	3.251(2)	Sn5-M	2.590(3)	2.669(4)
Sn3-6	2.989(2)	3.975(2)	Sn6-M	2.617(2)	2.705(2)
Sn3-4	3.049(3)	3.051(2)	Sn7-M	2.621(2)	2.726(3)
Sn1-4	2.989(2)	3.082(2)	Sn8-M	2.586(2)	2.665(2)
Sn4-8	2.943(3)	3.024(2)	Sn9-M	2.761(3)	2.751(2)
Sn8-9	2.923(3)	3.076(2)	Sn7-4	3.015(3)	3.061(4)
Sn5-8	3.353(2)	3.193(2)	Sn7-3	3.099(3)	3.333(3)
Sn5-9	2.988(3)	3.058(2)	Sn7-6	3.184(3)	3.333(2)
Sn6-9	2.981(2)	3.026(2)	Sn1-8	3.429(4)	3.402(3)
Sn7-9	3.038(3)	3.103(4)	Sn1-3	3.916(3)	4.140(3)
Sn7-8	3.287(2)	3.192(4)	Sn6-5	3.751(3)	4.289(3)

The crystallographic data for M@Sn₉SnCy₃³⁻ (M= Ni (**3**), Pd (**4**)) are given in Table 4.3. Both unit cells are isomorphic monoclinic space group, P2₁/n with 3 [K(2,2,2-crypt)]⁺ and en/tol solvent molecules. The Pd@Sn₉SnCy₃³⁻ ion **4** was crystallized in the [K(2,2,2crypt)]₃[(Sn₉SnCy₃)_{0.32}(**4**)_{0.68}] salt. Similarly, the Ni@Sn₉SnCy₃³⁻ (**3**) was also obtained with occupation of Ni@Sn₉H³⁻ (**1**) in a 9:1 ratio

with respect to the $\text{Sn}_9\text{SnCy}_3^{3-}$ ion in the lattice. Although the occurrence of two different clusters on the same crystallographic site of the lattice causes crystallographic disorder, they were successfully modeled and independently refined by Dr. Peter Zavalij.

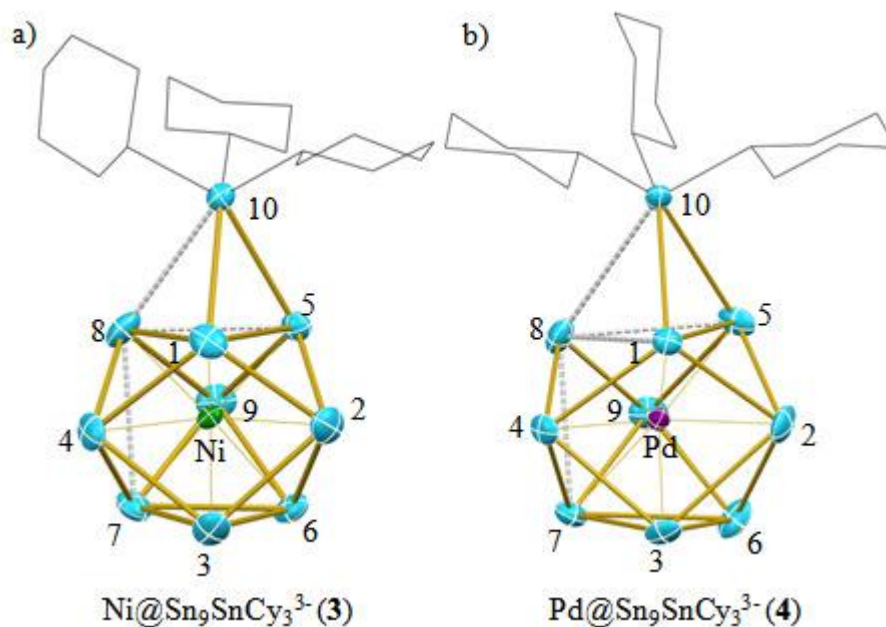


Figure 4.2. ORTEP drawings of the $\text{M@Sn}_9\text{SnCy}_3^{3-}$ clusters; a) $\text{M} = \text{Ni}$ **3**, b) $\text{M} = \text{Pd}$ **4**. Thermal ellipsoids are set at the 50% probability level. The dotted lines represent the contacts between $3.4 < x < 3.7 \text{ \AA}$, whereas solid lines denotes the bond lengths less than 3.4 \AA . The hydrogens of the cyclohexyl groups are not shown.

Table 4.3. Crystallographic data for the M@Sn₉SnCy₃³⁻ (M= Pd, Ni^b)

Compound	[K(2,2,2crypt)] ₃ [4].1/2en	[K(2,2,2-crypt)] ₃ [3].tol
	[Pd@Sn ₉ SnCy ₃] _{0.68} [Sn ₉ SnCy ₃] _{0.32}	[Ni@Sn ₉ SnCy ₃]
formula weight	2784.98	
temperature (K)	110(2)	
wavelength (Å)	0.71073	0.71073
crystal system	Monoclinic	Monoclinic
space group	P2 ₁ /n	P2 ₁ /n
unit cell dimensions		
a (Å)	16.32(5)	16.33(2)
b (Å)	23.49(8)	23.54(3)
c (Å)	27.71(9)	27.72(4)
α (°)	90	90
β (°)	105.00(1)	104.86(2)
γ (°)	90	90
volume (Å ³)	10260.6(6)	10302.2
Z	4	
D _{calc} (Mg/m ³)	1.803	
Abs. coeff. (mm ⁻¹)	2.684	
final R indices (all data) ^a		
R1, I>2σ(I)	0.0398	
wR2	0.0775	

^a R₁ = Σ||F_o|-|F_c||/Σ|F_o|, wR₂ = [Σw(F_o²-F_c²)²/Σw(F_o²)²]^{1/2}, ^bPreliminary data

As shown in Figure 4.2, the structures of cluster ions **3** and **4** are similar and have virtual C_s symmetry where the mirror planes are defined by Sn10, Sn7, Sn8 and M (Ni and Pd). The Ni and Pd centered clusters have *exo*-bonded SnCy₃ groups, and they are isostructural with the M@Sn₉H³⁻ cluster ions with similar positions and binding of the substituent groups, revealed from the calculated optimized energy structure of the hydride substituted ions in Figure 4.1b.

The endohedral metal atoms have direct effect on the bonding of *exo*-substituents. As discussed earlier in Chapter 3, the SnCy₃ group on the non-endohedral Sn₉SnCy₃³⁻ cluster is covalently bonded to only one of the vertices of the

cluster and it makes a secondary longer contact to another Sn vertex. In contrast, the SnCy₃ groups in clusters **3** and **4** symmetrically bridge two tin atoms (Sn1 and Sn5) of the M@Sn₉ cluster cores, where the SnCy₃ groups have longer secondary contacts with Sn8 that gives a 5+1 coordination number. Similar bonding was also reported for the Ge₉SnPh₃³⁻ cluster ion where the SnPh₃ group symmetrically bridges two Ge vertices and has a longer contact to a third Ge vertex.^[78]

The selected Sn-Sn and Sn-M bond lengths of clusters **3** and **4** are listed in the Table 4.4. The M@Sn₉ core can be viewed as a distorted tricapped trigonal prism where Sn8-Sn7, Sn5-Sn6 and, Sn1-Sn3 define the prism heights. For example, the three prism heights for the ion **4** are elongated by 8.4% (Sn7-Sn8), 17.9% (Sn5-Sn6) and 2.0% (Sn1-Sn3) relative to the non-interstitial Sn₉SnCy₃³⁻ cluster. Moreover, the 5+1 coordination geometry of the SnCy₃ group results in elongation of the Sn1-8, Sn8-5 bond distances, compared to non-interstitial clusters. The average 21 Sn-Sn contacts within the cluster cores of the Ni and Pd endohedral M@Sn₉ clusters are 3.144±0.242 Å and 3.210±0.26 Å, respectively. These average distances are longer than the average contacts of non-interstitial Sn₉SnCy₃³⁻ ion, $d(\text{Sn-Sn})_{\text{avg}} = 3.044 \pm 0.17$ Å. The average M-Sn bond lengths are 2.626±0.06 Å for M=Ni and 2.679±0.03 Å for M=Pd, for the M@Sn₉SnCy₃³⁻ clusters. Similar to the M@Sn₉H³⁻ clusters, the average bond distances of cluster **3** and **4** are sequentially elongated, which are consistent with the relative covalent radii of the parent endohedral transition metal atoms.

Table 4.4. Selected Bond Lengths [\AA] for the $M@Sn_9SnCy_3^{3-}$ ($M= Ni, Pd$) clusters.

Distances	Pd	Ni	Distances	Pd	Ni
Sn1-Sn2	2.950(2)	2.935(1)	Sn4-Sn7	3.130(1)	3.005(1)
Sn1-Sn4	2.970(1)	3.007(1)	Sn5-Sn9	3.080(1)	2.916(1)
Sn2-Sn3	3.180(2)	3.049(1)	Sn6-Sn7	3.200(2)	3.102(1)
Sn2-Sn5	3.000(1)	2.939(1)	Sn6-Sn9	3.110(2)	3.036(1)
Sn2-Sn6	3.070(2)	3.051(1)	Sn7-Sn9	3.030(1)	3.011(1)
Sn3-Sn4	3.050(1)	3.036(1)	Sn8-Sn9	3.010(1)	2.962(1)
Sn3-Sn6	3.100(1)	2.996(1)	Sn7-Sn8	3.463(2)	3.489(1)
Sn3-Sn7	3.180(1)	3.077(1)	Sn4-Sn8	3.030(1)	2.988(1)
Sn1-Sn8	3.565(6)	3.348(1)	Sn5-Sn8	3.470(1)	3.400(1)
Sn1-Sn5	3.353(7)	3.301(1)	Sn1-Sn10	3.144(5)	3.316(1)
Sn8-Sn10	3.622(8)	3.456(1)	Sn5-Sn10	3.282(6)	3.150(1)
Sn1-Sn3	3.727(2)	3.728(1)	Sn5-Sn6	3.844(2)	3.653(1)
Sn1-M	2.680(1)	2.545(1)	Sn4-M	2.622(6)	2.687(1)
Sn2-M	2.724(8)	2.689(1)	Sn5-M	2.683(9)	2.599(1)
Sn3-M	2.730(1)	2.612(1)	Sn6-M	2.771(9)	2.636(1)
Sn7-M	2.601(7)	2.595(1)	Sn8-M	2.622(9)	2.564(1)
Sn9-M	2.683(9)	2.713(1)			

The $M@Sn_9SnCy_3^{3-}$ ions ($M= Ni, Pd$) can be described using a Wade-Mingos cluster bonding analysis. They are 9-vertex, 22-electron *nido* clusters, considering the contribution from the $SnCy_3$ groups are 1 e^- donors. They are isoelectronic to the $M@E_9H^{3-}$ ($E= Ge, Sn$) clusters. While the endohedral d^{10} transition metal atoms do not contribute electrons to the cluster bonding as in the $M@Sn_9R^{3-}$ ions, a vertex transition metal contributes TE -12, where TE is the total electrons at the metal center electrons to cluster bonding as in the $Pd@Sn_9PdSnCy_3^{3-}$ (**5**) ion.

The Pd@Sn₉PdSnCy₃³⁻ (**5**) was obtained as [K(2,2,2-crypt)]⁺ salts in a triclinic crystal lattice, space group P-1. The crystallographic data are given in Table 4.5.

Table 4.5. Crystallographic data for the Pd@Sn₉PdSnCy₃³⁻ ion.

Compound	[K(2,2,2crypt)] ₃ [5]·tol·½en [Pd@Sn ₉ PdSnCy ₃]
formula weight	3018.09
temperature (K)	150(2)
wavelength (Å)	0.71073
crystal system	Triclinic
space group	P-1
Unit cell dimentions	
a (Å)	14.778(7)
b(Å)	15.842(7)
c (Å)	24.572(2)
a (°)	84.160(7)
β (°)	81.131(7)
γ (°)	75.614(7)
volume (Å ³)	5493.9(4)
Z	2
D _{calc} (Mg/m ³)	1.824
ab. coeff.,mm ⁻¹	2.72
final R indices	
R1, I>2σ(I)	0.029
wR2, (all data) ^a	0.0601

$$^aR_1 = \frac{\sum||F_o| - |F_c||}{\sum|F_o|}, \quad wR_2 = \left[\frac{\sum w(F_o^2 - F_c^2)^2}{\sum w(F_o^2)^2} \right]^{1/2}$$

As shown in Figure 4.3, the structure is a 10-vertex ion, where Pd1 occupies an endohedral site and Pd2 occupies a vertex site of cluster. The Pd@Sn₉PdSnCy₃³⁻ ion has a virtual C_{3v} symmetry, with a 3-fold axes defined by the Pd2-Pd1 vector. The -SnCy₃ group is attached to the vertex atom of the Pd2 bending slightly off of the 3-fold axis, Pd1-Pd2-Sn10 = 158.1(1)°.

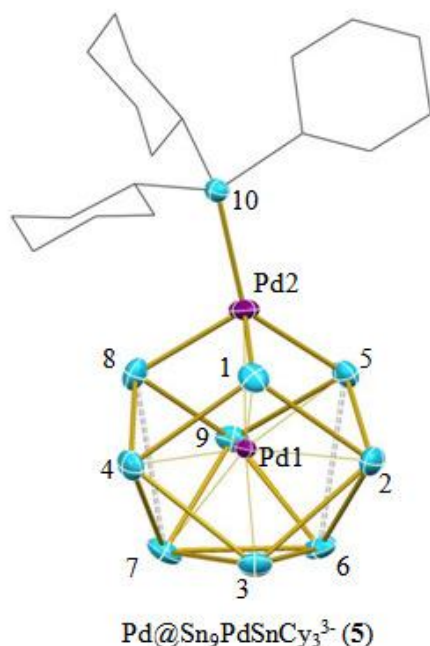


Figure 4.3. ORTEP drawing of the Pd@Sn₉PdSnCy₃³⁻ ion. Thermal ellipsoids are set at the 50% probability level. The dotted lines represent the contacts in the range 3.4 < x < 3.7 Å, whereas solid lines denotes the bond lengths less than 3.4 Å. The hydrogens of the cyclohexyl groups are not shown.

The selected bond lengths of ions **5** are listed in Table 4.6. The average Sn-Sn distance is 3.062±0.06Å. The Pd-Pd contact is 2.72(4) Å, which is consistent with a Pd-Pd single bond. The Pd1-Sn(1-9) bond lengths are in a narrow range of 2.667(3)-2.776(3) Å. The Sn-Sn prism heights are slightly shortened by 0.7% (Sn7-Sn8), 2.9% (Sn5-Sn6) and 5.9% (Sn1-Sn3) compared to the Pd@Sn₉SnCy₃³⁻ (**4**) cluster. In comparison with the **4**, insertion of the Pd2 atoms in the capping site of the cluster **5** resulted in breaking the Sn-Sn contacts on the top triangular base, such that Sn1-8 and Sn1-5 distances are 4.132(1) Å and 3.879(4) Å, respectively.

Using a Wade-Mingos analysis, the cluster electron count for **5** is 20e⁻, where the contributions are minus 1 e⁻ for vertex Pd2 atom and the SnCy₃ group (TE-12; where TE = 10 + 1 = 11), zero for endohedral Pd1, 9Sn @ 2e⁻ each, and 3e⁻ from the charge.

Therefore, it corresponds to a 10-vertex hyper-*closo* cluster. It is isoelectronic and isostructural to the similar hyper-*closo* clusters; Pt@Sn₉Pt(PPh₃)²⁻, Ni@Ge₉Ni(CO)²⁻, Ni@Ge₉Ni(CPh)³⁻, and Ni@Ge₉Pd(PPh₃)²⁻.^[99, 100, 117]

Table 4.6. Selected Bond Lengths [Å] for the Pd@Sn₉PdSnCy₃³⁻ ion.

Sn1-2	3.029(4)	Sn7-8	3.519(4)
Sn1-4	3.025(4)	Sn5-6	3.438(4)
Sn2-3	3.078(4)	Pd1-Sn1	2.668(4)
Sn2-5	2.961(4)	Pd1-Sn2	2.772(3)
Sn2-6	3.160(4)	Pd1-Sn3	2.744(3)
Sn3-4	3.123(4)	Pd1-Sn4	2.776(3)
Sn3-6	3.065(4)	Pd1-Sn5	2.705(3)
Sn3-7	3.058(4)	Pd1-Sn6	2.732(3)
Sn4-8	2.970(4)	Pd1-Sn7	2.732(3)
Sn4-7	3.737(4)	Pd1-Sn8	2.711(4)
Sn5-9	3.012(4)	Pd1-Sn9	2.764(3)
Sn6-7	3.055(4)	Pd2-Sn1	2.593(4)
Sn6-9	3.109(4)	Pd2-Sn5	2.651(4)
Sn7-9	3.124(4)	Pd2-Sn8	2.612(4)
Sn8-9	3.022(4)	Pd2-Sn10	2.552(3)

4.2.3. NMR Spectroscopic Studies

A summary of the NMR and structure data of the M@Sn₉R³⁻ (M= Ni, Pd, R= H, SnCy₃) ions and their non-interstitial analogs is given in the Table 4.7.

Table 4.7. Summary of the average Sn-Sn bond distances and NMR data of the Sn₉R³⁻ and M@Sn₉R³⁻ ions (R= H, SnCy₃ and M= Ni, Pd)

Cluster Ion	X nuclei	Bond lengths ^d (Sn1-9) _{avg}	$\delta^{119}\text{Sn}$ (Sn1-9)	δX	$J^{119}\text{Sn}-^{117}\text{Sn}$ (intravertex)	$J^{119}\text{Sn-X}$
^a Sn ₉ H ³⁻	H	3.035 ±0.12	-1271	6.1	390	21
^c Sn ₉ SnCy ₃ ³⁻	SnCy ₃	3.044±0.17	-1172	155	272	1331, 1272
(1) Ni@Sn ₉ H ³⁻	H	3.123±0.26	-837	-28	59	51
(2) ^b Pd@Sn ₉ H ³⁻	H	3.248±0.34	-326	-24	~43	43
(3) Ni@Sn ₉ SnCy ₃ ³⁻	SnCy ₃	3.144±0.24	-1006	-85	<147	850
(4) Pd@Sn ₉ SnCy ₃ ³⁻	SnCy ₃	3.210±0.26	-503	-26	<130	880

^aThe NMR data were collected in en (Chapter 2). ^bThe NMR data were collected in en/tol solutions. ^cDiscussed in Chapter 3. ^d21 Sn-Sn contacts.

The ^{119}Sn , $^{119}\text{Sn}^{[160]}$ and ^1H NMR spectra of the $\text{M@Sn}_9\text{H}^{3-}$ ($\text{M}=\text{Ni}$ (**1**), Pd (**2**)) 3 anions are given in Figure 4.4 and 4.5 respectively. Each of the clusters **1** and **2** has one, time-averaged ^{119}Sn signal at -837 ppm and -326 ppm, respectively. These signals show coupling to a single proton atom with a $J(^1\text{H}-^{119/117}\text{Sn})$ coupling constants of 51 Hz and 43 Hz respectively. The $J(^{119}\text{Sn}-^{117}\text{Sn})$ coupling constant for the 9-equivalent Sn nuclei is 59 Hz for the cluster **1** and approximately 43 Hz for **2** (Figure 4.5a). Similarly, the ^{119}Sn signal of the previously reported $\text{Pt@Sn}_9\text{H}^{3-}$ ion is at $\delta^{119}\text{Sn} = -367$ ppm with an approximate $J(^{119}\text{Sn}-^{117}\text{Sn})$ coupling constant of 46 Hz.^[115] The $^{119}\text{Sn}\{^1\text{H}\}$ NMR spectra are shown in Figure 4.4b and 4.5b.

Compared to the non-interstitial Sn_9H^{3-} cluster ($\delta^{119}\text{Sn}$, -1271 ppm), the ^{119}Sn signals of clusters **1** and **2** are shifted downfield upon insertion of the d^{10} endohedral transition metals. The downfield chemical shifts have also been reported for endohedral clusters of the $\text{Pt@Sn}_9\text{Pt}(\text{PPh}_3)^{2-}$, $\text{Pt}_2\text{@Sn}_{17}^{4-}$ and $\text{Pd}_2\text{@Sn}_{18}^{4-}$ ions.^[115, 117, 174] While Pd and Pt analogs of the similar clusters have similar chemical shifts, the resonance for the Ni analog is more upfield. The M@Pb_{12}^{2-} series ($\text{M} = \text{Ni}, \text{Pd}, \text{Pt}$) also shows a similar trend with increasing ^{207}Pb chemical shift in the order of $\text{Pt} \approx \text{Pd} > \text{Ni}$.^[122]

The proton signals of the cluster hydrides are at -28 ppm and -24 ppm for the Ni (**1**) and Pd (**2**) endohedral clusters, respectively. Proton chemical shifts are similar to the previously reported $\text{Pt@Sn}_9\text{H}^{3-}$ ion $\delta^1\text{H} = -22$ ppm. The $^{119/117}\text{Sn}$ satellites on the proton resonances are 7-line multiplet with an integration ratio of 0.04 : 0.24 : 0.65 : 1.0 : 0.65 : 0.25:0.04 arising from coupling to 9-Sn atoms. The Sn-H coupling

constants of all $M@Sn_9H^3-$ clusters with values in range of 43-51 Hz are relatively small compared to the organostannane hydrides having typical values of 2000 Hz.^[175] Recently, Sn-Sn compounds with bridged hydrides have been synthesized by Power et al. Similar to our study, they reported a small Sn-H coupling constant for these compounds (89 Hz).^[162]

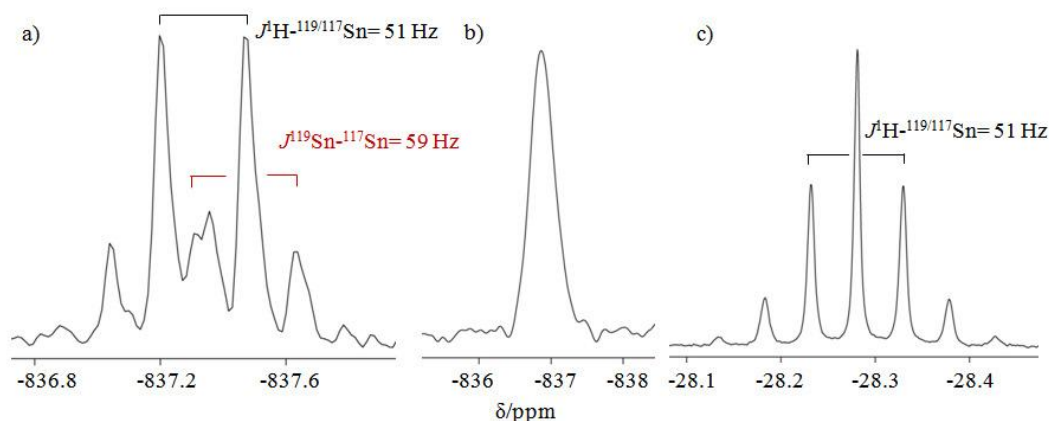


Figure 4.4. NMR spectra of the $Ni@Sn_9H^3-$ ion taken from pyridine- d_5 at room temperature. a) ^{119}Sn , b) $^{119}Sn\{^1H\}$, c) 1H . The operating frequencies for ^{119}Sn and 1H are 186 MHz and 500 MHz, respectively.

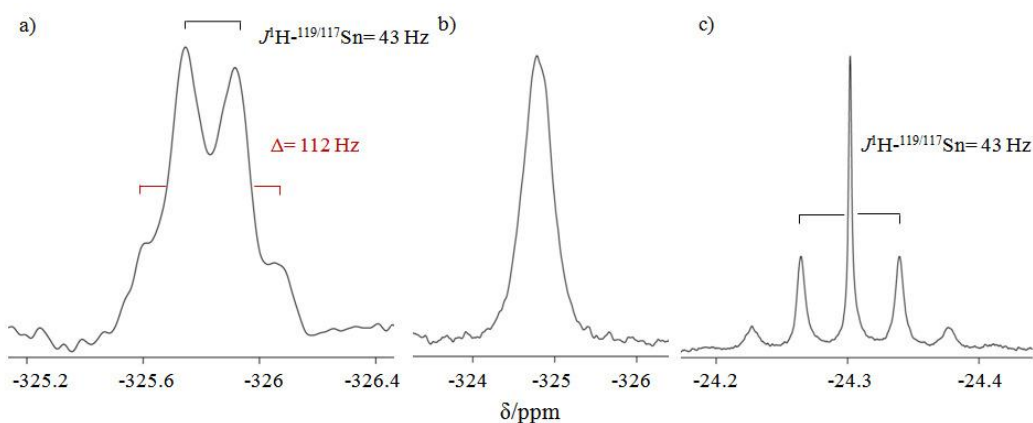


Figure 4.5. NMR spectra of the $Pd@Sn_9H^3-$ ion taken from pyridine- d_5 at room temperature. a) ^{119}Sn , b) $^{119}Sn\{^1H\}$, c) 1H . The operating frequencies for ^{119}Sn and 1H are 223 MHz and 600 MHz, respectively.

The proton signals of the ion **1** and **2** and the previously reported Pt analog are in the range of -22 ppm to -28 ppm ($\delta^1\text{H}$: Pt \approx Pd>Ni). A similar sequence of the proton chemical shift has been reported for a complex of trans-MH(Cl)(PBz₃)₂ ($\delta^1\text{H}$: -23 ppm for Ni, -14 ppm for Pd, -17.3 ppm for Pt).^[176]

The ¹H NMR spectrum of the Ni@Ge₉H³⁻ cluster has a resonance at -15.2 ppm as shown in Figure 4.6. The ¹H signal is a singlet without any satellite pattern since the Ge nucleus is quadrupolar (I= 9/2). However, this cluster is also expected to have an exchange mechanism similar to the M@Sn₉H³⁻ clusters (M= Ni, Pd).

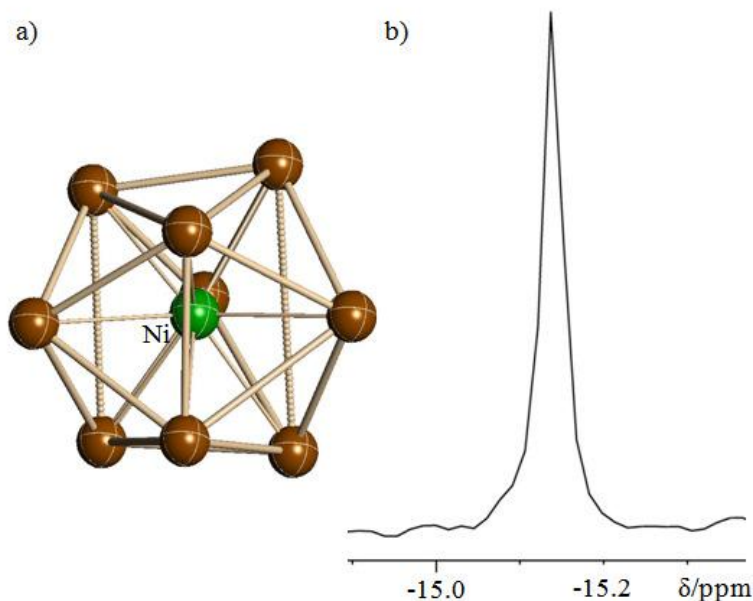


Figure 4.6. ¹H NMR spectrum of the Ni@Ge₉H³⁻ in (b) taken from en solutions at room temperature at operating frequency of 500 MHz. Structure in (a) is taken from the reference^[126].

The time averaged ¹¹⁹Sn NMR signals of **1** and **2** indicate a fast intramolecular exchange of all nine Sn atoms in the clusters. Concurrently, the hydrogen is scrambling around the highly dynamic clusters of **1** and **2**, evidenced by an average coupling of a proton to the 9-equivalent Sn nuclei. Similar exchange mechanism has

also been observed for the Sn_9H^{3-} ion (Chapter 2). The process is entirely intramolecular in that $J(^1\text{H}-^{119}\text{Sn})$ and $J(^{119}\text{Sn}-^{117}\text{Sn})$ couplings are maintained in the fast-exchange limit.

The $\delta^1\text{H}$ values show upfield shifts with the centered transition metals in the $\text{M@Sn}_9\text{H}^{3-}$ ions (M= Ni, Pd) compared to the Sn_9H^{3-} cluster (6.1 ppm), suggesting a M-H interaction. The $\text{Ni@Ge}_9\text{H}^{3-}$ ion also have an upfield chemical shift for the hydride ligand, $\delta^1\text{H} = -15.2$ ppm. However, the position and connectivity of the proton atoms to the clusters are not revealed from the structure analysis. The Sn_9 framework is symmetrical with typical M-Sn bonds lengths (2.6 Å) in the solid state structure, and there is no indication of a direct M-H bond. Theoretical calculations also shows that the shortest distance through space between endohedral Ni atom and H ligand is 3.149 Å, whereas hydride ligand is attached to the Sn vertex atoms with 2.056 Å and 2.095 Å contacts. In comparison, the HP_7^{2-} and $\text{HP}_7\text{W}(\text{CO})_3^{2-}$ clusters ($\delta^1\text{H} = 7.2$ vs. 4.2 ppm) do not show any substantial difference in proton chemical shifts, where the hydrogen atom is attached to the phosphorus and three-bond distant from the capping $\text{W}(\text{CO})_3$ group in the latter.^[149, 165]

The spherical symmetry in the $\text{M@Sn}_9\text{H}^{3-}$ ions and mobility of the hydride ligand do not exist in the nortricyclic structured metallated phosphido clusters. Thus, it is possible that a rearrangement in the M@Sn_9 cluster core can allow a direct M-H bond during the exchange mechanism Sn vertices. In addition to the upfield chemical shift after insertion of endohedral transition metals, the reported $\text{Pt@Sn}_9\text{H}^{3-}$ ion has a small coupling constant $J(^{195}\text{Pt}-^1\text{H}) = 32$ Hz, less than the magnitude of a one-bond coupling $^1J(^{195}\text{Pt}-^1\text{H}) = 1080$ Hz for the $\text{P}_7\text{PtH}(\text{PPh}_3)^{2-}$ ion.

In the alternative scenario, the measured M-H coupling constant in the $\text{Pt@Sn}_9\text{H}^{3-}$ ion can be a result the averaged two-bond coupling constants (${}^2J^{195}\text{Pt-}^1\text{H}$) over 9-Sn nuclei. On the other hand, the measured coupling constant of $J(\text{Sn-H})$ representing an averaged coupling over 9-Sn atoms are small in the range of 43-51 Hz, where the hydride atoms have direct bonding to the Sn atoms. As a result, a two-bond coupling of the (${}^2J^{195}\text{Pt-}^1\text{H}$) is expected to be very small. Therefore, the measured constant may not represent the averaged two-bond coupling constants.

The $\text{M@Sn}_9\text{SnCy}_3^{3-}$ clusters (M= Ni (**3**), Pd (**4**)) have two ^{119}Sn resonances as shown in Figure 4.7a and 4.7b, that are very similar to the spectrum of the non-endohedral $\text{Sn}_9\text{SnCy}_3^{3-}$ cluster. While cluster **3** has two ^{119}Sn resonances at -1006 ppm and -85 ppm, cluster **4** resonances are at -503 ppm and -26 ppm. The intensity ratio of the two resonances is approximately 1:9, consistent with the two sets of chemically inequivalent number of Sn nuclei in the clusters. Therefore, the signals with smaller intensity represent the tin atoms of the $-\text{SnCy}_3$ groups, and the signals with higher intensity represent the M@Sn_9 cluster cores. The resonances are mutually coupled to each other with $J_{\text{Sn-Sn}} = 850$ and 880 Hz for **3** and **4**, respectively. As discussed earlier in Chapter 3, this coupling constant between the Sn atom of substituent group and cluster core for the $\text{Sn}_9\text{SnCy}_3^{3-}$ cluster has a larger magnitude of $J(^{119}\text{Sn-}^{119}\text{Sn}) = 1331$ Hz and $J(^{119}\text{Sn-}^{117}\text{Sn}) = 1272$ Hz.

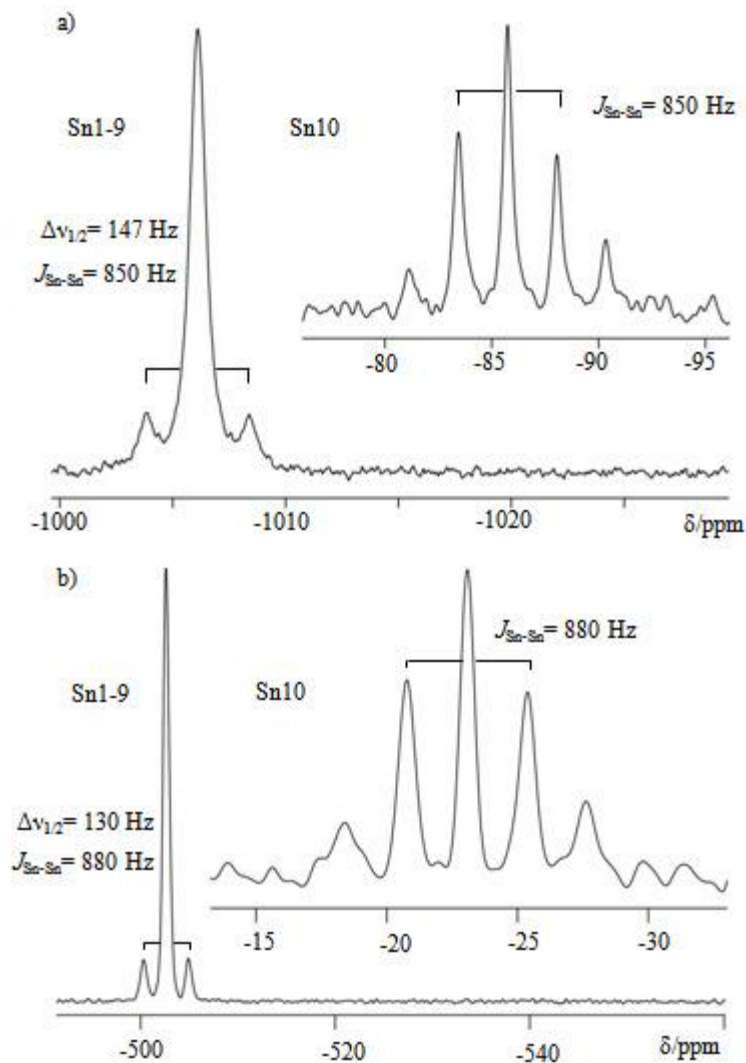


Figure 4.7. ^{119}Sn NMR spectra of the $\text{M}@\text{Sn}_9\text{SnCy}_3^{3-}$ taken from pyridine at room temperature at 186 MHz operating frequency. a) $\text{M} = \text{Ni}$ The signal at -1006 ppm assigned for the $\text{Ni}@\text{Sn}_9$ cluster core. The signal at -86 ppm (inset) is assigned to the SnCy_3 group. b) $\text{M} = \text{Pd}$. The signal at -503 ppm assigned for the $\text{Pd}@\text{Sn}_9$ cluster core. The signal at -26 ppm (inset) is assigned to the SnCy_3 group.

The $J(^{119}\text{Sn}-^{117}\text{Sn})$ coupling constants for the 9-equivalent Sn nuclei of the $\text{M}@\text{Sn}_9$ cluster cores could not be resolved. However, since the SnCy_3 group couples to 9-Sn nuclei of the $\text{M}@\text{Sn}_9$ cluster core, the exchange mechanism is intramolecular. Thus, the intramolecular $J(^{119}\text{Sn}-^{117}\text{Sn})$ coupling constants of the $\text{M}@\text{Sn}_9$ core have to

be smaller than the line width at $\frac{1}{2}$ height, which are 147 Hz and 130 Hz for the cluster ions **3** and **4**, respectively.

The endohedral derivatives of the substituted clusters **1-4**, $M@Sn_9R^{3-}$ ($R= H, SnCy_3$), discussed above are all highly dynamic ions. A single time-averaged ^{119}Sn signal with intensities consistent for a 9-equivalent-Sn atom pattern for all the $M@Sn_9$ cluster cores indicates a fast intramolecular exchange mechanism of 9-equivalent Sn atoms in the clusters. In addition, the satellite patterns on the X nuclei ($X= H, SnCy_3$) reveal that the nuclearity is consistent with the coupling of a to 9 equivalent Sn nuclei, which shows scrambling of the substituent groups around the clusters.

The effects of transition metal inclusion on the structure of Sn_9H^{3-} and $Sn_9SnCy_3^{3-}$ cluster and solution dynamics (^{119}Sn NMR) are discussed. In the $M@Sn_9R^{3-}$ cluster ions, the scrambling of the substituent group persists similar to fluxionality in the Sn_9R^{3-} precursor ions. The presence of an endohedral transition metal atom has systematic influences to both chemical shifts and J coupling. The analyses of the data show that an endohedral transition metal decreases the J coupling of the intravertex 9-Sn cluster core, which is also consistent with elongation of the Sn-Sn average bond lengths in the structures. Similar behavior has also been reported for other dynamic endohedral clusters such as; $Cu@Sn_9^{3-}$, $Pd@Sn_{18}^{4-}$, $Pt_2@Sn_{17}^{4-}$, and $Pt@Sn_9Pt(PPh_3)^{2-}$.^[115-117]

The $Pd@Sn_9PdSnCy_3^{3-}$ ion dissolved in pyridine- d_5 show two ^{119}Sn NMR signals in a 9:1 intensity ratio at -567 ppm and 126 ppm, respectively (Figure 4.8). On the basis of intensities, the signal at -567 ppm is assigned to the time-averaged

10-vertex Pd@Sn₉Pd- cluster and the 126 ppm signal is assigned to the -SnCy₃ substituent. Both of the signals are broad singlets with no discernible couplings.

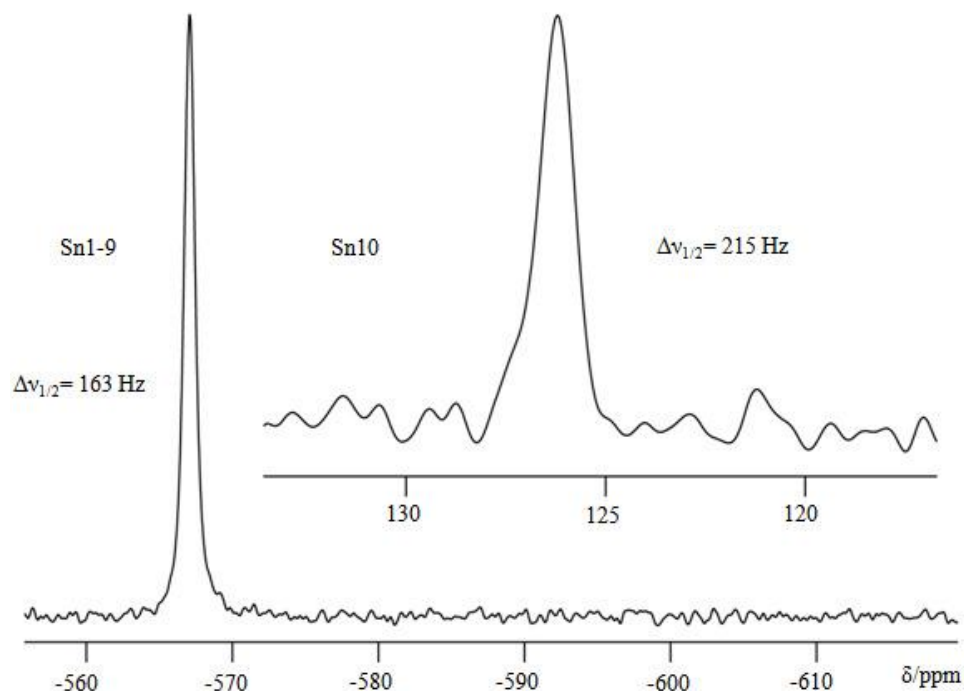


Figure 4.8. ¹¹⁹Sn NMR spectrum of the Pd@Sn₉PdSnCy₃³⁻ taken in pyridine-d₅ at room temperature at 186 MHz. The signal at -567 ppm assigned for the Pd@Sn₉Pd cluster. The signal at 126 ppm (inset) is assigned to the SnCy₃ group.

The unresolved intra-vertex $J(^{119}\text{Sn}-^{117}\text{Sn})$ coupling constant is less than 163 Hz, which is the peak width at $\frac{1}{2}$ height. The single ¹¹⁹Sn resonance for the 9-Sn atoms of the Pd@Sn₉Pd cluster shows that all nine Sn nuclei are still in fast exchange. This observation suggests that the SnCy₃ group remains bound to Pd₂ at all the times, but the data do not exclude a scrambling of the SnCy₃ group with a correspondingly low coupling constant. On the other hand, such a scrambling process would represent a formal reductive elimination, leaving a highly unsaturated Pd₂ atom. For comparison, an isoelectronic and isostructural Pt@Sn₉Pt(PPh₃)₂²⁻ cluster, which has a

rigid Pt-Pt-PPh₃ linear subunit inserted into the Sn₉ framework with a non-labile PPh₃ ligand that retains its coupling to both Pt atoms at all temperatures. In addition, the nine Sn vertices of Pt@Sn₉Pt(PPh₃)²⁻ also show one ¹¹⁹Sn signal at -862 ppm with unresolved intra-vertex $J(^{119}\text{Sn}-^{117}\text{Sn})$ couplings of less than 150 Hz.

4.3. Conclusion

The mass and charge balanced stepwise reactions of group 14 *exo*-compounds with transition metal complexes are studied. Reactions are graphically illustrated in Figure 4.9. The Ni@Sn₉SnCy₃³⁻ ion is synthesized through the conversions of Sn₉⁴⁻ → Sn₉H³⁻ → Ni@Sn₉H³⁻ → Ni@Sn₉SnCy₃³⁻. In addition, the Pd@Sn₉PdSnCy₃³⁻ ion is synthesized through the conversions of Sn₉⁴⁻ → Sn₉SnCy₃³⁻ → Pd@Sn₉SnCy₃³⁻ → Pd@Sn₉PdSnCy₃³⁻.

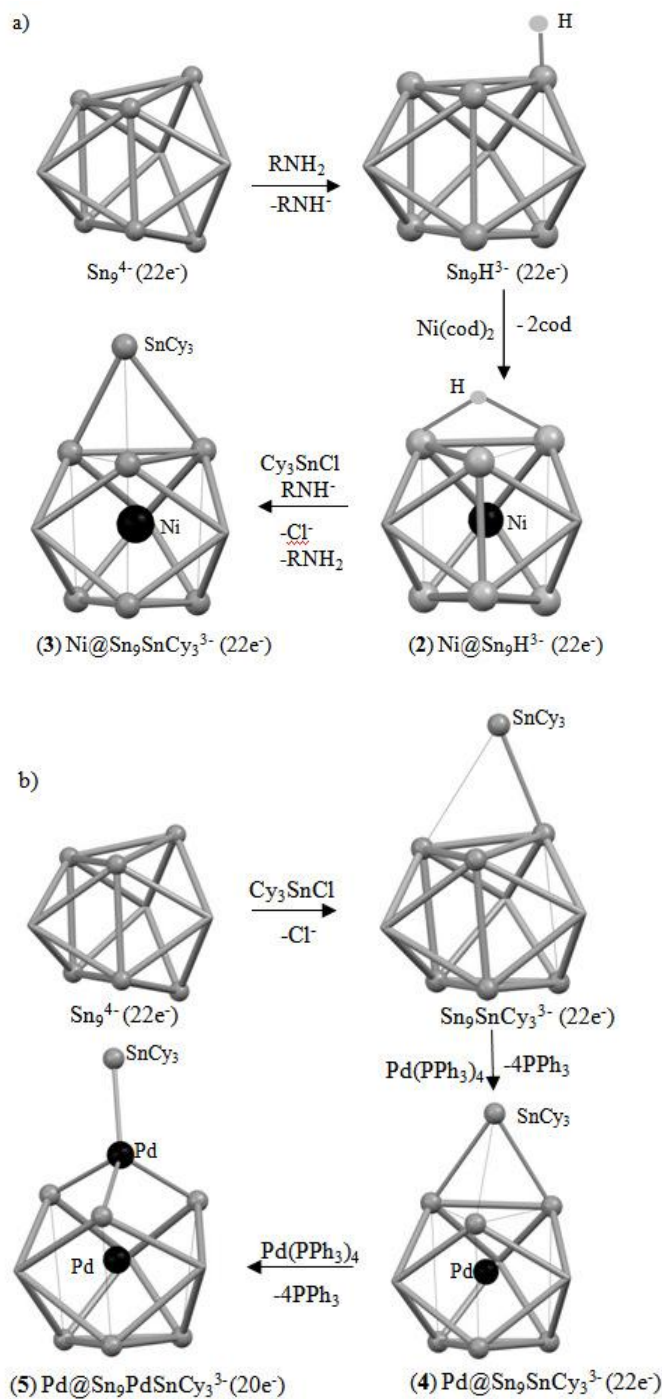


Figure 4.9. Graphical representations of stepwise conversions; a) $\text{Sn}_9^{4+} \rightarrow \text{Sn}_9\text{H}^{3-} \rightarrow \text{Ni@Sn}_9\text{H}^{3-} \rightarrow \text{Ni@Sn}_9\text{SnCy}_3^{3-}$, b) $\text{Sn}_9^{4+} \rightarrow \text{Sn}_9\text{SnCy}_3^{3-} \rightarrow \text{Pd@Sn}_9\text{SnCy}_3^{3-} \rightarrow \text{Pd@Sn}_9\text{PdSnCy}_3^{3-}$. Dark spheres are Ni atoms for the clusters **2** and **3**, and Pd metals for the ions **4** and **5**. Light spheres are Sn atoms that define the top and the bottom of the trigonal prism. The remaining vertices are capping sites. Solid lines denote normal Sn-Sn bonds whereas thin lines represent the heights of the virtual trigonal prisms and long contacts ranging between $3.4\text{\AA} < x < 3.7\text{\AA}$.

The $\text{Pt@Sn}_9\text{H}^{3-}$ was reported in earlier studies, and in this chapter, new members of the hydrido clusters $\text{M@Sn}_9\text{H}^{3-}$ (M= Ni, Pd) has been obtained. ^{119}Sn NMR studies showed that $\text{M@Sn}_9\text{H}^{3-}$ forms from inclusion reaction of the transition metal into the Sn_9H^{3-} ion. Similarly, the $\text{Sn}_9\text{SnCy}_3^{3-}$ ion gives inclusion product, $\text{Pd@Sn}_9\text{SnCy}_3^{3-}$ ion from the reaction with $\text{Pd}(\text{PPh}_3)_4$. These transition metal inclusion studies provide mechanistic information regarding the formation of endohedral clusters. The Ni@Ge_9^{3-} ion was reported as a paramagnetic ion previously.^[126] In this study, $\text{Ni@Ge}_9\text{H}^{3-}$ ion has been identified to have a hydride ligand. The structural distortions of the clusters are indirect indications of the H atom location. This study showed that co-crystallization is a challenging problem for obtaining crystallographically pure endohedral derivatives of the substituted clusters due to similar crystallographic structures with the non-interstitial components.

Our solution studies also show that the pKa of the E_9H^{3-} does not significantly change for the $\text{M@E}_9\text{H}^{3-}$ ions with an endohedral group 10 metal atoms. The unusual upfield chemical shift $\delta^1\text{H}$ of the $\text{M@E}_9\text{H}^{3-}$ ions (E = Sn for M = Ni, Pd, Pt and E = Ge for M= Ni) compared to the non-interstitial Sn_9H^{3-} ion suggesting a direct M-H bond. However, in the solid state and DFT calculations of the ions showed that hydride substituents are bridging on two of the Sn vertices, and there is no direct bonding between the interstitial metal atoms and hydride substituents. The solution studies suggest that M-H bond might be forming during the exchange mechanism.

The $\text{M@Sn}_9\text{SnCy}_3^{3-}$ clusters (M=Ni, Pd) are synthesized from two different synthetic routes as shown in Figure 4.9. The $\text{Ni@Sn}_9\text{SnCy}_3^{3-}$ cluster (**3**) is formed by exchanging the hydride ligand with SnCy_3 group. On the other hand, $\text{Pd@Sn}_9\text{SnCy}_3^{3-}$

cluster (**4**) is formed as a result of inclusion reaction of Pd metal into the $\text{Sn}_9\text{SnCy}_3^{3-}$ ion. These studies show that the identical cluster ions can be obtained in various synthetic routes in controlled reactions. Thus, understanding of the reaction mechanisms of Zintl ions with transition metals can lead to controlled synthesis of new cluster compounds.

Recall from chapter 3 that, Sn_9R^{3-} ions with alkyl substituent have a stationary substituent group, which removes the *exo*-bonded Sn atom from exchanging from the other vertices. However, similar to the dynamic non-interstitial Sn_9H^{3-} ions ($\text{R}=\text{H}$, SnCy_3), the endohedral derivatives of the substituted clusters **1-4**, $\text{M}@\text{Sn}_9\text{R}^{3-}$ ($\text{R}=\text{H}$, SnCy_3), are all highly dynamic ions. The presence of an endohedral transition metal atom has systematic influences to both chemical shifts and *J* coupling, but they do not affect the fluxionality of the Sn_9 cluster core and scrambling of the substituent groups around the cluster.

Finally, a new oxidative insertion process for the conversion of the $\text{Pd}@\text{Sn}_9\text{SnCy}_3^{3-}$ ion to the $\text{Pd}@\text{Sn}_9\text{PdSnCy}_3^{3-}$ ion in this class of clusters is shown. Insertion of the second Pd metal resulted in decrease of the cluster bonding electrons from $22 e^-$ to $20 e^-$ due to oxidative insertion process. Moreover, in this 10-vertex cluster, solution dynamics suggest a non-mobile SnCy_3 substituent group, while the $\text{Pd}@\text{Sn}_9\text{Pd}$ cluster is still in a fast exchange on the NMR time scale.

4.4. Experimental Section

4.4.1. General Data

All reactions were performed in a nitrogen atmosphere drybox. The ^1H , ^{13}C and ^{119}Sn NMR spectra for 1, 3 and 4 were recorded on a Bruker DRX500 AVANCE spectrometer operating at 500 MHz, 125 MHz and 186 MHz, respectively. The ^1H and ^{119}Sn spectra of the $\text{Pd@Sn}_9\text{H}^{3-}$ were recorded on a Bruker AVANCE 600 spectrometer operating at 600 and 223 MHz, respectively. The ^{119}Sn chemical shifts were calibrated to an external Me_4Sn standard in C_6D_6 (0 ppm) at room temperature. The ^1H and ^{13}C chemical shifts were calibrated to TMS as an external reference.

4.4.2. Chemicals

Melts of nominal composition K_4Sn_9 and K_4Ge_9 were made by fusion of stoichiometric ratios of the elements at high temperature under N_2 atmospheres. 4,7,13,16,21,24-Hexaoxa-1,10-diazobicyclo[8,8,8]hexacosane (2,2,2-crypt) was purchased from Fisher Scientific. Cy_3SnCl was purchased from Aldrich. $\text{Ni}(\text{cod})_2$, $\text{Pd}(\text{PPh}_3)_4$ and $\text{Pt}(\text{PPh}_3)_4$ were purchased from STREM chemicals. Anhydrous ethylenediamine (en) were purchased from Fisher, vacuum-distilled from K_4Sn_9 , and stored under dinitrogen. Toluene was distilled from sodium/benzophenone under dinitrogen and stored under dinitrogen. Pyridine was distilled from KOH under dinitrogen and stored under dinitrogen.

4.4.3. Synthesis

Synthesis of [K(2,2,2-crypt)]₃[Pd@Sn₉H].en

In a glass vial, K₄Sn₉ (80 mg, 0.065 mmol) and Pd(PPh₃)₄ (75 mg, 0.065 mmol) were dissolved in 2 mL of ethylenediamine (en). 2,2,2-crypt (98 mg, 0.26 mmol) was added to the solutions as a solid. After the solutions were stirred and heated at 60 °C for 30 minutes, the orange-red colored solutions were filtered through tightly packed glass wool and the solutions were layered with 2 mL of toluene. In five days, the orange crystals of [K(2,2,2-crypt)]₃[Pd@Sn₉H].en (~ 16 mg.) were obtained in a crystalline yield of %10 based on amount of K₄Sn₉. $\delta^{119}\text{Sn}$ (ppm, en/tol) -326 (9 Sn, $J(^{119}\text{Sn}-^{117}\text{Sn})$; ~ 43 Hz), $\delta^1\text{H}$ -24 (1 H, $J(^1\text{H}-^{119/117}\text{Sn})$; 43 Hz).

Synthesis of [K(2,2,2-crypt)]₃[Ni@Sn₉H].en

In a glass vial, K₄Sn₉ (80 mg, 0.065 mmol) and 2,2,2-crypt (98 mg, 0.26 mmol) were dissolved in 2 mL of en. Ni(cod)₂ (18 mg, 0.065 mmol) was added to this solutions as solid. The dark red solutions were stirred for three hours and filtered through tightly packed glass wool. The solutions were layered with 2 mL of toluene. In seven days, red crystals of [K(2,2,2-crypt)]₃[Ni@Sn₉H]_{0.46}[Sn₉H]_{0.54} (~ 101 mg.) were obtained in a 32% crystalline yield of Ni@Sn₉H³⁻, based on amount of K₄Sn₉. When the amount of Ni(cod)₂ was approximately doubled (37 mg, 0.13 mmol), red crystals of [K(2,2,2-crypt)]₃[Ni@Sn₉H]_{0.90}[Sn₉H]_{0.1} were obtained in a week (~116 mg.) in a %72 crystalline yield based on the amount K₄Sn₉. $\delta^{119}\text{Sn}$ (ppm, pyridine-d₅) -837 (9 Sn, $J(^{119}\text{Sn}-^{117}\text{Sn})$; 59 Hz), $\delta^1\text{H}$ / ppm -28 (1 H, $J(^1\text{H}-^{119/117}\text{Sn})$; 51Hz).

Synthesis of [K(2,2,2-crypt)]₃[Ni@Ge₉H]

Synthesis was followed exact same procedure as reported earlier.^[126] In a glass vial, K₄Ge₉ (84 mg, 0.104 mmol) and 2,2,2-crypt (117 mg, 0.310 mmol) were dissolved in 2 mL of en. Ni(cod)₂ (64 mg, 0.232 mmol) was added as a solid. After the solutions were stirred for three hours, the dark red-black solutions were filtered through tightly packed glass wool. $\delta^1\text{H}$ NMR (ppm, en); -15.2.

Synthesis of [K(2,2,2-crypt)]₃[Ni@Sn₉SnCy₃].en

In a glass vial 1, K₄Sn₉ (80 mg, 0.065 mmol) and 2,2,2-crypt (98 mg, 0.26 mmol) were dissolved in 2 mL of ethylenediamine. Ni(cod)₂ (40 mg, 0.14 mmol) was added as a solid. After the solution was stirred for three hours, the dark red solution was filtered through tightly packed glass wool. In a glass vial 2, a toluene solution of ClSnCy₃ (21 mg, 0.052 mmol) was prepared. The solution in vial 2 was added to vial 1 dropwise. The solution was stirred for 1 hr. and filtered through tightly packed glass wool. In 48 hours, red crystals of [K(2,2,2-crypt)]₃[Ni@Sn₉SnCy₃]_{0.9}[Ni@Sn₉H]_{0.1} (40 mg,) were obtained in a 20 % crystalline yield based on the K₄Sn₉ precursor. $\delta^{119}\text{Sn}$ NMR (ppm, pyridine) -1006 (9 Sn, $J(^{119}\text{Sn}-^{119/117}\text{Sn})$; 850 Hz), -85. $\delta^1\text{H}$ NMR (ppm, pyridine) 3.48 (s, 2,2,2-crypt), 3.40 (t, 2,2,2-crypt), 2.38 (t, 2,2,2-crypt), 1.98 (m, -Cy), 1.68 (m, -Cy), 1.46 (m, -Cy), 1.28 (m, -Cy). $\delta^{13}\text{C}$ NMR (ppm, pyridine) 70.8 (2,2,2-crypt), 67.9 (2,2,2-crypt), 54.2 (2,2,2-crypt), 34.6 (-Cy), 31.1 (-Cy), 28.6 (-Cy), 28.3 (-Cy).

Synthesis of [K(2,2,2-crypt)]₃[Sn₉SnCy₃]_{0.32}[Pd@Sn₉SnCy₃]_{0.68}·1/2en

In vial 1, [K(2,2,2-crypt)]₃[Sn₉SnCy₃] (80 mg, 0.028 mmol) was dissolved in 2ml of en/py (2:1) mixture. The solution was filtered through tightly packed glass

wool and added dropwise onto Pd(PPh₃)₄ (35.5 mg, 0.028 mmol) in vial 2. An additional 0.2 mL of py was added to tightly packed glass wool to wash down the remaining precursor. The solution in vial 2 was stirred for 2 hrs. The resulting dark red solution was filtered through tightly packed glass wool, and layered with 1 mL of toluene. In 2 weeks red prism-shaped crystals of [K(2,2,2-crypt)]₃[Sn₉SnCy₃]_{0.32}[Pd@Sn₉SnCy₃]_{0.68}1/2en were formed on the bottom of the vial. Crystalline Yield of Pd@Sn₉SnCy₃³⁻: 31 mg, ~27% based on amount of [Sn₉SnCy₃]³⁻ precursor.

Alternative synthesis of [Pd@Sn₉SnCy₃]³⁻; In a glass vial 1, crystals of the [K(2,2,2-crypt)]₃[Sn₉SnCy₃] (80 mg, 0.028 mmol) were dissolved in 2mL of en/py (2:1) mixture. Solid Pd(PPh₃)₄ (35.5 mg, 0.028 mmol) was added to vial 1 in three aliquots while stirring the solution. After stirring the resulting dark red solution for two hours, it was filtered through tightly packed glass wool, and layered with 1 mL of toluene. In three weeks, pure red polycrystalline powders (based on ¹¹⁹Sn, ¹³C NMR analysis) of the Pd@Sn₉SnCy₃³⁻ salts were formed on the bottom of the vial. Yield: 23 mg, ~30% based on the amount of [K(2,2,2-crypt)]₃[Sn₉SnCy₃] used. ¹¹⁹Sn NMR (ppm, pyridine-d₅): -503 (9 Sn, *J*(¹¹⁹Sn-^{119/117}Sn); 880 Hz), -26 (1 Sn, *J*(¹¹⁹Sn-^{119/117}Sn); 880 Hz). ¹H NMR (ppm, pyridine-d₅): δ= 4.49 (s, 2,2,2-crypt), 3.43 (t, 2,2,2-crypt), 2.419 (t, 2,2,2-crypt), 1.90 (m, -Cy), 1.69 (m, -Cy), 1.48 (m, -Cy), 1.26 (m, -Cy). ¹³C NMR (ppm, pyridine-d₅): δ= 71.2 (2,2,2-crypt), 68.7 (2,2,2-crypt), 54.9 (2,2,2-crypt), 35.15 (-Cy), 31.59 (-Cy), 29.82 (-Cy), 29.05 (-Cy).

Synthesis of [K(2,2,2-crypt)]₃[Pd@Sn₉PdSnCy₃]³⁻·tol·1/2en

Crystalline [K(2,2,2-crypt)]₃[Sn₉SnCy₃] (80 mg, 0.028 mmol) was dissolved in 2 mL of en/py (2:1) mixture in a glass vial 1. The solution from vial 1 was filtered through tightly packed glass wool, and added dropwise onto Pd(PPh₃)₄ (72 mg, 0.056 mmol) in vial 2. An additional 0.2 mL of pyridine was added to tightly packed glass wool to wash down the remaining precursor. The solution in vial 2 was stirred for 2 hrs. The resulting dark red solution was filtered through tightly packed glass wool, and layered with 2 mL of toluene. Within 7 days, black prism shaped crystals formed on the bottom of the vial. Yield: ~60%, 50 mg based on amount of Sn₉SnCy₃³⁻ precursor. ¹¹⁹Sn NMR (ppm, pyridine-d₅): -567 (9 Sn, Δv_{1/2} 163 Hz), 126 (1 Sn, Δv_{1/2} 215 Hz). ¹H NMR (ppm, pyridine-d₅): δ= 3.45 (s, 2,2,2-crypt), 3.38 (t, 2,2,2-crypt), 2.37 (t, 2,2,2-crypt), 1.84 (m, -Cy), 1.66 (m, -Cy), 1.44 (m, -Cy), 1.30 (m, -Cy). ¹³C NMR (ppm, pyridine-d₅): δ= 71.3 (2,2,2-crypt), 68.48 (2,2,2-crypt), 54.68 (2,2,2-crypt), 35.48 (-Cy), 31.59 (-Cy), 29.00 (-Cy), 26.50 (-Cy).

Crystallographic Studies

The crystal structure of the Pd@Sn₉H³⁻ ion (**2**) was determined at the single crystal X-ray facility at Chemistry and Biochemistry Department, University of Maryland, by Dr. James Fettinger. The crystal structures of the other compounds, **1**, and **3-5** were determined at single crystal X-ray facility at Chemistry and Biochemistry Department, University of Maryland, by Dr. Peter Zavalij.

The theoretical DFT calculations of the minimized energy structure of the Ni@Sn₉H³⁻ ion have been done by Prof. Andrei Vedernikov.

Chapter 5: Ni@Sn₉M(CO)₃⁴⁻ (M= Cr, Mo)

5.1. Introduction

The E₉M(CO)₃⁴⁻ ions (E= Sn, Pb, M= Cr, Mo, W) are the first examples of isolated transition metal-Zintl ion adducts from the reaction of E₉⁴⁻ and M(CO)₃L complexes (L= mes, tol, thf), as reported by Eichhorn et al.^[94, 95] Later, similar derivatives of these cluster ions have been reported with other transition metals such as, E₉Ir(cod)₂³⁻ (E= Sn, Pb), E₉MC₆H₅³⁻ (E= Si, Ge, Sn, Pb, M= Cd, Zn), and Ge₉Cu(PⁱPr₃)₃³⁻.^[101-103, 108, 123] Although, 9-atom clusters have shown to accommodate an interstitial transition metal, there are no interstitial examples of these clusters.

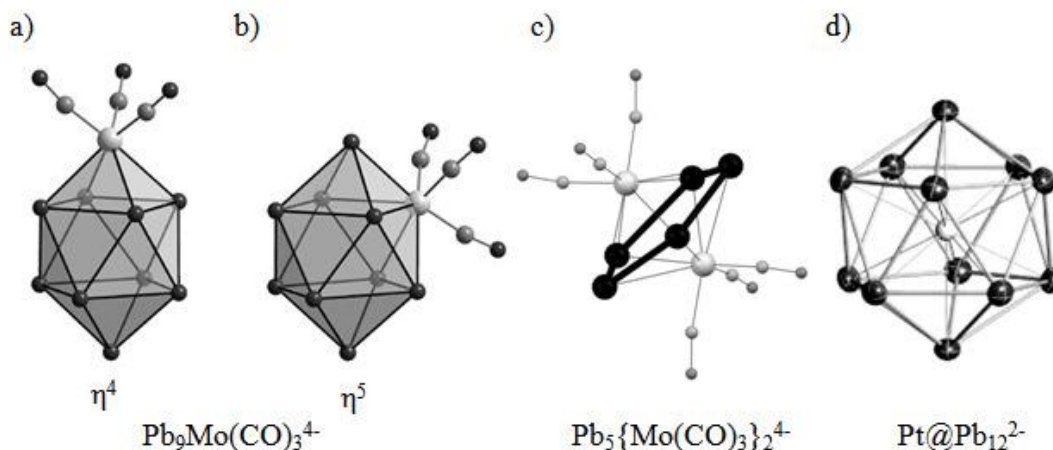


Figure 5.1. Structures of the Pb clusters from the reaction of Pb₉⁴⁻ with corresponding transition metal precursors. a) η^4 -Pb₉Mo(CO)₃⁴⁻; b) η^5 -Pb₉Mo(CO)₃⁴⁻; c) Pb₅^[96]₂⁴⁻ and d) Pt@Pb₁₂²⁻ ions. Figures are taken from the references^[96, 111, 120]

Two isomers have been reported for the Sn₉W(CO)₃⁴⁻ and Pb₉Mo(CO)₃⁴⁻ clusters, where the M(CO)₃ units are attached to the clusters in η^4 and η^5 fashion as

shown in Figure 5.1a and 5.1b.^[96, 97] Studies with the $\text{Sn}_9\text{W}(\text{CO})_3^{4-}$ ion have shown that the two isomers of the cluster interconvert by an isomerization mechanism. Formation of the $\eta^5\text{-Pb}_5^{4-}$ ion^[96], which has an unusual structure with a *cyclo*- Pb_5^{2-} fragment is coordinated by two $\text{Mo}(\text{CO})_3^-$ (Figure 5.1c) has been proposed as a disproportionation product of the $\eta^5\text{-Pb}_9\text{Mo}(\text{CO})_3^{4-}$ ion.^[111]

The η^5 isomer is thought to be an important transition state to high symmetry clusters and eventually fuller-type clusters. The icosahedral clusters $\text{Ir}@\text{Sn}_{12}^{3-}$ and $\text{M}@\text{Pb}_{12}^{2-}$ (M= Ni, Pd, Pt) are examples of high symmetry in the group 14 Zintl ions.^[121, 122] Eichhorn et al. reported that in the reaction of Pb_9^{4-} with $\text{Pt}(\text{PPh}_3)_4$ complex resulting in $\text{Pt}@\text{Pb}_{12}^{2-}$ ion (Figure 5.1d).^[122] In this reaction, C_6H_6 and Ph_2P^- were reported as by-products. Fassler et al. succeeded in converting $\eta^4\text{-Sn}_9\text{Ir}(\text{cod})^{3-}$ into $\text{Ir}@\text{Sn}_{12}^{3-}$ ion.^[123] However, detailed reaction mechanisms of formation for these clusters are not clear. Fassler et al. pointed out a possible disproportionation reaction might creating a five-membered ring fragment in the course of reaction, which is also a common feature in the pentagonal prism non-deltahedral $\text{M}@\text{Ge}_{10}^{3-}$ (M= Fe, Co) ions.^[103, 124] Understanding of the reaction mechanism might lead to obtaining fuller-type cluster ions of group 14 ion similar to the $\text{As}@\text{Ni}_{12}@\text{As}_{20}^{3-}$ ion.^[5] In a recently study, a fuller-type $\text{Eu}@\text{Sn}_6\text{Bi}_8^{4-}$ ion has been isolated and intermediate ion was found to be a $\text{Sn}_3\text{Bi}_4^{6-}$ ion.^[130] The proposed structure for this intermediate ion is analogous to the nortricyclic As_7^{3-} ion with 5-membered units in the structure.

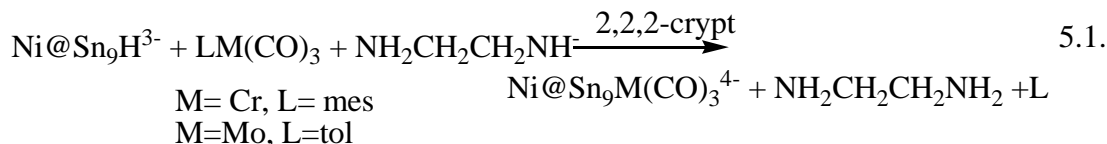
In this study, we present the synthesis and structural properties of two new ternary examples of the endohedral cluster ions, $\eta^5\text{-Ni}@\text{Sn}_9\text{M}(\text{CO})_3^{4-}$ ions (M= Cr, Mo). They are first examples of ternary Sn clusters with two d-block transition metals

with different d-electron counts, and are obtained in step-wise reactions via the $\text{Ni@Sn}_9\text{H}^{3-}$ intermediate cluster ion.

5.2. Results and Discussion

5.2.1. Synthesis

Ethylenediamine (en) solution of $\text{Ni@Sn}_9\text{H}^{3-}$, prepared *in-situ*, in the presence of $[\text{K}(2,2,2\text{-crypt})]^+$ cations, reacts with toluene solutions of $\text{Cr}(\text{CO})_3\{\text{C}_6\text{H}_3(\text{CH}_3)_3\}$ and $\text{Mo}(\text{CO})_3\{\text{C}_6\text{H}_5(\text{CH}_3)\}$ complexes, to give the $\text{Ni@Sn}_9\text{M}(\text{CO})_3^{4-}$ clusters (M = Cr, Mo) respectively according to eq.5.1. The resulting air and moisture sensitive $\text{Ni@Sn}_9\text{M}(\text{CO})_3^{4-}$ clusters were obtained as black crystalline prism-like $[\text{K}(2,2,2\text{-crypt})]^+$ salts in 25% (M=Cr), and 21% (M=Mo) yields. The $\text{Ni@Sn}_9\text{Cr}(\text{CO})_3^{4-}$ ion has been characterized by IR spectroscopy and single crystal XRD. The $\text{Ni@Sn}_9\text{Mo}(\text{CO})_3^{4-}$ ion has been characterized by IR spectroscopy, single crystal XRD and ^{13}C NMR spectroscopy.



The stepwise conversions are schematically shown in Figure 5.2. As mentioned in chapter 2, the Sn_9H^{3-} ion forms from a reaction of Sn_9^{4-} ions with the solvent molecules (en). Further reactions of Sn_9H^{3-} ion with $\text{Ni}(\text{cod})_2$ gives an endohedral $\text{Ni@Sn}_9\text{H}^{3-}$ ion as discussed in Chapter 4. The $\text{Ni@Sn}_9\text{H}^{3-}$ ion, prepared *in-situ*, reacts with a $\text{M}(\text{CO})_3\text{L}$ complexes to form the $\text{Ni@Sn}_9\text{M}(\text{CO})_3^{4-}$ ions as described above. It is anticipated that the conversion of $\text{Ni@Sn}_9\text{H}^{3-}$ to $\text{Ni@Sn}_9\text{M}(\text{CO})_3^{4-}$ ions

must be conducted in the presence of a base ($\text{NH}_2\text{CH}_2\text{CH}_2\text{NH}^-$) suggesting a relatively acidic “hydride” ligand in these particular reactions.

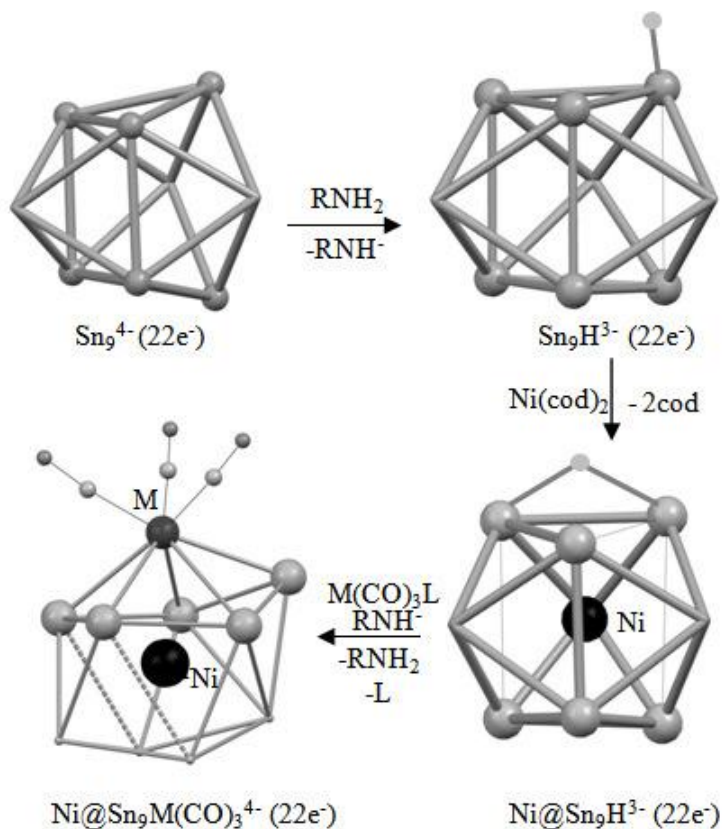


Figure 5.2. Conversion of $\text{Sn}_9^{4+} \rightarrow \text{Sn}_9\text{H}^{3-} \rightarrow \text{Ni}@\text{Sn}_9\text{H}^{3-} \rightarrow \text{Ni}@\text{Sn}_9\text{M}(\text{CO})_3^{4-}$ ($\text{M} = \text{Cr}, \text{Mo}$). The dark spheres are Ni and M transition metal atoms as labeled. Large light spheres are Sn atoms, which denotes the trigonal prisims for Sn_9^{4+} , Sn_9H^{3-} and $\text{Ni}@\text{Sn}_9\text{H}^{3-}$ ions, whereas they represents a pseudo-five membered ring in the $\text{Ni}@\text{Sn}_9\text{M}(\text{CO})_3^{4-}$ ion. Solid lines denote normal Sn-Sn bonds whereas thin lines represent the heights of the virtual trigonal prisims and long contacts ranging between $3.4 < x < 3.7 \text{ \AA}$. RNH_2 represents the ethylenediamine molecule.

The $\text{Ni}@\text{Sn}_9\text{H}^{3-}$ ion is an important intermediate ion, which can possibly convert into other cluster ions. Conversion the $\text{Ni}@\text{Sn}_9\text{H}^{3-}$ ion into $\text{Ni}@\text{Sn}_9\text{SnCy}_3^{3-}$ ion is explained in Chapter 4. In this chapter, conversion of the $\text{Ni}@\text{Sn}_9\text{H}^{3-}$ to $\eta^5\text{-Ni}@\text{Sn}_9\text{M}(\text{CO})_3^{4-}$ cause in the polarization of Sn-H bond as a result of coordination of

the $M(\text{CO})_3$ moiety. It is known that the $M(\text{CO})_3$ moiety is an electronwithdrawing group, which is revealed from significant of π -backdonation resulting. As a result of this polarization, H^+ is dissociated from the cluster, and form ethylenediamine molecules with the presence of a base ($\text{NH}_2\text{CH}_2\text{CH}_2\text{NH}^-$). On the other hand, conversion of the isolated $\text{Ni@Ge}_9\text{H}^{3-}$ ion into $\text{Ni@Ge}_9\text{Ni}(\text{CO})^{2-}$ has been reported with a 2-electron lost, which possibly proceeds by H_2 gas evolution.

5.2.2. Solid State Structure

The crystallographic data for the $\eta^5\text{-Ni@Sn}_9\text{M}(\text{CO})_3^{4-}$ ions are given in Table 5.1. The selected bond distances and angles for the $\eta^5\text{-Ni@Sn}_9\text{Mo}(\text{CO})_3^{4-}$ ion are given in Table 5.2. The $[\text{K}(2,2,2\text{-crypt})]^+$ salt of $\eta^5\text{-Ni@Sn}_9\text{Cr}(\text{CO})_3^{4-}$ is a triclinic, space group P-1, whereas the $[\text{K}(2,2,2\text{-crypt})]_4[\text{Ni@Sn}_9\text{Mo}(\text{CO})_3]_3\cdot\text{en}$ is a monoclinic, space group $\text{P}2_1/\text{n}$. Structure of the Cr analog in the isolated crystal lattice highly disordered with three superimposed clusters of $\eta^5\text{-Ni@Sn}_9\text{Cr}(\text{CO})_3^{4-}$ on the same crystallographic site in different orientations, which hindered an accurate refinement. Although detailed structural analysis was not possible, the geometry of the cluster ion is consistent with the Mo analog, which was successfully refined.

Both $\eta^5\text{-Ni@Sn}_9\text{M}(\text{CO})_3^{4-}$ (M= Cr, Mo) clusters are a 10-vertex *closo* structures with interstitial Ni atoms (Figure 5.3a and c). They adopt a bicapped square anti-prismic geometry, where the $M(\text{CO})_3$ fragments are attached to the square planes of the 10-vertex units, as shown in Figures 5.3. Both clusters have virtual C_s symmetry with a mirror plane passes through Sn8, M, and C1 atoms. The $\text{Cr}(\text{CO})_3$ and $\text{Mo}(\text{CO})_3$ groups occupy a waist vertex of the square plane (Sn2-Sn4-Sn8-M) with five Sn-M contacts representing a rare η^5 isomer. The average angles between

the Sn atoms on the top square plane are $90\pm 5.2^\circ$ and $90\pm 2.7^\circ$ on the bottom square. The O-C-Mo units slightly deviate from linearity with an average angle of $175^\circ \pm 1$, as also reported for the non-interstitial η^5 coordinated clusters. They are isostructural to the η^5 - $\text{Sn}_9\text{W}(\text{CO})_3^{4-}$ and η^5 - $\text{Pb}_9\text{Mo}(\text{CO})_3^{4-}$ ions, and reminiscent to the ligand stabilized $\{\text{Si}(\text{SiMe}_3)_3\}_3\text{Ge}_9\text{Cr}(\text{CO})_3^-$ cluster.^[63, 97, 177]

Table 5.1. Crystallographic data for the $\text{Ni}@\text{Sn}_9\text{M}(\text{CO})_3^{4-}$ (M= Cr^b, Mo) ion.

Compound	[K(2,2,2crypt)] ₄ .en	
	[Ni@Sn ₉ Cr(CO) ₃]	[Ni@Sn ₉ Mo(CO) ₃]
formula weight	2985.41	3029.35
temperature (K)	150 (2)	150 (2)
wavelength (Å)	0.71073	0.71073
crystal system	triclinic	monoclinic
space group	P-1	P2 ₁ /n
unit cell dimensions		
a (Å)	14.798 (2)	17.632 (14)
b (Å)	15.399 (8)	25.031 (2)
c (Å)	15.819 (8)	25.770 (2)
α (°)	117.69 (1)	90
β (°)	113.51 (1)	92.279 (2)
γ (°)	92.462 (1)	90
volume (Å ³)	2808.03	11363(2)
Z		4
D _{calc} (Mg/m ³)		1.771
Abs. coeff. (mm ⁻¹)		2.422
final R indices(all data) ^a		
R1, I>2σ(I)		0.0398
wR2		0.0903

^a $R_1 = \sum||F_o| - |F_c|| / \sum|F_o|$, $wR_2 = [\sum w(F_o^2 - F_c^2)^2 / \sum w(F_o^2)^2]^{1/2}$ ^b Preliminary result

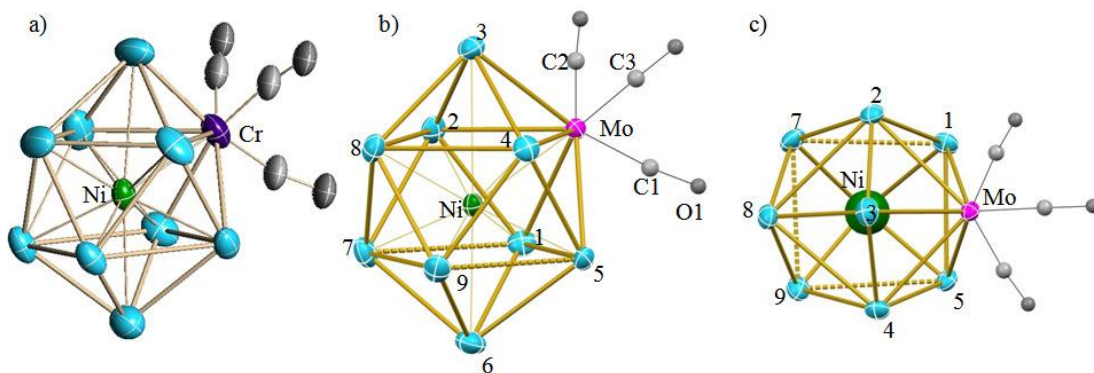


Figure 5.3. ORTEP drawings of the $\eta^5\text{-Ni@Sn}_9\text{M(CO)}_3^{4-}$ ions, a) $\text{M}=\text{Cr}$, b) $\text{M}=\text{Mo}$, and c) top view of $\eta^5\text{-Ni@Sn}_9\text{Mo(CO)}_3^{4-}$ ion. Thermal ellipsoids are set to 50% probability level. The dotted lines represent the contacts between $3.4 < x < 3.7 \text{ \AA}$, whereas solid lines denotes the bond lengths less than 3.4 \AA .

The 19 Sn-Sn bond distances of the $\eta^5\text{-Ni@Sn}_9\text{Mo(CO)}_3^{4-}$ ion are in the range of $2.951(2) - 3.514(2) \text{ \AA}$ (avg. $3.124 \pm 0.18 \text{ \AA}$). The longest Sn-Sn distances are between the atoms that reside within the bottom waist $d(\text{Sn}1\text{-}5\text{-}7\text{-}9)_{\text{avg}} = 3.372 \pm 0.16 \text{ \AA}$, which are slightly longer than the distances within the top waist $d(\text{Sn}2\text{-}4\text{-}8)_{\text{avg}} = 3.338 \pm 0.04 \text{ \AA}$ (Figure 5.3c). The shortest Sn-Sn distance in the $\eta^5\text{-Ni@Sn}_9\text{Mo(CO)}_3^{4-}$ cluster ion is between the apical Sn3 atom and the square plane defined by the Mo-Sn4-Sn8-Sn2 atoms ($d(\text{Sn-Sn})_{\text{avg}} = 2.985 \pm 0.04 \text{ \AA}$). The reported non-interstitial $\eta^4\text{-Sn}_9\text{Mo(CO)}_3^{4-}$ ion, where Mo(CO)_3 group caps the top waist, and 20 Sn-Sn distances are in a range of $2.919(2) - 3.282(2) \text{ \AA}$ (avg $3.027 \pm 0.1 \text{ \AA}$).^[98] Although, η^5 isomer of Mo analog of the non-interstitial ion have not been reported, having a similar covalent radii the W analog has also similar Sn-Sn distances with an average $3.039 \pm 0.12 \text{ \AA}$.^[97] Therefore, the presence of an interstitial Ni atom together with $\eta^5\text{-Mo(CO)}_3$ coordination resulted in the elongation of the Sn-Sn bond distances in consistent with other known endohedral Sn clusters.

The Sn-Ni distances differ according to location of the Sn atoms of the η^5 -Ni@Sn₉Mo(CO)₃⁴⁻ ion. The 7 Sn-Ni distances of the Sn atoms of the square planes are symmetrical in a narrow range of 2.607(2) - 2.644(2) Å and are consistent with the other Ni endohedral clusters such as, η^4 -Ni@Sn₉Ni(CO)₃³⁻ and Ni₂@Sn₁₇⁴⁻ ions.^[117, 128] On the other hand, 2 Sn-Ni distances on the apical sites are non-equally elongated, Sn6-Ni= 2.885 Å and Sn3-Ni= 3.288 Å. The elongation of apical vertex-Ni atom contacts has also been reported for Ni@Pb₁₀²⁻ ion,^[178] a bicapped square-anti prism, however elongations are symmetrical unlike to the η^5 -Ni@Sn₉Mo(CO)₃⁴⁻ ion.

Total coordination number of the vertex Mo atom in the η^5 -Ni@Sn₉Mo(CO)₃⁴⁻ ion is nine, including five Sn-Mo contacts and one Mo-Ni contact. The Mo-Sn distances range between 2.976 (2) - 3.116(2) Å ($d_{\text{avg}} = 3.06 \pm 0.08$ Å), slightly longer compared to the η^4 -Sn₉Mo(CO)₃⁴⁻ ion ($d_{\text{avg}} = 2.99 \pm 0.02$ Å)^[98]. However, similar elongation also exist in η^5 isomers of the Pb₉Mo(CO)₃⁴⁻ ion compared to the η^4 isomer.^[96] Moreover, the Mo atom in the title cluster makes closer contacts to the Sn1-Sn3-Sn5 atoms than to the Sn2-Sn4 atoms, which is also reported for the η^5 -Pb₉Mo(CO)₃⁴⁻ ion. Thus, the endohedral Ni atom does not have a substantial effect on the Mo-Sn distances. The Mo-Ni distance in the Ni@Sn₉Mo(CO)₃⁴⁻ cluster ion is 2.788(2) Å, which is longer than the reported values for the coordination compounds, such as Ni₃Mo(μ_3 -CO)₃(η^5 -C₅H₅)₃(η^5 -C₅H₄Me) (2.593 Å),^[179] as expected due to high coordination number of Mo atom and negative charge of the cluster.

Compared to the η^4 -Sn₉Mo(CO)₃⁴⁻ ion, the average M-C bond length is longer for Ni@Sn₉Mo(CO)₃⁴⁻ (1.94 Å vs. 1.88 Å); while, the average C-O bond length is slightly shorter (1.189 Å vs 1.193 Å). A similar observation has also been reported

for the comparison of η^4 and η^5 isomers of the non-interstitial $\text{Sn}_9\text{W}(\text{CO})_3^{4-}$ and $\text{Pb}_9\text{Mo}(\text{CO})_3^{4-}$ ions, where η^5 isomers have longer M-C and shorter C=O contacts compared to the η^4 isomers.

Both $\eta^5\text{-Ni@Sn}_9\text{M}(\text{CO})_3^{4-}$ anions (M= Cr, Mo) are 22 e^- *closo* clusters in a Wade-Mingos description. In this analysis, there are 18 electrons for the 9-atom Sn cluster (2×9), and 4 electrons due to the charge giving 22 e^- cluster bonding electrons (c.b.e.). Being a d^{10} interstitial atom, Ni does not any contribution to the c.b.e. The $\text{M}(\text{CO})_3$ ligand also does not have any contribution to the c.b.e. since a vertex transition metal contributes TE -12 electrons to cluster bonding where TE is the total electrons at the metal center (TE = 6 +6 = 12 for d^6 transition metal atoms and three CO groups). This situation corresponds to a $2n+2$ ($n=10$) *closo* cluster. The Mo and Cr complexes are the 18 electron complexes according to neutral electron count formalism, with 6 e^- donation from the cluster ions and the 2 e^- donor CO ligands. They are isoelectronic to similar types of transition metal derivatives of group 14 Zintl ions, *e.g.* $\text{E}_9\text{M}(\text{CO})_3^{4-}$ (M= Cr, Mo, W, E= Sn, Pb), $\text{E}_9\text{Ir}(\text{cod})_2^{3-}$ (E= Sn, Pb), $\text{E}_9\text{ZnC}_6\text{H}_5^{3-}$ (E= Si, Ge, Sn, Pb), and $\text{Ge}_9\text{Cu}(\text{P}^i\text{Pr}_3)^{3-}$ ions.^[101-103, 108, 121]

Table 5.2. Selected Bond Lengths [\AA] and angles ($^\circ$) for the $\eta^5\text{-Ni@Sn}_9\text{Mo(CO)}_3^{4-}$ ion.

Sn1-Sn2	3.014(2)	Sn3-Sn4	2.973(2)	Sn6-Sn7	2.945(2)
Sn1-Sn5	3.146(2)	Sn3-Sn8	3.030(2)	Sn6-Sn9	2.970(2)
Sn1-Sn6	3.031(2)	Sn4-Sn5	2.992(2)	Sn7-Sn8	3.002(2)
Sn2-Sn3	2.951(2)	Sn4-Sn9	3.114(2)	Sn8-Sn9	3.004(2)
Sn2-Sn7	3.102(2)	Sn5-Sn6	3.069(2)	Sn5-Sn9	3.420(2)
Sn7-Sn9	3.410(2)	Sn7-Sn1	3.514(2)	Sn2-Mo	3.171(2)
Sn2-Sn8	3.365(2)	Sn8-Sn4	3.310(2)	Sn1-Mo	3.005(2)
Sn3-Mo	2.976(2)	Sn4-Mo	3.116(2)	Sn5-Mo	3.055(2)
Mo-Ni	2.788(2)	Sn1-Ni	2.607(2)	Sn2-Ni	2.644(2)
Sn3-Ni	3.289(2)	Sn4-Ni	2.639(2)	Sn5-Ni	2.631(2)
Sn6-Ni	2.889(2)	Sn7-Ni	2.608(2)	Sn8-Ni	2.637(2)
Sn9-Ni	2.613(2)	Mo-C1	1.936(5)	Mo-C2	1.950(5)
Mo-C3	1.940(5)	C1-O1	1.196(6)	C2-O2	1.182(5)
C3-O3	1.189(6)				
Angles					
Sn2-Mo-Sn4	91.49(4)	Sn2-Sn8-Sn4	84.84 (7)	Sn8-Sn2-Mo	90.82(5)
Sn1-Sn5-Sn9	92.71(4)	Sn5-Sn9-Sn7	88.90(8)	Sn5-Sn1-Sn7	91.64(8)
C1-Mo-Ni	120.18(15)	C1-Mo-Sn3	170.11(14)	O1-C1-Mo	173.9(5)
O2-C2-Mo	175.4(4)	O3-C3-Mo	175.0(5)	Mo-Ni-Sn5	68.57(4)
Sn8-Ni-Sn9	69.81(2)	Sn9-Ni-Sn5	81.41(3)	Sn7-Ni-Sn9	81.55(4)

5.2.3. IR Spectroscopy

The $\nu(\text{C-O})$ regions of infrared spectrum (IR), taken from pyridine (py) solutions of the crystalline samples ($M = \text{Cr, Mo}$) are shown in Figure 5.4. Py solvent does not have any IR bands in this region. The IR spectra show broad $\nu(\text{C-O})$ stretching vibrations at 1827 cm^{-1} and 1745 cm^{-1} for $M = \text{Cr}$, and 1847 cm^{-1} and 1761 cm^{-1} for the $M = \text{Mo}$ complexes. These recorded frequencies are in the region consistent with $\eta^4\text{-Sn}_9\text{M(CO)}_3^{4-}$ ($M = \text{Cr, Mo}$) and $\eta^5\text{-Pb}_9\text{Mo(CO)}_3^{4-}$ ions ($1829\text{-}1697 \text{ cm}^{-1}$), which have been taken from KBr pellets.^[63, 97, 98]

In C_s symmetry, the $M(CO)_3$ fragment gives three IR active $\nu(C-O)$ stretching modes with $2a + a$ symmetries. However, the observed two IR active $\nu(C-O)$ bands for the $\eta^5-Ni@Sn_9M(CO)_3^{4-}$ complexes correspond to a local C_{3v} symmetry with $a_1 + e$ symmetries. Only two stretching modes have also been observed for C_s symmetric $Sn_9M(CO)_3^{4-}$ complexes (M= Cr, Mo, W).^[97]

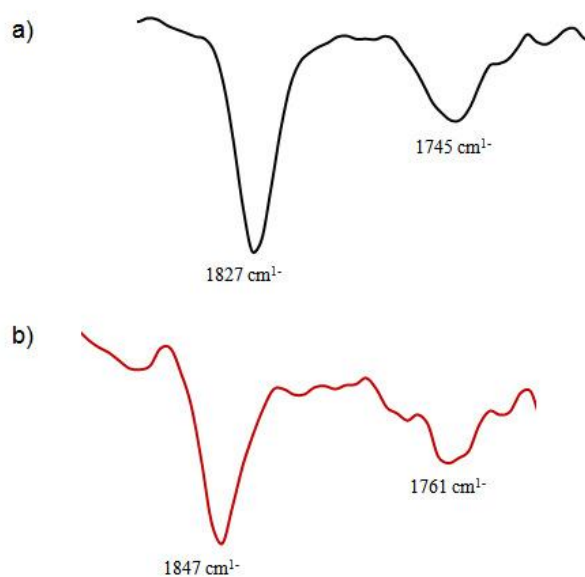


Figure 5.4. The $\nu(C=O)$ region of the IR spectra of taken from the pyridine solutions; a) $\eta^5-Ni@Sn_9Cr(CO)_3^{4-}$ and b) $\eta^5-Ni@Sn_9Mo(CO)_3^{4-}$.

Compare to the $\eta^4-Sn_9Mo(CO)_3^{4-}$ ion ($\nu= 1829\text{ cm}^{-1}, 1708\text{ cm}^{-1}$), the recorded frequencies are slightly blue shifted, consistent with a slightly shorter C=O bond lengths for the $\eta^5-Ni@Sn_9Mo(CO)_3^{4-}$ ion indicating a less CO π -backbonding.

5.2.4. NMR Spectroscopic Studies

The ^{13}C NMR spectrum of the $\eta^5\text{-Ni@Sn}_9\text{Mo(CO)}_3^{4-}$ ion has a resonance at 247.6 ppm corresponding to the CO ligands, slightly shifted to downfield comparing to the $\text{Sn}_9\text{Mo(CO)}_3^{4-}$ at 240 ppm.

The $\eta^5\text{-Ni@Sn}_9\text{Mo(CO)}_3^{4-}$ clusters are diamagnetic based on the even number of electrons with a Wade-Mingos description and the presence of a ^{13}C NMR signal. ^{119}Sn spectra were searched in blocks in the region of 3000-(-3000) ppm, but corresponding ^{119}Sn resonances could not be found in various solvents including en/tol reaction mixture, pyridine, dimethylformamide (room temperature and $-40\text{ }^\circ\text{C}$), and acetonitrile.

In the previous solution studies, it was shown that the non-interstitial $\text{Sn}_9\text{M(CO)}_3^{4-}$ ions (M= Cr, Mo, W) have three ^{119}Sn resonances in 4 :4 :1 intensity ratio corresponding to C_{4v} symmetric E_9 cluster core.^[97, 98] Although these cluster ions can be considered as static due to three resonances with large $J(^{119}\text{Sn}\text{-}^{119/117}\text{Sn})$ coupling constants, further studies showed the presence of an isomerization of between η^4 and η^5 structures of the $\text{Sn}_9\text{W(CO)}_3^{4-}$ ion.^[97] On the other hand, the $\eta^4\text{-Sn}_9\text{Ir(cod)}^3$ ion, has one time-averaged ^{119}Sn resonance suggesting an intramolecular exchange mechanism.^[121] However, it is unclear why we have not detected a ^{119}Sn NMR signal for the $\eta^5\text{-Ni@Sn}_9\text{M(CO)}_3^{4-}$ clusters.

5.3. Conclusion

In this study, two new ternary endohedral clusters of $\eta^5\text{-Ni@Sn}_9\text{M(CO)}_3^{4-}$ (M= Cr, Mo) have been isolated. The $\eta^5\text{-Ni@Sn}_9\text{M(CO)}_3^{4-}$ ions have a rare 5-

coordinating $M(\text{CO})_3$ units and are the adopt a bicapped square antiprism geometry similar to the Ni@Pb_{10}^{2-} and $\text{Ni@Sn}_9\text{Ni}(\text{CO})_3^{3-}$ ions.

With 22 c.b.e according to a Wade-Mingos description, they are isoelectronic with the non-interstitial $\text{E}_9\text{M}(\text{CO})_3^{4-}$ (Sn, Pb) ions. This study showed that similar 10-vertex *closo* clusters such as E_9ML^{3-} ions (E= Ge, Sn, Pb, ML= Ir(cod), Cu(PCy₃), Zn(mes), Cd(C₆H₅)) can also be centered with a transition metal.

The $\eta^5\text{-Ni@Sn}_9\text{M}(\text{CO})_3^{4-}$ ions are also ternary Sn clusters with two transition metals of d-electrons. As potential building blocks for catalytically active nanoparticles, such diversity of electronic structures might result in enhancing catalytical activity of such materials.

The synthesis of the title clusters were obtained by step-wise conversion of $\text{Sn}_9\text{H}^{3-} \rightarrow \text{Ni@Sn}_9\text{H}^{3-} \rightarrow \text{Ni@Sn}_9\text{Mo}(\text{CO})_3^{4-}$ with both mass and charge balanced reaction equations. Unlike to the binary d¹⁰ transition metal-Zintl ions such as, $\text{Pt@Sn}_9\text{Pt}(\text{PPh}_3)^{2-}$, and $\text{Ni@Ge}_9\text{Ni}(\text{CO})_3^{2-}$ ions, the formation of $\text{Ni@Sn}_9\text{Mo}(\text{CO})_3^{4-}$ ions does not involve an oxidative process.

5.4. Experimental Section

5.4.1. General Data

All reactions were performed in a nitrogen atmosphere drybox. The ¹³C NMR spectra were recorded on a Bruker DRX500 AVANCE spectrometer at 125 MHz operating frequency and chemical shifts were calibrated to TMS as an external reference. The infrared spectra were taken from the dissolved crystalline products of

the title clusters in pyridine solutions in a Nicolet FTIR. The percentage yields were calculated by considering the amount of alloy precursor K_4Sn_9 that was used.

5.4.2. Chemicals

Melts of nominal composition K_4Sn_9 was prepared by fusion of stoichiometric ratios of the elements at high temperature under N_2 atmosphere. 4,7,13,16,21,24-Hexaoxa-1,10-diazobicyclo[8,8,8]hexacosane (2,2,2-crypt) were purchased from Fisher Scientific. $Ni(cod)_2$ and $Cr(CO)_3(mes)$ were purchased from STREM Chemicals. Anhydrous ethylenediamine (en) and dimethylformamide (DMF) were purchased from Fisher, vacuum distilled from K_4Sn_9 , and stored under dinitrogen. Toluene was distilled from sodium/benzophenone under dinitrogen and stored under dinitrogen.

Synthesis of $[K(2,2,2-crypt)]_4[Ni@Sn_9Cr(CO)_3].en$

In a glass vial, K_4Sn_9 (80 mg, 0.065 mmol) and 2,2,2-crypt (98 mg, 0.26 mmol) were dissolved in 2 mL of en. To this solution $Ni(cod)_2$ (40 mg, 0.14 mmol) was added as solid. After string for 3 hrs, the dark red solution was filtered through tightly packed glass wool. In a glass vial 2, toluene solution of the $Cr(CO)_3(mes)$ complex (12 mg, 0.047 mmol) was prepared and added to vial 1 dropwise. The solutions were stirred for 1 hr. and filtered through tightly packed glass wool. After 4 days, the prism shaped black crystals of the $[K(2,2,2-crypt)]_4[Ni@Sn_9Cr(CO)_3].en$ (48 mg, 25 %) were obtained. IR (py): $\nu= 1827, 1745\text{ cm}^{-1}$ (CO).

Synthesis of $[K(2,2,2\text{-crypt})]_4[Ni@Sn_9Mo(CO)_3].en$

In a glass vial, K_4Sn_9 (80 mg, 0.065 mmol) and 2,2,2-crypt (98 mg, 0.26 mmol) were dissolved in 2 mL of en. To this solution, $Ni(cod)_2$ (40 mg, 0.14 mmol) was added as solid. After stirring for three hours, the dark red solution was filtered through tightly packed glass wool. In vial 2, toluene solution of the $Mo(CO)_3(tol)$ complex (15 mg, 0.055 mmol) was prepared and added to vial 1 dropwise. The solution was stirred for 1 hr. and filtered through tightly packed glass wool. After 3 days, the prism shaped black crystals of the $[K(2,2,2\text{-crypt})]_4[Ni@Sn_9Mo(CO)_3].en$ (42 mg, 21 %) were obtained. $\delta^{13}C$ (ppm, dmf) 246.7. IR (py): $\nu = 1847, 1761\text{ cm}^{-1}$ (CO)

Chapter 6: Fused Deltahedral Clusters

6.1. Introduction

Using transition metal complexes with labile ligands such as PPh_3 and cyclooctadiene (cod), ligand-free naked metal atoms can be inserted inside the E_9^{4-} ions to form endohedral clusters. In some cases, the reactions with such transition metal complexes can result in endohedral clusters with a higher nuclearity than 9, such as Ni@Pb_{10}^{2-} .^[178] Among the high nuclearity clusters, fused deltahedral Zintl ions can encapsulate more than one transition metal atom. Earlier studies reported different nuclearities in the homoleptic two-focus Sn and Ge clusters, depending on the group 14 elements and the endohedral transition metal atoms. The Sn clusters contain Pt or Ni atoms and form 17-atom Sn-framework structures such as the $\text{Pt}_2\text{@Sn}_{17}^{4-}$ (Figure 6.1a) and $\text{Ni}_2\text{@Sn}_{17}^{4-}$ (Figure 6.1c) ions.^[115, 128] The fused deltahedral Ge clusters also differs in their structures and nuclearity. The $\text{Pd}_2\text{@Ge}_{18}^{4-}$ ion is a single-cage 18-atom cluster with two endohedral Pd atoms (Figure 6.1b).^[127] On the other hand, the $\text{Ni}_3\text{@Ge}_{18}^{4-}$ ion has two Ni@Ge_9 units that are connected by a third Ni atom (Figure 6.1d).^[126] Although there are structural similarities for these fused deltahedral clusters, reasons for the different nuclearity and the variety in the resulted geometry are not clear.

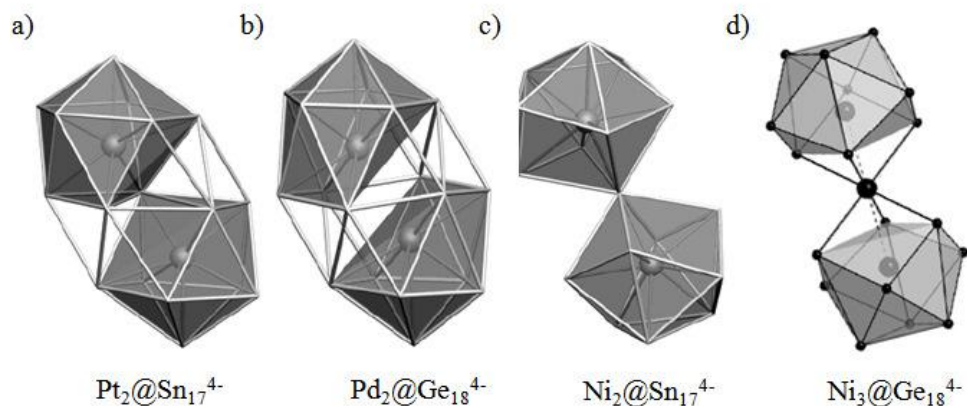


Figure 6.1. Polyhedral structures of the fused deltahedral clusters; a) $\text{Pt}_2@ \text{Sn}_{17}^{4-}$, b) $\text{Pd}_2@ \text{Ge}_{18}^{4-}$, c) $\text{Ni}_2@ \text{Sn}_{17}^{4-}$, d) $\text{Ni}_3@ \text{Ge}_{18}^{4-}$ (taken from the references [115]).

Unlike the burgeoning class of Zintl ions, heteroatomic Zintl clusters are not well known. The limited examples isolated from the nominal composition of ternary phases (e.g. KSnBi) are $\text{Sn}_2\text{Bi}_2^{2-}$, $\text{Pb}_2\text{Sb}_2^{2-}$, InBi_3^{2-} , and GaBi_3^{2-} ions. [87, 88, 180] Other studies have shown that 9-atom clusters such as $\text{In}_4\text{Bi}_5^{3-}$ and TlSn_8^{3-} have been isolated from the corresponding ternary phases. [86, 181]

The group 14 heteroatom cluster series of the $\text{Sn}_{9-x}\text{Ge}_x^{4-}$, and $\text{Sn}_{9-x}\text{Pb}_x^{4-}$ ($1 < x < 8$) compositions were obtained by extraction of A-Sn-Ge and A-Sn-Pb intermetallics with ethylenediamine solution, and they have been observed in solution and in gas phase as early as the 1980s. [38, 140] However, attempted isolation of heteroatomic clusters resulted in polycrystalline products or single crystals of the segregated homoatomic clusters. A recent study showed that the mixture of K_4Sn_9 and K_4Ge_9 binary phases in ethylenediamine (en) solution does not show any heteroatom ions in the mass spectrometer. [90] However, the same mixture in dimethylformamide (dmf) solution forms the $\text{Sn}_{9-x}\text{Ge}_x^{4-}$ ion series. This phenomenon was attributed to the high dielectric constant of dmf compared to en. In the same

study, two clusters of this series have been isolated in the form of substituted clusters $\text{Sn}_8\text{GeR}^{3-}$, $\text{Sn}_7\text{Ge}_2\text{R}^{3-}$ ($\text{R} = -\text{CH}=\text{CH}_2$). To our knowledge, isolated examples of heteroatom group 14 Zintl ions with transition metal atoms have not been reported. However, $\text{Ni}_2@\text{Sn}_7\text{Bi}_5^{3-}$ ion has been isolated in a recent study, from the ternary phase $\text{K}_2\text{Sn}_2\text{Bi}_2$ and $\text{Ni}(\text{cod})_2$ complex.^[131]

Although Rudolph's studies could not be completed during his lifetime, his research group reported solution studies for the proposed $\text{L}_2\text{MTISn}_8^{5-}$ clusters ($\text{M} = \text{Pd}, \text{Pt}$; $\text{L} = \text{en}$).^[93] However, isolation of these proposed heteroatom clusters have not been reported, and their exact composition and structure are still unknown.

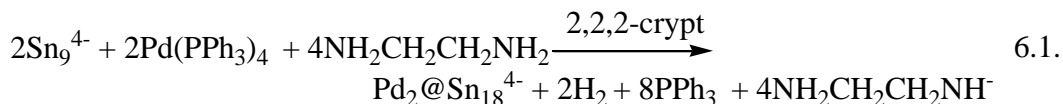
In this study, a fused deltahedral cluster ion, $\text{Pd}_2@\text{Sn}_{18}^{4-}$, has been isolated and characterized. The synthesis and the structure of this ion have also been concurrently published by Sun et al.^[182] However, we also explored its highly dynamic properties in solution, and found that it is the largest known deltahedral ion with fast-global exchange.^[174] The second fused deltahedral cluster, $\text{Ni}@\text{Sn}_8(\mu\text{-Ge})\text{Ni}@\text{Sn}_8^{4-}$, is the first example of an isolated heteroatomic cluster of group 14 elements with a transition metal atom. It suggests a dynamic exchange across a Ge focal point.

6.2. Results and Discussion

6.2.1. Synthesis

Ethylenediamine (en) solutions of K_4Sn_9 react with toluene solutions of $\text{Pd}(\text{PPh}_3)_4$ in the presence of 2,2,2-crypt to give $\text{Pd}_2@\text{Sn}_{18}^{4-}$ cluster ion according to proposed eq.6.1. The reaction requires a 4-electron oxidation of two Sn_9^{4-} ions giving

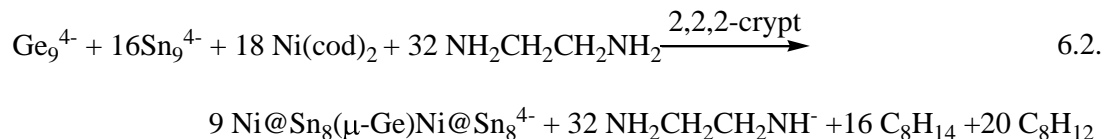
the $\text{Pd}_2@\text{Sn}_{18}^{4-}$ ion. The dark red brown crystals of the $\text{Pd}_2@\text{Sn}_{18}^{4-}$ cluster are obtained as $[\text{K}(2,2,2\text{-crypt})]^+$ salt in 15% yield. Air and moisture sensitive $[\text{K}(2,2,2\text{-crypt})]_4[\text{Pd}_2@\text{Sn}_{18}] \cdot 3\text{en}$ salt has been characterized by single crystal X-ray diffraction and ^{119}Sn NMR spectroscopy. The $\text{Pd}_2@\text{Sn}_{18}^{4-}$ ions are thermally unstable in en and dmf solutions at temperatures higher than 60 °C and 10 °C, respectively.



As discussed in Chapter 4, the reaction 6.1. gives $\text{Pd}_2@\text{Sn}_{18}^{4-}$ ion and a minor product of $\text{Pd}@\text{Sn}_9\text{H}^{3-}$ ion, evidenced by NMR studies. The ^{119}Sn NMR spectrum of the reaction mixture initially contains the resonance signal of only $\text{Pd}_2@\text{Sn}_{18}^{4-}$ ion cluster. The spectrum, taken after two days, has shown that the solution contains both the $\text{Pd}_2@\text{Sn}_{18}^{4-}$ and the $\text{Pd}@\text{Sn}_9\text{H}^{3-}$ ions. A similar observation has also been reported for the reaction of K_4Sn_9 and $\text{Pt}(\text{PPh}_3)_4$, which gives a major product of $\text{Pt}_2@\text{Sn}_{17}^{4-}$ ion and $\text{Pt}@\text{Sn}_9\text{H}^{3-}$ as a minor product.

The $\text{Ni}@\text{Sn}_8(\mu\text{-Ge})\text{Ni}@\text{Sn}_8^{4-}$ cluster is synthesized from K_4Sn_9 , K_4Ge_9 binary phases and the $\text{Ni}(\text{cod})_2$ complex in en solutions in the presence of 2,2,2-crypt. As shown in the proposed equation 6.2, cyclooctadiene is reduced to cyclooctene. The reduction of cyclooctadiene ligands to cyclooctene has been reported in earlier studies for synthesis of $\text{Ni}_2@\text{Sn}_{17}^{4-}$.^[128]

The dark red crystalline $\text{Ni}@\text{Sn}_8(\mu\text{-Ge})\text{Ni}@\text{Sn}_8^{4-}$ ions were isolated as $[\text{K}(2,2,2\text{-crypt})]^+$ salts in 30% yield based on the amount of K_4Sn_9 precursor. The air and moisture sensitive $[\text{K}(2,2,2\text{-crypt})]_4[\text{Ni}@\text{Sn}_8(\mu\text{-Ge})\text{Ni}@\text{Sn}_8]$ salt has been characterized by ^{119}Sn NMR spectroscopy and single crystal XRD.



6.2.2. Solid State Structure

The crystallographic data and selected bond distances for the $\text{Pd}_2@\text{Sn}_{18}^{4-}$ ion are given in Table 6.1. and 6.2. The $[\text{K}(2,2,2\text{crypt})]_4[\text{Pd}_2@\text{Sn}_{18}] \cdot 3\text{en}$ salt is a triclinic, space group P-1.

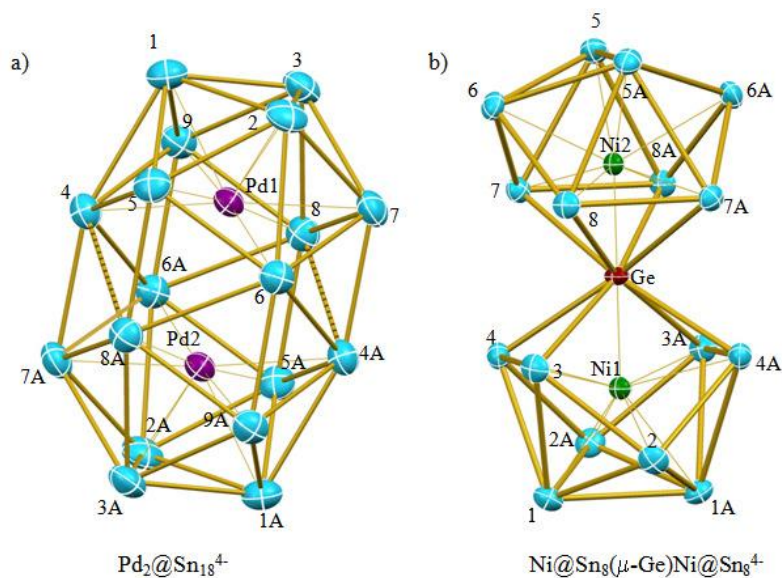


Figure 6.2. ORTEP drawing of the structures; a) $\text{Pd}_2@\text{Sn}_{18}^{4-}$ and, b) preliminary structure of $\text{Ni@Sn}_8(\mu\text{-Ge})\text{Ni@Sn}_8^{4-}$ ion. Thermal ellipsoids are set to the 50% probability level.

Table 6.1. Crystallographic data for the Pd₂@Sn₁₈⁴⁻ ion.

Compound	[K(2,2,2-crypt)] ₄ [Pd ₂ Sn ₁₈]·3en
formula weight	4191.88
temperature (K)	200(2)
wavelength (Å)	0.71073
crystal system	Triclinic
space group	P-1
unit cell dimensions	
a (Å)	14.797(9)
b(Å)	15.874(1)
c (Å)	15.934(1)
α (°)	115.28(1)
β (°)	98.24(1)
γ (°)	100.87(1)
volume (Å ³)	3216.3(3)
Z	1
D _{calc} (Mg/m ³)	2.164
abs. coeff. (mm ⁻¹)	3.885
final R indices(all data) ^a	
R ₁ , I>2σ(I)	0.0476
wR ₂	0.0955

$$^a R_1 = \frac{\sum ||F_o| - |F_c||}{\sum |F_o|}, \quad wR_2 = \left[\frac{\sum w(F_o^2 - F_c^2)^2}{\sum w(F_o^2)^2} \right]^{1/2}$$

The Pd₂@Sn₁₈⁴⁻ cluster has a capsule-like structure (Figure 6.2a), defined by a two-focus *closo*-Sn₁₈ deltahedral with two endohedral Pd atoms. The cluster has a virtual D_{3d} point symmetry, where three-fold rotation axis and the mirror plane passes through top and bottom triangular faces Sn1-2-3 and the two central Pd atoms. The structure is isostructural to the Pd₂@Ge₁₈⁴⁻ ion and similar to that of Pt₂@Sn₁₇⁴⁻ except that the planar six-membered ring at the center of Pd₂@Sn₁₈⁴⁻ is replaced by a disordered five-membered ring in the Pt complex.^[115, 127]

The polyhedron has 48 edges and 32 triangular faces defined by six 6-coordinate Sn atoms around the waist of the cluster and twelve 5-coordinate Sn atoms at the ends of the cluster. The centered Pd metal atoms are 9-coordinate in each of the clusters similar to the Pd endohedral Sn₉ clusters, which were discussed in Chapter 4.

The Sn-Sn contacts for $\text{Pd}_2@\text{Sn}_{18}^{4-}$ are in the range of 3.004(1) – 3.394(1) Å with an average of 3.11(1) Å. The Pd-Sn distances are in a more narrow range of 2.849(1) – 2.883(1) Å, with an average of 2.87 Å, which is slightly longer than the average Pd-Sn distance of the $\text{Pd}@ \text{Sn}_9\text{SnCy}_3^{3-}$ cluster ion ($d_{\text{Pd-Sn}} = 2.68$ Å) (Chapter 4). The Pd-Pd separation is 3.385 (2) Å, and much longer than the Pd-Pd distance (2.72 Å) in the $\text{Pd}@ \text{Sn}_9\text{PdSnCy}_3^{3-}$ ion, where the PdSnCy_3 occupies a vertex site.

Table 6.2. Selected Bond Lengths [Å] for the $\text{Pd}_2@ \text{Sn}_{18}^{4-}$ ion.

Pd1-Sn5	2.849(1)	Pd1-Sn1	2.865(1)	Pd1-Sn8	2.869(1)
Pd1-Sn2	2.877(1)	Pd1-Sn3	2.878(1)	Pd1-Sn4	2.882(1)
Pd1-Sn9	2.883(1)	Pd1-Sn7	2.882(1)	Pd1-Sn6	2.883(1)
Sn1-Sn2	3.004(1)	Sn1-Sn3	3.022(1)	Sn1-Sn9	3.048(1)
Sn1-Sn5	3.061(1)	Sn1-Sn4	3.251(1)	Sn2-Sn3	3.006(1)
Sn2-Sn5	3.048(1)	Sn2-Sn7	3.065(1)	Sn2-Sn6	3.274(1)
Sn3-Sn7	3.052(1)	Sn3-Sn9	3.056(1)	Sn3-Sn8	3.246(1)
Sn4-Sn9	3.040(1)	Sn4-Sn7	3.069(1)	Sn4-Sn5	3.146(1)
Sn4-Sn8	3.212(1)	Sn5-Sn8	3.063(1)	Sn5-Sn6	3.089(1)
Sn6-Sn7	3.054(1)	Sn6-Sn9	3.080(1)	Sn6-Sn8	3.248(1)
Sn7-Sn8	3.065(1)	Sn7-Sn4	3.069(1)	Sn8-Sn5	3.063(1)
Sn8-Sn9	3.096(1)	Sn8-Sn4	3.212(1)	Sn9-Sn6	3.080(1)

Summary of the preliminary crystallographic data for the $\text{Ni}@ \text{Sn}_8(\mu\text{-Ge})\text{Ni}@ \text{Sn}_8^{4-}$ ion is given in Table 6.3. The $[\text{K}(2,2,2\text{crypt})]_4[\text{Ni}@ \text{Sn}_8(\mu\text{-Ge})\text{Ni}@ \text{Sn}_8]$ salt is monoclinic, space group C2/c.

The $\text{Ni}@ \text{Sn}_8(\mu\text{-Ge})\text{Ni}@ \text{Sn}_8^{4-}$ ion is a two-focus cluster of 8 Sn atoms with two Ni interstitial atoms, $\text{Ni}@ \text{Sn}_8$, sharing a common Ge vertex (Figure 6.2b). The complex has a virtual D_{2d} point symmetry, with the mirror plane passes through the

Sn5, Ge and Sn1 atoms. The structure is isostructural to the homoatomic $\text{Ni}_2@\text{Sn}_{17}^{4-}$ cluster and it is also reminiscent of $\text{Sn}_{17}\{\text{GaCl}(\text{dpp})\}_4$ metalloid cluster.^[128, 183]

Table 6.3. Crystallographic data for the $\text{Ni}@\text{Sn}_8(\mu\text{-Ge})\text{Ni}@\text{Sn}_8^{4-}$ ion.

Compound	$[\text{K}(2,2,2\text{-crypt})]_4[\text{Ni}@\text{Sn}_8(\mu\text{-Ge})\text{Ni}@\text{Sn}_8]$
temperature (K)	150
wavelength (Å)	0.71073
crystal system	Monoclinic
space group	C2/c
unit cell dimensions	
a (Å)	30.713 (2)
b (Å)	16.588 (1)
c (Å)	28.844 (2)
α (°)	90
β (°)	121.09 (1)
γ (°)	90
volume (Å ³)	12583.7

In the $\text{Ni}@\text{Sn}_8(\mu\text{-Ge})\text{Ni}@\text{Sn}_8^{4-}$ ion, two $\text{Ni}@\text{Sn}_8$ units are connected by a common vertex Ge atom, different from the common vertex Sn atom in the $\text{Ni}_2@\text{Sn}_{17}^{4-}$ ion. The Ge atom has 8 contacts to Sn atoms with a pseudo cubic structure ($d_{\text{Sn-Ge}} = 3.04 - 3.07$ Å), which are much shorter than the Sn-Ge distances for the reported $\text{Sn}_8\text{GeR}^{3-}$ and $\text{Sn}_7\text{Ge}_2\text{R}^{3-}$ ions (R = C_2H_3) (3.50 - 3.80 Å).^[90] The Ge atom has two other contacts to the interstitial Ni atoms (2.247 Å and 2.251 Å). Distances are consistent with the Ge-interstitial Ni distances of other known ions such as $\text{Ni}@\text{Ge}_9\text{Ni}(\text{CO})^{2-}$, ranging between 2.35 Å - 2.44 Å.^[99] The $\text{Ni}_2@\text{Sn}_{17}^{4-}$ ion has the highest coordination number for the shared vertex Sn atom.^[128] Likewise, the $\text{Ni}@\text{Sn}_8(\mu\text{-Ge})\text{Ni}@\text{Sn}_8^{4-}$ ion is the first example for the highest coordination number of the Ge atom with a cubic environment in a molecular Zintl clusters.

The $\text{Ni}@\text{Sn}_8(\mu\text{-Ge})\text{Ni}@\text{Sn}_8^{4-}$ polyhedron has 30 Sn-Sn contacts ranging between 2.967 Å - 3.219 Å (avg 3.05 Å). The Sn-Sn distances excluding the shared

vertex are also very similar to the $\text{Ni}_2@\text{Sn}_{17}^{4-}$ ion with average Sn-Sn distances of 3.05 Å.^[128] Therefore, a Sn or a Ge atom on the common vertex site does not have a significant effect on the Sn-Sn distances of the polystannides.

Both cluster ions of $\text{Pd}_2@\text{Sn}_{18}^{4-}$ and $\text{Ni}@\text{Sn}_8(\mu\text{-Ge})\text{Ni}@\text{Sn}_8^{4-}$ demonstrate deviation from Wade-Mingos electron counting description. Considering 2 e⁻ contributions for each vertex atoms of these two-focus cluster and 4 e⁻ due to charge, the $\text{Pd}_2@\text{Sn}_{18}^{4-}$ ion has 40 cluster bonding electrons, whereas the $\text{Ni}@\text{Sn}_8(\mu\text{-Ge})\text{Ni}@\text{Sn}_8^{4-}$ ion has 38 cluster bonding electrons. The $\text{Pd}@\text{Sn}_9^{2-}$ and $\text{Ni}@\text{GeSn}_8^{2-}$ fragments of both clusters can be considered as a 20 e⁻ *closo* structure, since, according to Wade-Mingos description, a cluster with n=9 vertex atoms corresponds to a 2n+2 electron configuration. Overall, clusters are two focus clusters, and as a result, they deviate from the classical Wade-Mingos description. While $\text{Pd}_2@\text{Sn}_{18}^{4-}$ ion is isoelectronic with the $\text{Pd}_2@\text{Ge}_{18}^{4-}$ ion,^[127] $\text{Ni}@\text{Sn}_8(\mu\text{-Ge})\text{Ni}@\text{Sn}_8^{4-}$ is isoelectronic with $\text{Ni}_2@\text{Sn}_{17}^{4-}$ ion.^[128]

6.2.3. NMR Spectroscopic Studies

The ¹¹⁹Sn NMR spectrum of the $\text{Pd}_2@\text{Sn}_{18}^{4-}$ cluster contains a single resonance at -733.8 ppm as shown in Figure 6.3. The limiting ¹¹⁹Sn NMR spectrum is expected to have three mutually-coupled, equal-intensity resonances due to chemically-inequivalent sets of Sn atoms in a 6:6:6 ratio due to three-fold symmetry in the solid state structure. However, the limiting spectrum could not be reached at -50 C° in dimethylformamide (dmf) solution.

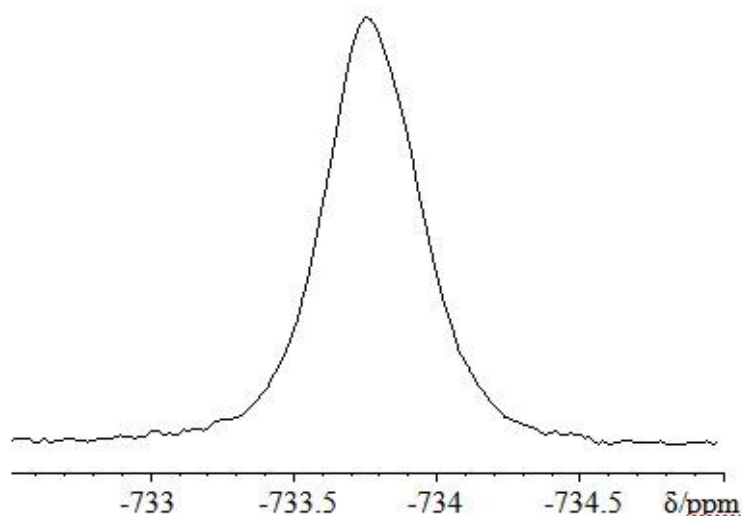


Figure 6.3. ^{119}Sn NMR spectrum of the $\text{Pd}_2@\text{Sn}_{18}^{4-}$ ion taken from dmf solutions at $-50\text{ }^\circ\text{C}$ and at 186 MHz operating frequency.

The chemical shift is temperature dependent and moves from -733.8 ppm at $-50\text{ }^\circ\text{C}$ downfield to -720 ppm at $+10\text{ }^\circ\text{C}$. Above $10\text{ }^\circ\text{C}$, the cluster begins to react with the dmf solvent and slowly decomposes. However, it is stable for several weeks in en solvents, where it shows a room temperature signal at -751.3 ppm . The lack of Sn-Sn coupling smaller than 120 Hz line width at $\frac{1}{2}$ height and the similarities to the $\text{Pt}_2@\text{Sn}_{17}^{4-}$ spectrum (single resonance at -742.3 ppm)^[115] indicate that all 18 Sn atoms of the $\text{Pd}_2@\text{Sn}_{18}^{4-}$ cluster are in fast exchange on the ^{119}Sn NMR time scale.

Although lack of ^{119}Sn - ^{117}Sn coupling constant for the equivalent 18-Sn nuclei would suggest an intermolecular exchange mechanism, the signal is broad, which can hinder the measurement of a coupling constant that is smaller than the line-broadening ($\nu_{1/2} = 120\text{ Hz}$). For example, the $\text{Cu}@\text{Sn}_9^{3-}$ cluster has a resolved $J(^{119}\text{Sn}$ - $^{117}\text{Sn})$ coupling constant with magnitude of 85 Hz.^[116] Another example is the $\text{Pt}_2@\text{Sn}_{17}^{4-}$ ion with a coupling constant of $J(^{119}\text{Sn}$ - $^{117}\text{Sn}) = 170\text{ Hz}$, which is an

indication of an intramolecular exchange mechanism of the vertex nuclei.^[115] The significant decrease in the coupling constant suggests that local $J(^{119}\text{Sn}-^{117}\text{Sn})$ values are substantially lower on average in the $\text{Pd}_2@\text{Sn}_{18}^{4-}$ cluster compared to the $\text{Pt}_2@\text{Sn}_{17}^{4-}$ ion. The average Pd-Sn distances in the $\text{Pd}_2@\text{Sn}_{18}^{4-}$ cluster is 2.87 Å, the average Pt-Sn contact (2.78 Å) in the $\text{Pt}_2@\text{Sn}_{17}^{4-}$ ion. While the average Sn-Sn contact of the two clusters are very similar, the $\text{Pt}_2@\text{Sn}_{17}^{4-}$ cluster has more short Sn-Sn contacts under 3.0 Å, compared to the Pd cluster. Therefore, the decrease in intra-vertex J coupling can be explained by the longer interatomic distances and a greater number of Sn atoms in the $\text{Pd}_2@\text{Sn}_{18}^{4-}$ ion compared to the $\text{Pt}_2@\text{Sn}_{17}^{4-}$ ion.

The ^{119}Sn NMR spectrum of the $\text{Ni}@\text{Sn}_8(\mu\text{-Ge})\text{Ni}@\text{Sn}_8^{4-}$ cluster ion was taken from the en/tol reaction mixture, Figure 6.4. It contains a single resonance at -1226 ppm at room temperature. This chemical shift is very similar to the temperature dependent single resonance at -1176 ppm (dmf, 44 °C) for the homoleptic $\text{Ni}_2@\text{Sn}_{17}^{4-}$ ion.^[128]

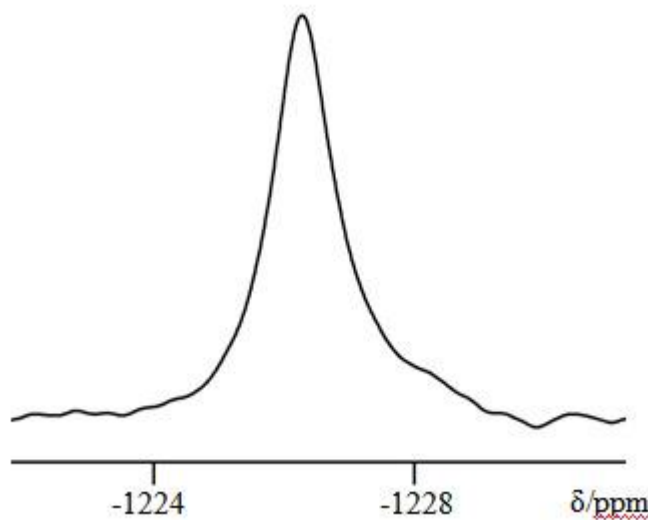


Figure 6.4. ^{119}Sn NMR spectrum of the $\text{Ni}@\text{Sn}_8(\mu\text{-Ge})\text{Ni}@\text{Sn}_8^{4-}$ ion taken from en/tol reaction mixture at room temperature and at 186 MHz operating frequency.

The limiting spectrum of the $\text{Ni@Sn}_8(\mu\text{-Ge})\text{Ni@Sn}_8^{4-}$ cluster is expected to have 3 resonances in a 8:4:4 ratio with a multiplet coupling pattern on each signal, due to chemically-inequivalent nuclei with a D_{2d} symmetry. However, a single ^{119}Sn resonance is observed in the spectrum, and this suggests that all 16 Sn atoms of the cluster are in fast-exchange at room temperature in the NMR time scale. The exchange mechanism is expected to be intramolecular due to similarities of ^{119}Sn resonance to other the fused deltahedral clusters such as the $\text{Ni}_2\text{@Sn}_{17}^{4-}$, $\text{Pd}_2\text{@Sn}_{18}^{4-}$.^[128, 174] While ^{119}Sn spectrum of $\text{Ni}_2\text{@Sn}_{17}^{4-}$ ion has a time averaged resonance at room temperature, it's limiting spectrum has been reached at $-64\text{ }^\circ\text{C}$ clearly indicates an intra-molecular exchange mechanism for this ion.

Intermediate reaction steps prior to the formation of $\text{Ni@Sn}_8(\mu\text{-Ge})\text{Ni@Sn}_8^{4-}$ ion were monitored by ^{119}Sn NMR spectroscopy. The assignments for the intermediate species are based on the obtained ^{119}Sn NMR results and the followed reaction steps and are speculative. For a precise characterization of the intermediate cluster species, supporting spectroscopic techniques are needed, however detailed analysis could not be completed.

In the first step, the nominal melt of composition K_4Sn_9 is dissolved in en, which gives a ^{119}Sn resonance at -1207.5 ppm , and $J(^{119}\text{Sn}\text{-}^{117}\text{Sn}) = 263\text{ Hz}$ (Figure 6.5a). This resonance corresponds to the Sn_9^{4-} ion with ion-pairing of K^+ ions, which was discussed in Chapter 2. After Sn_9^{4-} ion reacts with the $\text{Ni}(\text{cod})_2$ complex, this signal is replaced by a new signal at -1209 ppm (Figure 6.5b) with a line width at $1/2$ height $\nu_{1/2} = 12\text{ Hz}$ without any $^{119}\text{Sn}\text{-}^{117}\text{Sn}$ coupling. The resulting cluster ion was proposed to be Ni@Sn_9^{4-} having ion-pairing of K^+ ions since no sequestering agents

such as 2,2,2-crypt is used for the this reaction. The isolation attempts for the $\text{K}_4\text{Ni@Sn}_9$ cluster failed without using any sequestering agents.

The proposed Ni@Sn_9^{4-} ion is expected to have a similar nature to Rudolph's clusters, $\text{Sn}_9\text{Pt}(\text{PPh}_3)_2^{4-}$.^[92] Since Rudolph's clusters could not be isolated, their exact composition and structure are still unknown. However, from the ^{119}Sn and ^{31}P NMR spectroscopy, this cluster ion has been proposed as $\text{Sn}_9\text{Pt}(\text{PPh}_3)_2^{4-}$. Unlike the $\text{Sn}_9\text{Pt}(\text{PPh}_3)_2^{4-}$ cluster, which has a PPh_3 group attached to the Pt atom, the proton spectrum of Ni@Sn_9^{4-} does not show an ^1H NMR resonance for a coordinated cod ligand. Support of this proposal comes from an alternative synthesis from the $\text{Ni@Sn}_9\text{H}^{3-}$ cluster. These experiments are discussed below.

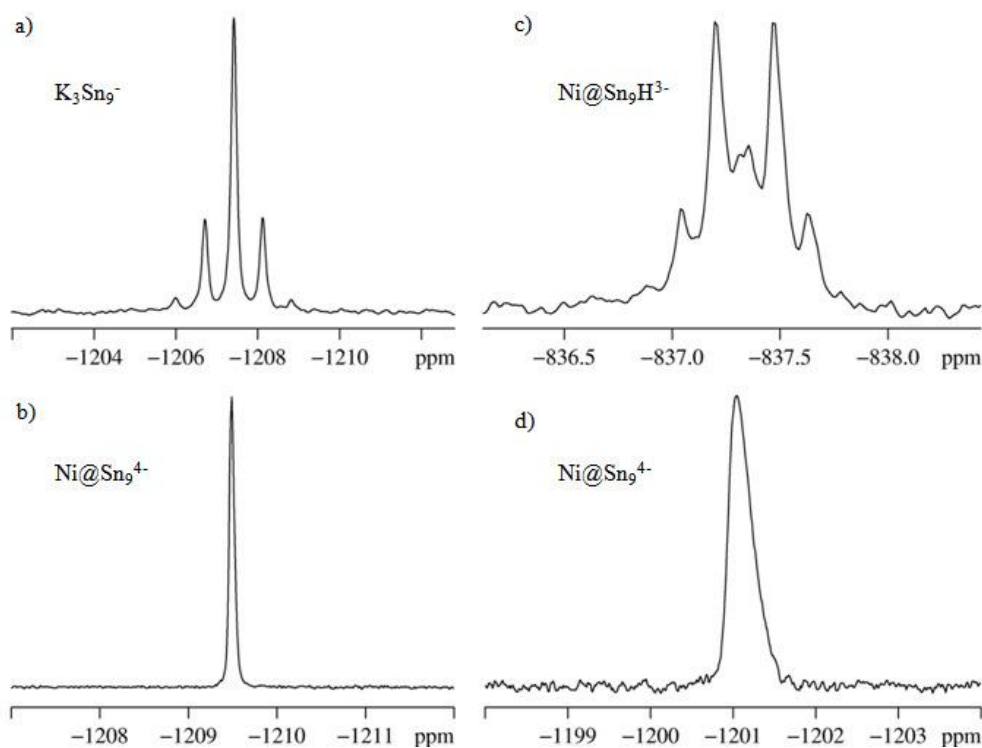


Figure 6.5. ^{119}Sn NMR spectra in ethylenediamine at room temperature at 186 MHz; a) K_4Sn_9 , b) reaction mixture of K_4Sn_9 with $\text{Ni}(\text{cod})_2$ complex, c) $\text{Ni@Sn}_9\text{H}^{3-}$ ion, and d) reaction mixture of KCl salt and $\text{Ni@Sn}_9\text{H}^{3-}$ ion, prepared *in-situ* in the presence of 2,2,2-crypt.

The $\text{Ni@Sn}_9\text{H}^{3-}$ ion is prepared from the reaction of K_4Sn_9 and $\text{Ni}(\text{cod})_2$ in the presence of 2,2,2-crypt as discussed earlier in Chapter 4. The *in-situ* prepared $\text{Ni@Sn}_9\text{H}^{3-}$ ion reacts with KCl in en solutions. After immediate reaction, the ^{119}Sn signal associated for the $\text{Ni@Sn}_9\text{H}^{3-}$ at -837.5 ppm shown in the Figure 6.5c is replaced by a new signal at -1201 ppm (Figure 6.5d). As mentioned in Chapter 2, addition of K^+ ions (KCl) to the solution containing Sn_9H^{3-} cluster and RNH^- anions facilitates the dissociation of the protons resulting in ion-paired Sn_9^{4-} ions. The singlet resonance at -1201 ppm also lacks any Sn-Sn coupling with a line-width at $\frac{1}{2}$ height = 50 Hz (at line broadening (lb) = 0). It is slightly shifted and broadened compared to the resonance signal for the proposed intermediate Ni@Sn_9^{4-} ion, which was obtained from direct reaction of K_4Sn_9 intermetallics and $\text{Ni}(\text{cod})_2$ in Figure 6.5b. This shift of the chemical shift has also been observed for the K_3Sn_9^- ions (Chapter 2) due to different for the different number of ion-pairing with the K^+ ions in the presence of 2,2,2-crypt. Recall that, ^{119}Sn resonance of the K_3Sn_9^- ions shifts to upfield with the increasing number of the equivalents of the 2,2,2-crypt. Thus, it is possible that slight upfield shift can be a result of different number of coordinating alkali metals to the Ni@Sn_9^{4-} ions, obtained in two alternative syntheses. However, similarities of the two signals supports that the resulting cluster ion from the reaction K_4Sn_9 and $\text{Ni}(\text{cod})_2$ can be Ni@Sn_9^{4-} . This single sharp ^{119}Sn resonance of this proposed Ni@Sn_9^{4-} ion lacks any ^{117}Sn satellite suggesting an intermolecular exchange mechanism and it is significantly different from the single broad ^{119}Sn resonances of the $\text{Ni}_2@\text{Sn}_{17}^{4-}$, $\text{Ni@Sn}_8(\mu\text{-Ge})\text{Ni@Sn}_8^{4-}$ and the $\text{Pd}_2@\text{Sn}_{18}^{4-}$ (see Figure 6.3) ions.^[128, 174] However,

the reason for an intermolecular exchange of the Ni@Sn_9^{4-} cluster is not clear and needs more studies.

A similar reaction mixture is prepared from the K_4Ge_9 and $\text{Ni}(\text{cod})_2$ complex in en solutions without using any 2,2,2-crypt sequestering agent. The resulting cluster is assumed to be the Ni@Ge_9^{4-} ion, analogous to the Ni@Sn_9^{4-} ion, but there is no NMR spectroscopic evidence for this assignment since Ge is a quadropolar nucleus.

The formation mechanisms and the reasons for the different nuclearities in the resulting fused deltahedral clusters are not straight forward. However, it can be anticipated that $\text{Pd}_2\text{@Sn}_{18}^{4-}$ cluster is a fusion product of the two Pd@Sn_9^{2-} cluster units. It is isostructural with the $\text{Pd}_2\text{@Ge}_{18}^{4-}$ and reminiscent to the similarly fused deltahedral polystannides, $\text{Ni}_2\text{@Sn}_{17}^{4-}$ and $\text{Pt}_2\text{@Sn}_{17}^{4-}$. Thus, by similar reasoning, the $\text{Ni@Sn}_8(\mu\text{-Ge})\text{Ni@Sn}_8^{4-}$ ion can be a result of the fusion of the Ni@Sn_9^{4-} and Ni@GeSn_8^{4-} clusters after an 4-electron oxidation process. The variety in the nuclearities for the fused deltahedral clusters, $\text{M}_2\text{@Sn}_{17/18}^{4-}$ ions, may also be a result of an intermolecular exchange of Sn vertices as observed for the proposed Ni@Sn_9^{4-} intermediate species.

6.3. Conclusion

Two new members of the fused-deltahedral clusters have been isolated and characterized in this study. The high-nuclearity homoleptic $\text{Pd}_2\text{@Sn}_{18}^{4-}$ ion is the largest deltahedral cluster isolated to-date. It is highly dynamic in the solution and showed a rapid global intramolecular exchange of 18 Sn atoms. The $\text{Ni@Sn}_8(\mu\text{-$

Ge)Ni@Sn₈⁴⁻ ion is the first isolated example of a heteroatomic 14 Zintl cluster with an interstitial transition metal.

The preparation of the Ni@Sn₈(μ-Ge)Ni@Sn₈⁴⁻ ion has been monitored by NMR studies. In these studies, an intermolecular exchange process has been observed by the NMR studies. As a result of this unusual dynamic exchange, a Ge-Sn heteroatom cluster has been obtained. Although it requires further studies and more evidence, the intermolecular exchange mechanism depending on the transition metal atom can be a reason for obtaining different nuclearity clusters with the same group transition metal atoms such as M₂@Sn₁₇⁴⁻ (M= Ni, Pt) and Pd₂@Sn₁₈⁴⁻.^[115, 127, 128]

This study also suggests that it is also possible to prepare various clusters with two different endohedral transition metal atoms encapsulated in the fused-deltahedral clusters. As a result, it is possible to obtain many other cluster ions with interesting bonding and electronic properties, which would expand this class of Zintl ions.

6.4. Experimental Section

6.4.1. General Data

All reactions were performed in a nitrogen atmosphere drybox. The ¹¹⁹Sn NMR spectra were recorded on a Bruker DRX500 AVANCE spectrometer operating at 500 MHz. The ¹¹⁹Sn chemical shifts were calibrated to Me₄Sn as an external reference in C₆D₆ (0 ppm) at room temperature. A 200 dummy scan is applied for the ¹¹⁹Sn NMR experiments. The percentage yields were calculated by considering the amount of alloy precursor K₄Sn₉ that was used.

6.4.2. Chemicals

Melts of nominal composition K_4Sn_9 and K_4Ge_9 were made by fusion of stoichiometric ratios of the elements at high temperature under N_2 atmosphere. 4,7,13,16,21,24-Hexaoxa-1,10-diazobicyclo[8,8,8]hexacosane (2,2,2-crypt) were purchased from Fisher Scientific. $Ni(cod)_2$, $Pd(PPh_3)_4$ were purchased from STREM Chemicals. Anhydrous ethylenediamine (en) and dimethylformamide (dmf) were purchased from Fisher, vacuum distilled from K_4Sn_9 , and stored under dinitrogen. Toluene was distilled from sodium/benzophenone under dinitrogen and stored under dinitrogen.

6.4.3. Synthesis

Synthesis of $[K(2,2,2-crypt)]_4[Pd_2@Sn_{18}].3en$

In vial 1, K_4Sn_9 (80 mg, 0.065 mmol) and 2,2,2-crypt (98 mg, 0.26 mmol) were dissolved in en (~ 2 mL) and stirred for ~5 min, yielding a red-brown solution. In vial 2, $Pd(PPh_3)_4$ (75 mg, 0.065 mmol) was dissolved in tol (~ 1 mL) yielding a pale-yellow solution. The solutions from vial 2 were added dropwise to vial 1 and the mixture was stirred for about 2 days, yielding a reddish brown solution. The solutions were then filtered through tightly packed glass wool. After 5 days, ~25 mg of reddish-black crystals of $[K(2,2,2-crypt)]_4[Pd_2@Sn_{18}]$ were obtained. Yield: ~ 15%.

Synthesis of $[K(2,2,2-crypt)]_4[Ni@Sn_8(\mu-Ge)Ni@Sn_8].2en$

In vial 1, K_4Sn_9 (80 mg, 0.065 mmol) was dissolved in 1 mL of ethylenediamine (en) and $Ni(cod)_2$ (36 mg, 0.13 mmol) was added as solid to this solution. In vial 2, $Ni(cod)_2$ (40 mg, 0.14 mmol) was added as solid to the solutions of the K_4Ge_9 (53 mg, 0.065 mmol) in 1 mL en. Both vials were stirred for 30 min and

filtered through tightly packed glass wool. The orange-brown solution in vial 1 was added to green colored solution in vial 2 and the mixture was stirred for 30 min. Toluene solutions of 2,2,2-crypt (190 mg, 0.5 mmol) were added dropwise. After an additional two hours of mixing, the solutions were filtered through tightly packed glass wool. The resulting red-brown solutions were layered with 1 mL of toluene and kept undisturbed for crystallization. The red-black crystals (38 mg) of the $[\text{K}(2,2,2\text{-crypt})]_4[\text{Ni}@\text{Sn}_8(\mu\text{-Ge})\text{Ni}@\text{Sn}_8].2\text{en}$ was formed after 1 week on the vial. Yield 30% based on the K_4Sn_9 intermetallic.

Crystallographic Studies

The crystal structures of the clusters were determined at single crystal X-ray facility at Chemistry and Biochemistry Department, University of Maryland, by Dr. Peter Zavalij.

Chapter 7: Conclusion

The Zintl ions and their transition metal derivatives have received a great deal of interest due to their remarkable structures. As the number of such species increases, so does the amount of knowledge about their structure, bonding nature and dynamic properties. However, the true nature of the E_9^{4-} ions ($E = \text{Si, Ge, Sn, Pb}$) has not been fully understood, leading to mischaracterizations of some cluster species, and creating difficulties in conducting controlled reactions towards discovering new clusters. The studies presented in this thesis uncover the nature of these ions by focusing on Sn_9^{4-} , and show stepwise reactions based on this new knowledge.

Earlier studies concluded that Sn_9^{3-} with distorted tricapped trigonal prism structure is a stable paramagnetic ion in equilibrium between Sn_9^{2-} , Sn_9^{4-} , and solvated electrons.^[136] Using extensive NMR analyses, our study shows that this ion is actually a proton substituted cluster Sn_9H^{3-} , similar to the other known substituted Sn_9R^{3-} ions ($\text{R} = \text{}^i\text{Pr, SnCy}_3$). Consequently, Sn_9^{4-} is a strong base with the Brønsted acidity strength of its conjugate acid, Sn_9H^{3-} , in the range of ${}^t\text{BuOH} > \text{Sn}_9\text{H}^{3-} > \text{}^i\text{Pr}_2\text{NH}$.

Earlier solution studies have demonstrated a strong ion pairing in a solution prepared from melts of nominal composition K_4Sn_9 .^[140] Our studies suggest that this binary phase ionizes in solution as K_3Sn_9^- ions, and using 2,2,2-crypt diminishes but does not completely eliminate the ion pairing. It has been known that the complex formation of sequestering agents and alkali metal cations depends on the counter anions and solvents, but none of the related studies considered a weakened sequestering of cations, when there is a strong coordinating anion such as Sn_9^{4-} . Our

study shows that Sn_9H^{3-} ions are subject to an equilibrium process with H^+ and K^+ ions, which can be manipulated by addition of an alkali metal halide salt favoring K_3Sn_9^- , or by adding excess 2,2,2-crypt favoring Sn_9H^{3-} ion.

The significance of this discovery becomes clear, considering that Sn_9^{4-} appears individually in most of the reactions with melts of nominal composition K_4Sn_9 in presence of 2,2,2-crypt in ethylenediamine solvent. In such reactions, the equilibrium between KSn_9^{3-} and Sn_9H^{3-} needs to be taken into account.

The Zintl ion chemistry is on the verge of exciting discoveries of new materials, namely cluster-assembled materials. Recent developments in group 14 Zintl ions, such as endohedral Zintl ions, transition metal linked molecular building blocks, and oxidatively coupled clusters, will advance this field towards discovering new types of nanomaterials. For this ultimate goal, there is a need to understand the reactivity of group 14 Zintl ions by means of controlled synthesis. However, studies with stepwise synthetic protocols were only few in numbers, and the reaction steps have not been very clear so far.

In this study, stepwise, mass and charge balanced reactions of exo-substituted clusters, Sn_9R^{3-} ($\text{R} = \text{H}, \text{SnCy}_3$), with the group 10 transition metal atoms have been studied. The conversion of Sn_9R^{3-} to $\text{M}@\text{Sn}_9\text{R}^{3-}$ provides mechanistic information of endohedral clusters' formation. Further reactions of the $\text{Ni}@\text{Sn}_9\text{H}^{3-}$ and $\text{Pd}@\text{Sn}_9\text{SnCy}_3^{3-}$ ions have shown different reactivity profiles of these endohedral substituted clusters. Starting from $\text{Ni}@\text{Sn}_9\text{H}^{3-}$, a ligand exchange reaction yields the $\text{Ni}@\text{Sn}_9\text{SnCy}_3^{3-}$ ion, while its reaction with group 6 transition metal complexes results in ternary $\text{Ni}@\text{Sn}_9\text{M}(\text{CO})_3^{4-}$ ($\text{M} = \text{Cr}, \text{Mo}$) ions. Furthermore, a new type of

reaction is introduced in this field, where the Pd metal is oxidatively inserted into the exo-bond Pd@Sn₉-SnCy₃ yielding a 10-vertex Pd@Sn₉PdSnCy₃³⁻ ion.

The group 14 fused deltahedral clusters with 2 endohedral transition metal atoms have been shown to form two-focus clusters in different nuclearities, such as Ni₂@Sn₁₇⁴⁻, Pd₂@Ge₁₈⁴⁻ ions.^[127, 128] In this study, two new fused deltahedral clusters have been isolated: Pd₂@Sn₁₈⁴⁻ is the largest-known deltahedral cluster to-date; and Ni@Sn₈(μ-Ge)Ni@Sn₈⁴⁻ is the first example of an endohedral heteroatom cluster. Although, more investigations for a complete understanding of formation of these ions are needed, stepwise mechanistic studies for the synthesis of Ni@Sn₈(μ-Ge)Ni@Sn₈⁴⁻ ion suggest a fusion mechanism of two endohedral cluster units. Moreover, NMR analyses led to discovery of an intermolecular exchange mechanism, which can be a possible reason for the different nuclearity in these two focus clusters.

Atomic mobility has significant implications in the reactivity of bimetallic nanoparticles (NPs) catalysts in heterogeneous transformation. Although, small NPs have been found to be more fluid with lower melting points, little is known about the dynamic processes of NPs due to the lack of suitable experimental techniques. However, NMR is a powerful method to investigate the liquid-like behavior of the Zintl ions, whose sizes are comparable to small NPs. Highly dynamic nature of Zintl ions with 9 or more vertices have been extensively studied in the past. Solution dynamics studies in this thesis have provided a deeper insight into the global dynamic exchange of the clusters with up to 18 vertices. Exchange mechanisms of the Sn₉R³⁻ ions (R= H, ⁱPr, SnCy₃, SnBu₃) are shown to be substituent dependent. The hydride, SnCy₃ and SnBu₃ substituent groups are involved in a rapid migration process around

the cluster, while the alkyl group remains bound to a specific Sn atom. The rapid migration process is also observed in endohedral derivatives of these substituted ions $M@Sn_9R^{3-}$ ($R= H, SnCy_3, M= Ni, Pd$) and systematic effects of the endohedral atoms is observed on the exchange process.

Throughout this thesis, syntheses of new Sn clusters have been discussed with the goal of answering some fundamental questions about their nature and reactivity. Besides shedding light on some of the earlier mischaracterizations and explaining the true nature of Sn_9^{4-} and coupling mechanism, our results expand the diversity of the group 14 Zintl ions. Zintl ions are potential building blocks to fabricate cluster-assembled nanomaterials, due to their high symmetry, chemical properties and electronic stabilities. However, fabricating a desired product is difficult without knowing reactive intermediates in a reaction. The stepwise conversions of Zintl ions shown in Chapters 4 and 5 demonstrate controlled synthesis with these ions, and advance cluster chemistry toward building new nanomaterials.

Appendix

This appendix contains syntheses and structural analysis results of other ions prepared in the course of this study.

Solid State Structures

The $\text{PtH}(\text{PPh}_3)(\text{SnCy}_3)_2^-$ is an anionic coordination complex crystallized as a $[\text{K}(2,2,2\text{-crypt})]^+$ salt without any solvent molecules in the monoclinic unit cell, $C2/c$. The crystallographic data is given in the Table A1.

As shown in Figure A1, the square planar complex with C_{2v} symmetry has two SnCy_3 ligands attached to the Pt center, trans to each other. The 109° (P-Pt-Sn1) and 102° (P-Pt-Sn2) angles are slightly larger than an ideal square planar homoleptic PtL_4 complex. Complex is a 16-electron complex according to both neutral atom and oxidation state formalisms. The Pt(II) complex has two $(\text{SnCy}_3)^-$, a hydride, and PPh_3 in the coordination sphere making the total charge of the compound -1. The selected bond lengths are listed in Table A3. The Pt-Sn1 and Pt-Sn2 bond lengths are 2.609(4) Å and 2.624(4) Å, respectively. A similar coordination compound of trans- $(\text{SnPh}_3)\text{Pt}(\text{PCy}_3)_2\text{H}$ was reported to have a Pt-Sn bond length of 2.654(6) Å.^[184]

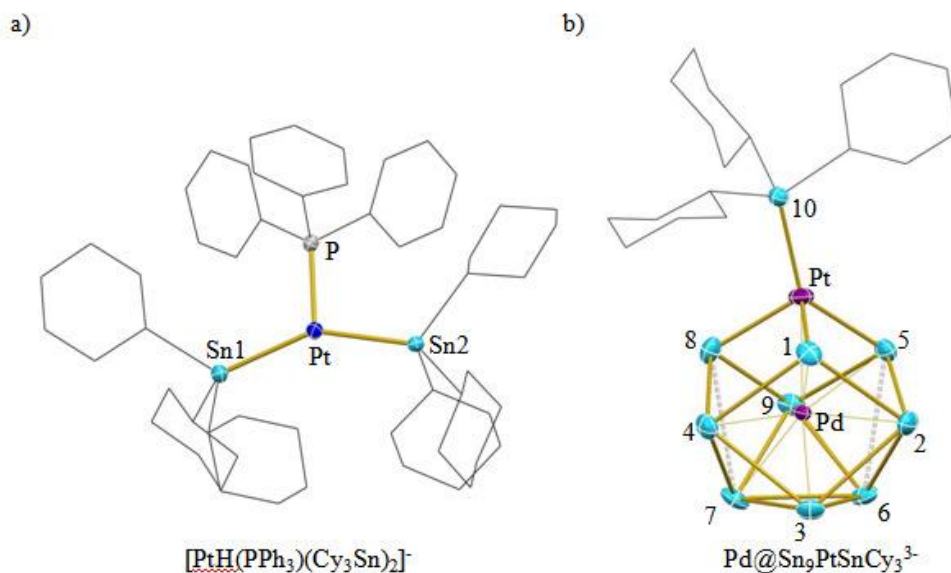


Figure A1. ORTEP drawing of the $\text{PtH}(\text{PPh}_3)(\text{SnCy}_3)_2^-$ complex (a) and $\text{Pd}@\text{Sn}_9\text{PtSnCy}_3^{3-}$ ion (b).

The $\text{Pd}@\text{Sn}_9\text{Pd}/\text{PtSnCy}_3^{3-}$ ion crystals have been obtained as $[\text{K}(2,2,2\text{-crypt})]^+$ salts in a triclinic crystal lattice, space group P-1. The crystallographic data is given in Table A1. The $\text{Pd}@\text{Sn}_9\text{Pd}/\text{PtSnCy}_3^{3-}$ has the fully occupied endohedral Pd atom, and Pd/Pt metals as the vertex atom for the two crystallographically independent clusters with a statistical mixture in a ratio of 0.72:0.28.

The selected bond distances are given in Table A3. The structure is 10-vertex, with a virtual C_{3v} symmetry, with a 3-fold axes defined by the Pt-Pd vector. The SnCy_3 group is attached to the Pt vertex atom bending slightly off of the 3-fold axis such that $\text{Pd1-Pd2/Pt-Sn10} = 160.7(4)^\circ$.

According to the Wade-Mingos analysis, the cluster electron count is 20: 2×9 electrons for the Sn atoms, 3 for the charge, and $-1 e^- \{10 (\text{Pt}) + 1 (\text{SnCy}_3) - 12\}$ (a vertex transition metal contributes TE -12 electrons to cluster bonding). Thus $20 e^-$ correspond to a 10-vertex hyper-closo cluster (2n).

Table A1. Crystallographic data for the $\text{PtH}(\text{PPh}_3)(\text{SnCy}_3)_2^-$ and $\text{Pd}@_{\text{Sn}_9}\text{PtSnCy}_3^{3-}$

Compound	[K(2,2,2-crypt)] [PtH(PPh ₃)(SnCy ₃) ₂]	[K(2,2,2-crypt)] ₆ .2tol.en [Pd@Sn ₉ Pd _{0.72} Pt _{0.28} SnCy ₃]
formula weight	1609.22	6084.96
temperature (K)	150(2)	150(2)
wavelength (Å)	0.71073	0.71073
crystal system	Monoclinic	Triclinic
space group	C2/c	P-1
unit cell dimensions		
a (Å)	22.474(2)	14.787(8)
b (Å)	16.364(2)	15.844(8)
c (Å)	40.114(3)	24.580(2)
a (°)	90	84.061(8)
β (°)	92.528(2)	81.053(8)
γ (°)	90	75.540(8)
volume (Å ³)	14737(2)	5495.7(5)
Z	8	1
Dcalc (Mg/m ³)	1.451	1.839
ab. coeff. (mm ⁻¹)	2.693	3.023
final R indices		
R1, I>2σ(I)	0.0417	0.0323
wR2, (all data) ^a	0.0949	0.0628

$$^a R_1 = \frac{\sum ||F_o| - |F_c||}{\sum |F_o|}, \quad wR_2 = \left[\frac{\sum w(F_o^2 - F_c^2)^2}{\sum w(F_o^2)^2} \right]^{1/2}$$

Table A2. Selected Bond Lengths [Å] and angles (°) for the $\text{PtH}(\text{PPh}_3)(\text{Cy}_3\text{Sn})_2^-$

Pt1-P1	2.267 (2)	Pt1-Sn2	2.609 (4)
Pt1-Sn1	2.625 (4)	Sn1-C11	2.216 (6)
Sn1-C21	2.217 (6)	Sn1-C31	2.259 (6)
Sn2-C41	2.215 (5)	Sn2-C61	2.222 (5)
Sn2-C51	2.226 (5)	P1-Pt1-Sn2	102.5 (3)
P1-Pt1-Sn1	109.7 (3)	Sn2-Pt1-Sn1	147.6 (2)

Table A3. Selected Bond Lengths [Å] for the Pd@Sn₉PtSnCy₃³⁻ ion.

Sn1-2	3.027(4)	Sn7-8	3.533(1)
Sn1-4	3.024(4)	Sn5-6	3.478(1)
Sn2-3	3.084(4)	Pd-Sn1	2.675(4)
Sn2-5	2.975(5)	Pd-Sn2	2.770(4)
Sn2-6	3.153(5)	Pd-Sn3	2.746(4)
Sn3-4	3.122(5)	Pd-Sn4	2.775(4)
Sn3-6	3.060(4)	Pd-Sn5	2.705(4)
Sn3-7	3.052(5)	Pd-Sn6	2.732(4)
Sn4-8	2.977(5)	Pd-Sn7	2.732(4)
Sn4-7	3.130(5)	Pd-Sn8	2.714(4)
Sn5-9	3.015(4)	Pd-Sn9	2.763(4)
Sn6-7	3.047(5)	Pt-Sn1	2.573(1)
Sn6-9	3.107(5)	Pt-Sn5	2.663(4)
Sn7-9	3.124(4)	Pt-Sn8	2.614(4)
Sn8-9	3.022(4)	Pt-Sn10	2.543(4)

Synthesis of [K(2,2,2-crypt)]₆[Pd@Sn₉PdSnCy₃]_{0.72}[Pd@Sn₉PtSnCy₃]_{0.28}·2tol·en

The crystalline [K(2,2,2-crypt)]₃[Sn₉SnCy₃] (80 mg, 0.028 mmol) was dissolved in 2mL of en/py (2:1) mixture in vial 1. The solutions from vial 1 were filtered through tightly packed glass wool, and added dropwise onto Pd(PPh₃)₄ (72 mg, 0.056 mmol) in vial 2. An additional 0.2 mL of pyridine was added to tightly packed glass wool to wash down remaining solutions. The solutions in vial 2 were stirred for 10 minutes. In vial 3, Pt(PPh₃)₄ (35 mg, 0.028 mmol) was dissolved in 1 mL of toluene. The solutions in vial 2 was added dropwise to vial 2. The resulting dark red solutions were filtered through tightly packed glass wool, and layered with 2 mL of toluene. Within seven days black needle shaped crystals formed on the bottom of the vial. Yield: 34 mg, 20% based on amount of [K(2,2,2-crypt)]₃[Sn₉SnCy₃] used.

Synthesis of [K(2,2,2-crypt)][PtH(PPh₃)(SnCy₃)₂]

In vial 1 the crystals of [K(2,2,2-crypt)]₃[Sn₉SnCy₃] (80 mg, 0.028 mmol) was dissolved in 2 mL of en. In vial 2, Pt(PPh₃)₄ (35 mg, 0.028 mmol) was dissolved in 1 mL of toluene. The solutions from vial 2 were added dropwise to the vial 1. The mixture in vial 1 was stirred for two hours. The resulting red-brown solutions were filtered through tightly packed glass wool, and layered with 2 mL of toluene. Within seven days brown plates formed on the bottom of the vial. Yield: ~30%, 14 mg based on amount of [K(2,2,2-crypt)]₃[Sn₉SnCy₃] that was used.

References

- [1] M. Baudler and K. Glinka, *Chem. Rev.* **1993**, *93*, 1623.
- [2] J. D. Corbett, *Angew. Chem., Int. Ed.* **2000**, *39*, 670.
- [3] S. Scharfe and T. F. Fassler, *Phil. Trans. Roy. Soc. Math. Phys. Engin. Sci.* **2010**, *368*, 1265.
- [4] S. C. Sevov and J. M. Goicoechea, *Organometallics* **2006**, *25*, 5678.
- [5] M. J. Moses, J. C. Fettinger and B. W. Eichhorn, *Science* **2003**, *300*, 778.
- [6] S. A. Claridge, A. W. Castleman, S. N. Khanna, C. B. Murray, A. Sen and P. S. Weiss, *Acs Nano* **2009**, *3*, 244.
- [7] M. C. Qian, A. C. Reber, A. Ugrinov, N. K. Chaki, S. Mandal, H. M. Saavedra, S. N. Khanna, A. Sen and P. S. Weiss, *Acs Nano* **2010**, *4*, 235.
- [8] R. C. Haushalter, C. M. O'Connor, J. P. Haushalter, A. M. Umarji and G. K. Shenoy, *Angew. Chem. Int. Ed.* **1984**, *23*, 169.
- [9] M. Moses *PhD Thesis* University of Maryland, **2004**.
- [10] M. M. Schubert, M. J. Kahlich, G. Feldmeyer, M. Huttner, S. Hackenberg, H. A. Gasteiger and R. J. Behm, *Phys. Chem. Phys.* **2001**, *3*, 1123.
- [11] S. Alayoglu, A. U. Nilekar, M. Mavrikakis and B. Eichhorn, *Nature Materials* **2008**, *7*, 333.
- [12] Z. Liu, G. Jackson and B. Eichhorn, *Angew. Chem. Int. Ed.* **2010**, *49*, 3173.
- [13] G. Somorjai, A. Contreras, M. Montano and R. Rioux, *Proc. Nat. Acad. Sci.* **2006**, *103*, 10577.
- [14] J. Greeley and M. Mavrikakis, *Nature Materials* **2004**, *3*, 810.
- [15] F. Fischer, T. Waitz, D. Vollath and N. Simha, *Prog. Mater. Sci.* **2008**, *53*, 481.
- [16] F. Tao, M. Grass, Y. Zhang, D. Butcher, J. Renzas, Z. Liu, J. Chung, B. Mun, M. Salmeron and G. Somorjai, *Science* **2008**, *322*, 932.
- [17] A. Joannis, *Comp. Rend.* **1891**, *113*, 795.
- [18] A. Joannis, *Comp. Rend.* **1892**, *114*, 585.
- [19] C. A. Kraus, *J. Am. Chem. Soc.* **1907**, *29*, 1557.
- [20] C. A. Kraus, *J. Am. Chem. Soc.* **1922**, *44*, 1216.
- [21] F. H. Smyth, *J. Am. Chem. Soc.* **1917**, *39*, 1299.
- [22] E. B. Peck, *J. Am. Chem. Soc.* **1918**, *40*, 335.
- [23] E. Zintl and A. Harder, *Z. Phys. Chem. Abt. A* **1931**, *154*, 47.
- [24] E. Zintl, Dullenkopf, W., *Z. Phys. Chem. Abt. B* **1932**, *16*.
- [25] E. Zintl, Kaiser, H., *Z. Anorg. Allg. Chem.* **1933**, *211*, 113.
- [26] L. Diehl and D. Kummer, *Angew. Chem. Int. Ed. Engl.* **1970**, *9*, 895.
- [27] L. Diehl, K. Khodadedeh, D. Kummer and J. Strahle, *Z. Naturforsch* **1976**, *318*, 594.
- [28] R. G. Teller, L. J. Krause and R. C. Haushalter, *Inorg. Chem.* **1983**, *22*, 1809.
- [29] W. Dahlmann and H. G. von Schnering, *Naturwiss.* **1972**, *59*, 420.
- [30] W. Dahlmann and H. G. von Schnering, *Naturwiss.* **1973**, *60*, 429.
- [31] H. G. von Schnering, *Angew. Chem. Int. Ed.* **1981**, *20*, 33.

- [32] S. C. Critchlow and J. D. Corbett, *Inorg. Chem.* **1984**, *23*, 770.
- [33] F. Kraus, T. Hanauer and N. Korber, *Inorg. Chem.* **2006**, *45*, 1117.
- [34] T. Hanauer, M. Grothe, M. Reil and N. Korber, *Helvetica Chim. Acta* **2005**, *88*, 950.
- [35] D. M. P. Mingos, *Nature-Physical Science* **1972**, 236, 99.
- [36] K. Wade, *Chemistry in Britain* **1975**, *11*, 177.
- [37] S. C. Critchlow and J. D. Corbett, *J. Chem. Soc. Chem. Commun.* **1981**, 236.
- [38] R. W. Rudolph, W. L. Wilson and R. C. Taylor, *J. Am. Chem. Soc.* **1981**, *103*, 2480.
- [39] P. A. Edwards and J. D. Corbett, *Inorg. Chem.* **1977**, *16*, 903.
- [40] J. Campbell and G. J. Schrobilgen, *Inorg. Chem.* **1997**, *36*, 4078.
- [41] A. Spiekermann, S. D. Hoffmann and T. F. Fassler, *Angew. Chem. Int. Ed.* **2006**, *45*, 3459.
- [42] D. Rios and S. C. Sevov, *Inorg. Chem.* **2010**, *49*, 6396.
- [43] C. H. E. Belin, J. D. Corbett and A. Cisar, *J. Am. Chem. Soc.* **1977**, *99*, 7163.
- [44] S. Joseph, C. Suchentrunk, F. Kraus and N. Korber, *Eur. J. Inorg. Chem.* **2009**, 4641.
- [45] S. C. Critchlow and J. D. Corbett, *J. Am. Chem. Soc.* **1983**, *105*, 5715.
- [46] T. J. Fässler and M. Hunziker, *Inorg. Chem.* **1994**, *33*, 5380.
- [47] T. F. Fassler and R. Hoffmann, *Z. Kristallog. New Cryst. Struct.* **2000**, *215*, 139.
- [48] L. Yong, S. D. Hoffmann and T. F. Fassler, *Z. Kristallog. New Cryst. Struct.* **2005**, *220*, 49.
- [49] J. D. Corbett and P. A. Edwards, *J. Am. Chem. Soc.* **1977**, *99*, 3313.
- [50] T. F. Fassler and R. Hoffmann, *Angew. Chem. Int. Ed.* **1999**, *38*, 543.
- [51] J. M. Goicoechea and S. C. Sevov, *J. Am. Chem. Soc.* **2004**, *126*, 6860.
- [52] T. F. Fassler, M. Hunziker, M. E. Spahr, H. Lueken and H. Schilder, *Z. Anorg. Allg. Chem.* **2000**, 626, 692.
- [53] J. M. Goicoechea and S. C. Sevov, *Inorg. Chem.* **2005**, *44*, 2654.
- [54] R. C. Burns and J. D. Corbett, *Inorg. Chem.* **1985**, *24*, 1489.
- [55] R. Hauptmann and T. F. Fassler, *Z. Anorg. Allg. Chem.* **2002**, 628, 1500.
- [56] R. Hauptmann and T. F. Fassler, *Z. Kristallog. New Cryst. Struct.* **2003**, *218*, 455.
- [57] R. Hauptmann and T. F. Fassler, *Z. Anorg. Allg. Chem.* **2003**, 629, 2266.
- [58] A. Ugrinov and S. C. Sevov, *App. Organometallic Chem.* **2003**, *17*, 373.
- [59] L. Yong, S. D. Hoffmann and T. F. Fassler, *Inorg. Chim. Acta* **2006**, *359*, 4774.
- [60] R. C. Haushalter, B. W. Eichhorn, A. L. Rheingold and S. J. Geib, *Chem. Commun.* **1988**, 1027.
- [61] L. Xu and S. C. Sevov, *J. Am. Chem. Soc.* **1999**, *121*, 9245.
- [62] A. Ugrinov and S. C. Sevov, *J. Am. Chem. Soc.* **2002**, *124*, 10990.
- [63] L. Yong, S. D. Hoffmann and T. F. Fassler, *Z. Anorg. Allg. Chem.* **2005**, *631*, 1149.
- [64] L. Yong, S. D. Hoffmann and T. F. Fassler, *Z. Anorg. Allg. Chem.* **2004**, *630*, 1977.
- [65] A. Ugrinov and S. C. Sevov, *Inorg. Chem.* **2003**, *42*, 5789.

- [66] C. Downie, Z. J. Tang and A. M. Guloy, *Angew. Chem. Int. Ed.* **2000**, *39*, 338.
- [67] G. S. Armatas and M. G. Kanatzidis, *Science* **2006**, *313*, 817.
- [68] A. M. Guloy, R. Ramlau, Z. J. Tang, W. Schnelle, M. Baitinger and Y. Grin, *Nature* **2006**, *443*, 320.
- [69] D. Sun, A. E. Riley, A. J. Cadby, E. K. Richman, S. D. Korlann and S. H. Tolbert, *Nature* **2006**, *441*, 1126.
- [70] G. S. Armatas and M. G. Kanatzidis, *J. Am. Chem. Soc.* **2008**, *130*, 11430.
- [71] G. S. Armatas and M. G. Kanatzidis, *Nature Materials* **2009**, *8*, 217.
- [72] J. Q. Wang, B. Wahl and T. F. Fassler, *Angew. Chem. Int. Ed.* **2010**, *49*, 6592.
- [73] M. Baudler, W. Faber and J. Hahn, *Z. Anorg. Allg. Chem.* **1980**, *469*, 15.
- [74] G. Fritz, J. Härer and E. Matern, *Z. Anorg. Allg. Chem.* **1983**, *504*, 38.
- [75] S. P. Mattamana, K. Promprai, J. C. Fettinger and B. W. Eichhorn, *Inorg. Chem.* **1998**, *37*, 6222.
- [76] A. Ugrinov and S. C. Sevov, *J. Am. Chem. Soc.* **2002**, *124*, 2442.
- [77] A. Ugrinov and S. C. Sevov, *J. Am. Chem. Soc.* **2003**, *125*, 14059.
- [78] A. Ugrinov and S. C. Sevov, *Chem. Eur. J.* **2004**, *10*, 3727.
- [79] M. W. Hull, A. Ugrinov, I. Petrov and S. C. Sevov, *Inorg. Chem.* **2007**, *46*, 2704.
- [80] M. W. Hull and S. C. Sevov, *J. Am. Chem. Soc.* **2009**, *131*, 9026.
- [81] D. Chapman and S. C. Sevov, *Inorg. Chem.* **2008**, *47*, 6009.
- [82] B. E. Eichler and P. P. Power, *Angew. Chem. Int. Ed.* **2001**, *40*, 796.
- [83] A. F. Richards, B. E. Eichler, M. Brynda, M. M. Olmstead and P. P. Power, *Angew. Chem. Int. Ed.* **2005**, *44*, 2546.
- [84] K. W. Klinkhammer, X. O. Yun and S. L. Yao, *Angew. Chem. Int. Ed.* **2004**, *43*, 6202.
- [85] R. C. Burns and J. D. Corbett, *J. Am. Chem. Soc.* **1981**, *103*, 2627.
- [86] R. C. Burns and J. D. Corbett, *J. Am. Chem. Soc.* **1982**, *104*, 2804.
- [87] S. C. Critchlow and J. D. Corbett, *Inorg. Chem.* **1985**, *24*, 979.
- [88] L. Xu and S. C. Sevov, *Inorg. Chem.* **2000**, *39*, 5383-5389.
- [89] B. S. Pons, D. J. Santure, R. C. Taylor and R. W. Rudolph, *Electrochim. Acta* **1981**, *26*, 365.
- [90] M. M. Gillett-Kunnath, I. Petrov and S. C. Sevov, *Inorg. Chem.* **2010**, *49*, 721.
- [91] T. F. Fassler and S. D. Hoffmann, *Angew. Chem. Int. Ed.* **2004**, *43*, 6242.
- [92] F. Teixidor, M. L. Leutkens, Jr. and R. W. Rudolph, *J. Am. Chem. Soc.* **1983**, *105*, 149.
- [93] M. L. Luetkens, F. Teixidor and R. W. Rudolph, *Inorg. Chim. Acta* **1984**, *83*, L13.
- [94] B. W. Eichhorn, R. C. Haushalter and W. T. Pennington, *J. Am. Chem. Soc.* **1988**, *110*, 8704.
- [95] B. W. Eichhorn and R. C. Haushalter, *J. Chem. Soc. Chem. Commun.* **1990**, 937.
- [96] L. Yong, S. D. Hoffmann and T. F. Fassler, *Eur. J. Inorg. Chem.* **2005**, 3663.
- [97] B. Kesanli, J. C. Fettinger, D. R. Gardner and B. W. Eichhorn, *Chem. Eur. J.* **2001**, 5277.

- [98] J. Campbell, H. P. A. Mercier, F. Holger, D. Santry, D. A. Dixon and G. J. Schrobilgen, *Inorg. Chem.* **2002**, *41*, 86.
- [99] J. M. Goicoechea and S. C. Sevov, *J. Am. Chem. Soc.* **2006**, *128*, 4155.
- [100] Z. M. Sun, Y. F. Zhao, J. Li and L. S. Wang, *J. Cluster Sci.* **2009**, *20*, 601.
- [101] D. O. Downing, P. Zavalij and B. W. Eichhorn, *Eur. J. Inorg. Chem.* **2010**, 890.
- [102] J. M. Goicoechea and S. C. Sevov, *Organometallics* **2006**, *25*, 4530.
- [103] B. B. Zhou, M. S. Denning, T. A. D. Chapman and J. M. Goicoechea, *Inorg. Chem.* **2009**, *48*, 2899.
- [104] A. Spiekermann, S. D. Hoffmann, F. Kraus and T. F. Fassler, *Angew. Chem. Int. Ed.* **2007**, *46*, 1638.
- [105] S. Joseph, M. Hamberger, F. Mutzbauer, O. Hartl, M. Meier and N. Korber, *Angew. Chem. Int. Ed.* **2009**, *48*, 8770.
- [106] A. Nienhaus, R. Hauptmann and T. F. Fassler, *Angew. Chem. Int. Ed.* **2002**, *41*, 3213.
- [107] B. B. Zhou, M. S. Denning, T. A. D. Chapman, J. E. McGrady and J. M. Goicoechea, *Chem. Commun.* **2009**, 7221.
- [108] S. Scharfe and T. F. Fassler, *Eur. J. Inorg. Chem.* **2010**, 1207.
- [109] A. Spiekermann, S. D. Hoffmann, T. F. Fassler, I. Krossing and U. Preiss, *Angew. Chem. Int. Ed.* **2007**, *46*, 5310.
- [110] B. Kesanli, B. W. Eichhorn and J. C. Fettinger, *Angew. Chem. Int. Ed.* **2001**, *40*, 2300.
- [111] L. Yong, S. D. Hoffmann, T. F. Fassler, S. Riedel and M. Kaupp, *Angew. Chem. Int. Ed.* **2005**, *44*, 2092.
- [112] C. Knapp, B. B. Zhou, M. S. Denning, N. H. Rees and J. M. Goicoechea, *Dalton Transactions* **2010**, *39*, 426.
- [113] B. Kesanli, D. R. Gardner, B. Scott and B. W. Eichhorn, *J. Chem. Soc. Dalton Trans.* **2000**, *8*, 1291.
- [114] J. Q. Wang and T. F. Fassler, *Z. Natur. Sec. B J. Chem. Sci.* **2009**, *64*, 985.
- [115] B. Kesanli, J. E. Halsig, P. Zavalij, J. C. Fettinger, Y.-F. Lam and B. W. Eichhorn, *J. Am. Chem. Soc.* **2007**, *129*, 4567.
- [116] S. Scharfe, T. F. Fassler, S. Stegmaier, S. D. Hoffmann and K. Ruhland, *Chem. Eur. J.* **2008**, *14*, 4479.
- [117] B. Kesanli, J. Fettinger, D. R. Gardner and B. Eichhorn, *J. Am. Chem. Soc.* **2002**, *124*, 4779.
- [118] N. Korber, *Angew. Chem. Int. Ed.* **2009**, *48*, 3216.
- [119] E. N. Esenturk, J. Fettinger and B. Eichhorn, *Polyhedron* **2006**, *25*, 521.
- [120] E. N. Esenturk, J. Fettinger, Y. F. Lam and B. Eichhorn, *Angew. Chem. Int. Ed.* **2004**, *43*, 2132.
- [121] J.-Q. Wang, S. Stegmaier, B. Wahl and T. F. Fässler, *Chem. Eur. J.* **2010**, *16*, 1793.
- [122] E. N. Esenturk, J. Fettinger and B. Eichhorn, *J. Am. Chem. Soc.* **2006**, *128*, 9178.
- [123] J. Q. Wang, S. Stegmaier, B. Wahl and T. F. Fassler, *Chemistry-a European Journal* **2010**, *16*, 1793-1798.

- [124] J. Q. Wang, S. Stegmaier and T. F. Fassler, *Angew. Chem. Int. Ed.* **2009**, *48*, 1998.
- [125] B. B. Zhou, M. S. Denning, D. L. Kays and J. M. Goicoechea, *J. Am. Chem. Soc.* **2009**, *131*, 2802.
- [126] J. M. Goicoechea and S. C. Sevov, *Angew. Chem. Int. Ed.* **2005**, *44*, 4026.
- [127] J. M. Goicoechea and S. C. Sevov, *J. Am. Chem. Soc.* **2005**, *127*, 7676.
- [128] E. N. Esenturk, J. C. Fettinger and B. W. Eichhorn, *J. Am. Chem. Soc.* **2006**, *128*, 12.
- [129] M. Waibel, F. Kraus, S. Scharfe, B. Wahl and T. F. Fassler, *Angew. Chem. Int. Ed.* **2010**, *49*, 6611
- [130] R. C. Felicitas Lips, and Stefanie Dehnen, *Angew. Chem. Int. Ed.* **2010**, *Asap*.
- [131] F. Lips, Dehnen, *Angew. Chem. Int. Ed.* **2010**, *Asap*.
- [132] R. W. T. Rudolph, R. C.; Young, D. C. in *The Nature of Naked Metal Clusters in Solution*, v3 (Ed. M. Tsutsui), Plenum, **1979**, pp. 997-1005.
- [133] B. Eichhorn, S. Kocak *Dynamic Properties of the Group 14 Zintl Ions and Their Derivatives in Structure and Bonding Vol. 137* (Ed. T. Fassler), Springer, Berlin, **2010**.
- [134] R. W. Rudolph, W. L. Wilson, F. Parker, R. C. Taylor and D. C. Young, *J. Am. Chem. Soc.* **1978**, *100*, 4629.
- [135] W. L. Wilson, R. W. Rudolph, L. L. Lohr, R. C. Taylor and P. Pyykko, *Inorg. Chem.* **1986**, *25*, 1535.
- [136] J. D. Corbett, *Chem. Rev.* **1985**, *85*, 383.
- [137] U. Gupta, A. C. Reber, P. A. Clayborne, J. J. Melko, S. N. Khanna and A. W. Castleman, *Inorg. Chem.* **2008**, *47*, 10953.
- [138] T. Birchall, R. C. Burns, L. A. Devereux and G. J. Schrobilgen, *Inorg. Chem.* **1985**, *24*, 890.
- [139] J. Rosdahl, T. F. Fassler and L. Kloo, *Eur. J. Inorg. Chem.* **2005**, 2888.
- [140] W. L. Wilson, R. W. Rudolph, L. L. Lohr, R. C. Taylor and P. Pyykko, *Inorg. Chem.* **1986**, *25*, 1535.
- [141] A.G. Davies, *Organotin Chemistry*, VHC, New York, **1997**.
- [142] E. Rivard and P. P. Power, *Dalton Transactions* **2008**, 4336.
- [143] V. F. K. U. Haussermann, K. Puhakainen in *Hydroheneous Zintl Phases, Vol. 137* (Ed. T. Fassler), Springer-Verlag, Berlin, **2010**.
- [144] M. Baudler and R. Heumüller, *Z. Naturforsch., Teil B* **1984**, *39*, 1306.
- [145] M. Baudler, R. Heumüller, J. Germershausen and J. Hahn, *Z. Anorg. Allg. Chem.* **1985**, *526*, 7.
- [146] M. Baudler and R. Heumüller, *Z. Anorg. Allg. Chem.* **1988**, *559*, 49.
- [147] N. Korber and H. G. Vonschering, *J. Chem. Soc. Chem. Commun.* **1995**, 1713.
- [148] S. Charles, B. W. Eichhorn, S. G. Bott and J. C. Fettinger, *J. Am. Chem. Soc.* **1996**, *118*, 4713.
- [149] F. R. Dai and L. Xu, *Inorg. Chimica Acta* **2006**, *359*, 4265.
- [150] G. Fritz and J. Härer, *Z. Anorg. Allg. Chem.* **1983**, *504*, 23.
- [151] G. Fritz, K. D. Hoppe, W. Hönle, D. Weber, C. Mujica, V. Manriquez and H. G. von Schnering, *J. Organomet. Chem.* **1983**, *249*, 63.

- [152] F. S. Kocak, P. Y. Zavalij, Y. F. Lam and B. W. Eichhorn, *Chem. Commun.* **2009**, 4197.
- [153] L. Diehl, K. Khodadedeh, D. Kummer and J. Strähle, *Chem. Ber.* **1976**, *109*, 3404.
- [154] N. Korber and A. Fleischmann, *J. Chem. Soc. Dalton Trans.* **2001**, 383.
- [155] T. F. Fassler and M. Hunziker, *Z. Anorg. Allg. Chem.* **1996**, 622, 837.
- [156] T. F. Fassler, *Coor. Chem. Rev.* **2001**, 215, 347.
- [157] L. Yong, S. D. Hoffmann and T. F. Fassler, *Z. Kristallog. New Cryst. Struct.* **2005**, 220, 49.
- [158] M. W. Hull and S. C. Sevov, *Angew. Chem. Int. Ed.* **2007**, 46, 6695.
- [159] M. W. Hull and S. C. Sevov, *Inorg. Chem.* **2007**, 46, 10953.
- [160] L. Dahlenburg, K. Herbst and A. Zahl, *J. Organomet. Chem.* **2000**, 616, 19.
- [161] M. L. Maddox, Flitcrof.N and H. D. Kaesz, *J. Organometallic Chem.* **1965**, 4, 50.
- [162] E. Rivard, R. C. Fischer, R. Wolf, Y. Peng, W. A. Merrill, N. D. Schley, Z. L. Zhu, L. Pu, J. C. Fettinger, S. J. Teat, I. Nowik, R. H. Herber, N. Takagi, S. Nagase and P. P. Power, *J. Am. Chem. Soc.* **2007**, 129, 16197.
- [163] I. S. Antipin, R. F. Gareyev, A. N. Vedernikov and A. I. Konovalov, *J. Phys. Org. Chem.* **1994**, 7, 181.
- [164] M. Baudler and K. Glinka, *Chem. Rev.* **1993**, 93, 1623.
- [165] S. Charles, J. A. Danis, S. P. Mattamana, J. C. Fettinger and B. W. Eichhorn, *Z. Anorg. Allg. Chem.* **1998**, 624, 823.
- [166] F. G. Bordwell, W. N. Olmstead and Z. Margolin, *J. Org. Chem.* **1980**, 45, 3295.
- [167] F. G. Bordwell, G. E. Drucker and H. E. Fried, *J. Org. Chem.* **1981**, 46, 632.
- [168] M. Brynda, R. Herber, P. B. Hitchcock, M. F. Lappert, I. Nowik, P. R. Power, A. V. Protchenko, A. Ruzicka and J. Steiner, *Angew. Chem. Int. Ed.* **2006**, 45, 4333.
- [169] C. Schrenk, I. Schellenberg, R. Pottgen and A. Schnepf, *Dalton Trans.* **2010**, 39, 1872.
- [170] A. Schnepf, *Chem. Soc. Rev.* **2007**, 36, 745.
- [171] H. Reuter, *Z. Kristallog. New Crystal Struct.* **2004**, 219, 327.
- [172] F. Teixidor, M. L. Luetkens and R. W. Rudolph, *J. Am. Chem. Soc.* **1983**, 105, 149.
- [173] F.S. Kocak, B. Eichhorn, *Chem. Eur. J.* **2010**, *Asap*.
- [174] F. S. Kocak, P. Zavalij, Y. F. Lam and B. W. Eichhorn, *Inorg. Chem.* **2008**, 47, 3515.
- [175] A. K. Sawyer, Y. E. Brown and E. L. Hanson, *J. Organomet. Chem.* **1965**, 3, 464.
- [176] A. L. Seligson, R. L. Cowan and W. C. Trogler, *Inorg. Chem.* **1991**, 30, 3371.
- [177] C. Schenk and A. Schnepf, *Chem. Commun.* **2009**, 3208.
- [178] E. N. Esenturk, J. Fettinger and B. Eichhorn, *Chem. Commun.* **2005**, 2, 247.
- [179] M. J. Chetcuti, J. C. Huffman and S. R. McDonald, *Inorg. Chem.* **1989**, 28, 238.
- [180] S. C. Critchlow and J. D. Corbett, *Inorg. Chem.* **1982**, 21, 3286.
- [181] F. R. Dai and L. Xu, *Chinese J. Struct. Chem.* **2007**, 26, 45.

- [182] Z. M. Sun, H. Xiao, J. Li and L. S. Wang, *J. Am. Chem. Soc.* **2007**, *129*, 9560.
- [183] G. Prabusankar, A. Kempter, C. Gemel, M. K. Schroter and R. A. Fischer, *Angew. Chem. Int. Ed.* **2008**, *47*, 7234.
- [184] H. C. Clark, G. Ferguson, M. J. Hampdensmith, H. Ruegger and B. L. Ruhl, *Can. J. Chem.* **1988**, *66*, 3120.